# Experiment No - 1
# Introduction of Vector Network Analyzer and Measurement of S-parameters of a DUT

Debashish Nandi, *Graduate Student Member, IEEE*
*Roll No.21204262*

***Abstract*— In this work, we present a detailed report on an introduction to Vector Network Analyzer (Agilent E5062A). A Vector Network Analyzer (VNA) helps in measuring complex impedance, scattering parameters (S-parameters), and phase information. In this work we have explored various features of a VNA and performed Open-Short-Load-Thru (OSLT) calibration on the VNA. Also, to demonstrate the importance of the VNA, we have characterized a 20 dB Directional Coupler by measuring important parameters such as Coupling, Isolation, Insertion Loss, Directivity. All the measurements have been carried out in the Microwave Measurement Laboratory in the Electrical Engineering Department of IIT Kanpur.**

***Index Terms*— Microwave Measurement, VNA, OSLT, Calibration, Device Under Test (DUT), Directional Coupler.**

## I. Introduction

IN the realm of microwave measurements and design, Vector Network Analyzers (VNAs) are indispensable tools that have revolutionized the way engineers and researchers work with high-frequency electronic circuits and systems [1], [2]. These sophisticated instruments have become the backbone of microwave engineering, providing precise and comprehensive insights into the behavior of complex RF components, thereby enabling the design, testing, and optimization of microwave circuits, antennas, filters, amplifiers, and transmission lines.At their core, VNAs are based on the principles of electrical impedance theory and wave propagation. They operate by transmitting a known test signal into a device under test (DUT) and then accurately measuring the reflected and transmitted signals. This measurement of the incident and reflected waves allows VNAs to determine a range of critical parameters, including the complex impedance, scattering parameters (S-parameters), phase information, and group delay. These parameters provide invaluable insights into how a component or system interacts with microwave signals across a wide frequency range. Some of the critical applications of VNAs are:

Component Characterization: VNAs excel at characterizing the performance of microwave components, such as filters, couplers, and attenuators. Engineers can assess critical parameters like insertion loss, return loss, and bandwidth, helping them select the right components for their designs.

Debashish Nandi is with the Nanolab, Department of Electrical Engineering, IIT Kanpur, Kanpur 208016, India (e-mail: debashish21@iitk.ac.in)

Amplifier Design: In microwave amplifier design, VNAs are used to evaluate gain, gain flatness, and stability. These measurements are vital in achieving optimal amplifier performance while minimizing distortion and instability issues.

Antenna Testing: VNAs are instrumental in the design and testing of antennas for wireless communication, radar systems, and satellite communications. Engineers can measure radiation patterns, impedance matching, and bandwidth to optimize antenna performance.

Transmission Line Analysis: Microwave transmission lines, such as coaxial cables and microstrip lines, must have precise impedance characteristics. VNAs assess impedance variations, propagation constants, and signal losses along these lines.

Frequency Converter Testing: For RF and microwave frequency converters, VNAs are used to evaluate conversion efficiency, spurious responses, and noise figure. This ensures the reliability of frequency translation in communication systems.

Material Characterization: Researchers use VNAs to determine the dielectric properties of materials, which is crucial in designing microwave components like microwave circuit boards and substrates.

Network Troubleshooting: VNAs are employed for troubleshooting and diagnosing problems in RF and microwave networks, identifying impedance mismatches and signal reflections that can degrade system performance.

Calibration and De-Embedding: VNAs are equipped with advanced calibration techniques to remove measurement errors introduced by cables, connectors, and test fixtures. This allows engineers to accurately isolate the behavior of the DUT.

VNAs continue to evolve, with advancements in frequency range, measurement speed, and dynamic range. Emerging trends include the integration of VNAs with software-defined capabilities and artificial intelligence for automated measurements and system optimization. As the demand for higher-frequency, higher-data-rate communication systems grows, VNAs will remain at the forefront of microwave measurements and design, enabling engineers and researchers to push the boundaries of modern technology.

In this Experiment-1 which is comprising of two sub-experiments, we familiarize ourselves with the Vector Network Analyzer by means of exploring features, OSLT calibration, and characterizing a 20dB directional coupler.

The organization of the report is as follows: The problem formulation is presented in Section II, followed by characterization in Section III. Section IV presents the results and

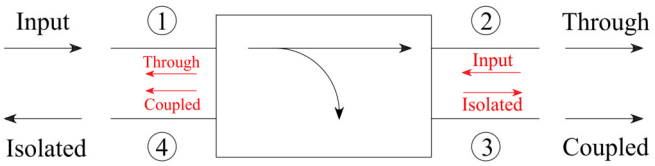


Fig. 1: A commonly used symbol for directional couplers

discussions, and we offer the concluding remarks in Section V.

## II. Problem Formulation

The experiments involved in this study are as follows:

*1)* **Study of Vector Network Analyzer (VNA):** In this experiment we familiarize ourselves with the Agilent E5062A Vector Network Analyzer (Fig. 2) by exploring its various operations and features which include Stimulus (frequency set-up), Average (IF bandwidth), Calibration, Format, Measurement, Marker Settings, Save/Recall etc. We also perform a Open-Short-Load-Thru (OSLT) calibration of the VNA.

*2)* **Characterization of a three port 20 dB Directional Coupler:** The objective of this experiment is to characterize a 20 dB Directional Coupler with the help of VNA. Here, we measure The S-Parameters of the DUT at 2.1 GHz and 1.8 GHz with and without calibration. Therefore, we characterize the insertion loss, return loss, coupling, isolation and directivity of the directional coupler.

**Available Information** : A symbolic representation of a directional coupler is shown in Fig. 1. If we consider the direction coupler as a four port network as shown in Fig. 1, we can define the following quantities [1], [3]:

The coupling factor (C) is given by

$$C = 10\log\frac{P_1}{P_3} = -20\log|S_{13}|dB \tag{1}$$

The Directivity (D) is given by

$$D = 10\log\frac{P_3}{P_4} = -20\log|S_{34}|dB \tag{2}$$

The Isolation (I) is given by

$$I = 10\log\frac{P_1}{P_4} = -20\log|S_{14}|dB \tag{3}$$

The Insertion Loss (L) is given by

$$L = 10\log\frac{P_1}{P_2} = -20\log|S_{12}|dB \tag{4}$$

The coupling factor (C) indicates the fraction of the input power that is coupled to the output port i.e., coupled port. The directivity (D) is a measure of the coupler's ability to isolate forward and backward waves (or the coupled and uncoupled ports). The isolation (I) is a measure of the power delivered to the uncoupled port i.e., isolated port. These quantities are related as

$$I = C + D \tag{5}$$

where I, C and D all are in dB.

However, in our experiment, the port-4 i.e., the isolated port is not accessible and hence the calculation of these quantities is not straightforward. Here, we use the reciprocity property of the directional coupler and port-2 as input port as shown in Fig. 1.

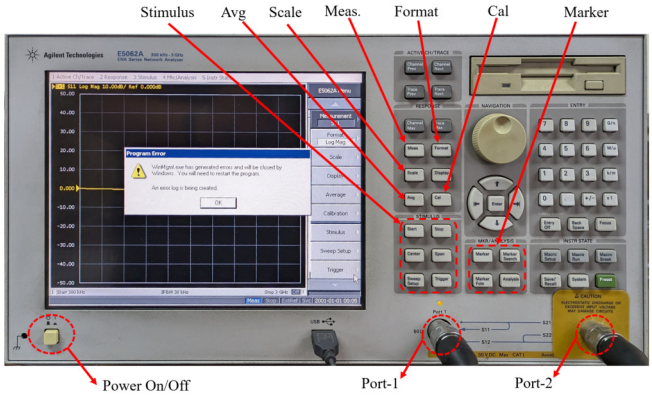


Fig. 2: Agilent E5062A Vector Network Analyzer

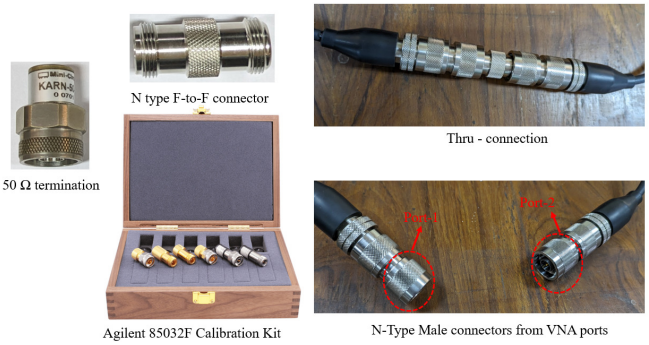


Fig. 3: Accessories used for this experiment

## III. Characterization

The Vector Network Analyzer used in this experiment is **Agilent E5062A** as shown in Fig. 3 which has a frequency range of 300 KHz to 3 GHz. Also, the calibration kit used is **Agilent 85032F** which contains precision 50 ohm type-N standards.

### A. Study of Vector Network Analyzer (VNA)

Fig. 2 shows the Vector Network Analyzer which is under study. In this experiment some of the very important features of a VNA, such as, the Stimulus (start and stop frequencies, span, centre frequency), Response (Measurement, Format, Scale, Display, Average, Calibration), Marker/Analysis, Save/Recall etc. have been explored.

Stimulus: Span helps us to set the frequency range in the VNA display while centre frequency can also be set. Otherwise, the start and stop frequencies are to be set/adjusted. The sweep settings help us to set the sweep type.

Response: In this section there are some of the very important features. The Measurement feature helps us to choose between the S-parameters to be measured ($S_{11}, S_{12}, S_{21}, S_{22}$), while the Format feature helps us in selecting the type of measurement (amplitude, phase, Smith chart etc.). The Average feature helps us to set the IF bandwidth and Scale helps us to set the vertical scale in the VNA display. Calibration is an

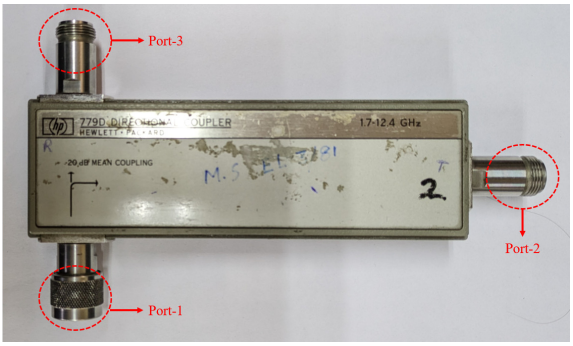


Fig. 4: HP 779D Directional Coupler with 20dB mean coupling

important feature which helps us to calibrate the VNA in 1-port, 2-port configuration. The selection of calibration kit is important while calibrating the VNA. Also, to complete the calibration, it is important to press 'done'.

Marker/Analysis: The marker helps us in reading the data from the display. The navigation tuner helps to move the marker to desired location. Also precise marker position can be set using the numerical entry.

Save/Recall: We can save the calibrated VNA state in its internal memory and recall whenever needed.

We have also performed Open-Short-Load-Thru (OSLT) calibration on the VNA using Agilent 85032F calibration kit. Here we have kept the centre frequency f = 2.1 GHz and span = 1 GHz, IF bandwidth = 30 KHz. We must be careful in connecting the proper connector (in our case female N-type components) to the VNA ports. While the open, short, load (0Ω) help us calibrating the individual ports, thru (as shown in Fig. 3) is essential in calibration of a two port system. The main purpose of calibration is to remove the systematic errors from components up to (and including) the measurement reference plane, which is typically at the end of the VNA measurement cables.

### *B.* Characterization of a three port 20 dB Directional Coupler

In this experiment, we measure the S-Parameters of a 20dB Directional coupler (HP 779D) as shown in Fig. 4, both with and without calibration of the VNA. The port nomenclature are shown in Fig. 4. The settings on the VNA is as follows: centre frequency f = 2.1 GHz and span = 1 GHz, IF bandwidth = 30 KHz. While measuring S-parameters, all the ports which are not in use, must be terminated with a matched load (50Ω). The measurement details at f = 2.1 GHz, is shown in Table. I and at f = 1.8 GHz, is shown in Table. II. The insertion loss is calculated as L = - $S_{21}$ (in dB) while return loss R = - $S_{11}$ (in dB). The Coupling Factor is calculated as C = - $S_{31}$ (in dB). To calculate the isolation, we use port-2 as input port which signifies port-3 to be the isolated port. Hence, isolation is given as I = - $S_{32}$ (in dB). At last the directivity is calculated from 5 as D = I - C (all quantities in dB). The results are tabulated in Table. III and IV.

## IV. Results and Discussion

This experiment is centred around the study of Vector Network Analyzer (SA). Firstly, in exp.A, we have explored various features of the VNA including Stimulus (start and stop frequencies, span, centre frequency), Response (Measurement, Format, Scale, Display, Average, Calibration), Marker/Analysis etc. We have also performed OSLT calibration on the VNA using Agilent 85032 Cal-kit. S-parameters of a directional coupler has been measured using the VNA where we measured the magnitudes in dB as given in Table. I and II. Though the phase of the S-parameters can also be measured easily in the VNA, these are not detailed in the report as they do not play a significant role in the mentioned characterization of the Directional Coupler. The Directional Coupler parameters namely Return Loss (R), Insertion Loss (L), Coupling (C), Isolation (I) and Directivity (D) are tabulated in Table. III and IV at frequencies f = 2.1 GHz and f = 1.8 GHz. We can observe that these parameter values deviate from the desired values in case of measurement with VNA without calibration which introduces error. Thus the measured values with calibrated VNA portray actual characteristics of the Directional Coupler. This brings out the significance of calibration in RF and Microwave measurements.

TABLE I: Measurement results of S-Parameters at f = 2.1 GHz

| S-Par | with cal (dB) | w/o cal (dB) |
|---|---|---|
| $S_{11}$ | -27.75 | -26.44 |
| $S_{21}$ | -0.14 | -1.05 |
| $S_{13}$ | -19.20 | -21.13 |
| $S_{31}$ | -19.20 | -20.98 |
| $S_{23}$ | -49.7 | -53.50 |
| $S_{32}$ | -49.7 | -53.50 |
| $S_{33}$ | -32.45 | -26.66 |

TABLE II: Measurement results of S-Parameters at f = 1.8 GHz

| S-Par | with cal (dB) | w/o cal (dB) |
|---|---|---|
| $S_{11}$ | -36.55 | -23.01 |
| $S_{21}$ | -0.11 | -0.95 |
| $S_{13}$ | -19.80 | -22.85 |
| $S_{31}$ | -19.80 | -22.85 |
| $S_{23}$ | -53.00 | -54.50 |
| $S_{32}$ | -53.00 | -54.50 |
| $S_{33}$ | -24.43 | -26.74 |

TABLE III: Calculated Parameters of Directional Coupler at f = 2.1 GHz

| Parameters | with cal (dB) | w/o cal (dB) |
|---|---|---|
| Return Loss (R) | 27.75 | 26.44 |
| Insertion Loss (L) | 0.14 | 1.05 |
| Coupling (C) | 19.20 | 21.13 |
| Isolation (I) | 49.7 | 53.50 |
| Directivity (D) | 30.50 | -32.37 |

TABLE IV: Calculated Parameters of Directional Coupler at f = 1.8 GHz

| Parameters | with cal (dB) | w/o cal (dB) |
|---|---|---|
| Return Loss (R) | 36.55 | 23.01 |
| Insertion Loss (L) | 0.11 | 0.95 |
| Coupling (C) | 19.80 | 22.85 |
| Isolation (I) | 53.00 | 54.50 |
| Directivity (D) | 33.20 | 31.65 |

## V. Conclusion

In this study, a comprehensive series of experimental investigations was conducted to gain a thorough understanding

of the diverse capabilities offered by the Agilent E5062A Vector Network Analyzer (VNA). The experimental approach began with an exploration of various features of the VNA, followed by an OSLT calibration procedure. Subsequently, a detailed characterization of a 20 dB directional coupler was performed at two distinct frequencies (2.1 GHz and 1.8 GHz). The analysis encompassed the evaluation of key parameters such as Coupling Factor, Directivity, Isolation, and Insertion Loss. Measurements were carried out for both calibrated and uncalibrated VNA setups. The findings from these experiments underscore the critical significance of VNA calibration. It is evident that calibrated measurements exhibit a closer alignment with theoretical predictions, emphasizing the importance of this calibration process in achieving accurate and reliable results.

The Vector Network Analyzer (VNA) holds a central position as an indispensable tool across a wide spectrum of applications within the field of RF and Microwave engineering. Its utility spans from the testing of integrated circuits to broader industrial applications. This experimental endeavor not only provided a solid foundation for proficiently operating the VNA but also deepened our understanding of its intricate functionalities.

## VI. ACKNOWLEDGMENT

Firstly, the author would like to thank his lab-mate Mr. Mayank Anupam for carrying out the experiments together and sharing concepts. The author would also like to acknowledge the efforts of course TAs in conducting the experiments smoothly and finally, Prof. A R Harish for his ever-present guidance and patience to answer all the questions.

## REFERENCES

[1] D. M. Pozar, “Microwave Engineering, 4th ed., Wiley, 2013.”
[2] A. R. Harish, “EE647A:Microwave Measurements and Design Lecture Notes, 2023.”
[3] ——, “EE647A:Microwave Measurements and Design Lab Handouts, 2023.”

# Experiment No. - 2: Measurement of Group Delay and characterization of Amplifier

Debashish Nandi, *Graduate Student Member, IEEE*
*Roll No.21204262*

***Abstract*— This study provides a comprehensive analysis of group delay measurement utilizing a Vector Network Analyzer (VNA) and the subsequent characterization of an amplifier. The utilization of a Vector Network Analyzer (VNA) facilitates the measurement of complex impedance, scattering parameters (S-parameters), and phase information. In this study, we conducted Open-Short-Load-Thru (OSLT) calibration of the Vector Network Analyzer (VNA), examined phase plots and electrical delay characteristics, and subsequently conducted a comprehensive S-parameter evaluation of an amplifier across several frequencies. Additionally, our investigation has focused on utilizing the power sweep capability in the Vector Network Analyzer (VNA) in order to determine the 1 dB compression point of the amplifier. The tests were conducted at the Microwave Measurement Laboratory located within the Electrical Engineering Department of IIT Kanpur.**

***Index Terms*— VNA, OSLT, Calibration, Group Delay, Electrical Delay, 1 dB compression point.**

## I. Introduction

IN the realm of microwave measurements and design [1], [2], the Vector Network Analyzer (VNA) has emerged as an indispensable tool in the field of electrical engineering and high-frequency electronics, enabling researchers and engineers to perform a wide range of intricate measurements and characterizations with precision and accuracy. This versatile instrument has found applications in diverse domains, and in this introduction, we delve into its usability, with a particular focus on its capabilities for group delay measurement of cables, phase plot analysis, and the comprehensive characterization of amplifiers via S-parameters. Additionally, we explore the VNA's power sweep functionality, which helps in determining the critical 1-dB compression point of amplifiers, offering a holistic perspective on its utility in contemporary research and engineering.

The accurate measurement of group delay in cables is paramount in applications ranging from telecommunications to high-speed data transmission. Group delay, a fundamental parameter, quantifies the time delay experienced by different frequency components of a signal as they pass through a cable. It is a critical metric in ensuring signal integrity and minimizing signal distortion, especially in applications where phase coherence is essential. VNAs equipped with time-domain analysis capabilities excel in precisely measuring group delay. By sending a known test signal through the cable under investigation and analyzing the phase response, VNAs can provide a detailed characterization of group delay across a range of frequencies. This capability is invaluable in optimizing cable design and performance, ensuring efficient data transmission, and minimizing signal degradation.

The characterization of amplifiers is crucial in numerous electronic applications, including telecommunications, radar systems, and wireless communication. S-parameters, which describe the relationship between input and output signals of a device, are pivotal in amplifier characterization. VNAs excel in the precise measurement of S-parameters, allowing engineers to assess amplifier performance comprehensively. By conducting S-parameter measurements at various frequencies, VNAs enable the determination of gain, bandwidth, input/output impedance matching, and other key amplifier characteristics. This information is vital for optimizing amplifier design, ensuring efficient signal amplification, and meeting specific performance requirements.

VNAs equipped with power sweep functionality can accurately determine the 1-dB compression point by varying the input power level and monitoring the corresponding output power. This capability allows engineers to assess the amplifier's behavior under different input power conditions, facilitating the design of amplifiers with the desired linearity and dynamic range.

In this Experiment-2 which is comprising of two sub-experiments, we measure group delay of a cable using Vector Network Analyzer by means of phase plots, and characterize an amplifier with S-parameters, 1-dB compression point etc.

The organization of the report is as follows: The problem formulation is presented in Section II, followed by characterization in Section III. Section IV presents the results and discussions, and we offer the concluding remarks in Section V.

## II. Problem Formulation

The experiments involved in this study are as follows:

*1)* **Study of Group Delay of a cable using VNA:** In this experiment, the Open-Short-Load-Thru (OSLT) calibration technique is employed on the Agilent E5062A Vector Network Analyzer (VNA) where we intend to measure the group delay of a cable. The group delay is calculated based on the phase plot of the cable, and its accuracy is afterwards confirmed by introducing electrical delay from the VNA.

*2)* **Study of Amplifier Characteristics using VNA:** The primary aim of this experiment is to conduct a characterization

Debashish Nandi is with the Nanolab, Department of Electrical Engineering, IIT Kanpur, Kanpur 208016, India (e-mail: debashish21@iitk.ac.in)

of the Mini Circuits ZKL-2R7 amplifier using a Vector Network Analyzer (VNA). In this study, the comprehensive S-Parameters of the amplifier are measured at different frequencies, and the 1-dB compression point is determined by utilizing the Power Sweep feature in the Vector Network Analyzer (VNA).

**Theoretical Formulation** : Group delay in a cable is a measure of the time delay experienced by different frequency components of a signal as they propagate through the cable. It quantifies how the cable affects the timing of different frequencies within a signal, indicating the amount of time it takes for each frequency component to traverse the cable.

Let us assume a modulated signal to be $x(t) = m(t)cos(\omega_c t)$ where the envelope of the signal id $m(t) = Acos(\omega_m t)$, $\omega_c$ is the angular frequency of the carrier and $\omega_m$ is the angular frequency of the message signal. m(t) is slowly changing envelope of the modulated signal, i.e., $\omega_m << \omega_c$. If the modulated signal is travelling in a cable (generally a Linear Time-Invariant or LTI system) with a transfer function $H(\omega) = |H(\omega)|e^{j\theta(\omega)}$, then the output signal at the end of the cable can be given by

$$y(t) = \frac{A}{2}|H(\omega)|[cos((\omega_c - \omega_m)t + \theta(\omega_c + \omega_m)) + cos((\omega_c - \omega_m)t + \theta(\omega_c - \omega_m))] \quad (1)$$

Where $\theta(\omega)$ is generally locally linear around $\omega = \omega_c$. Now if we Taylor expand $\theta(\omega+\Delta\omega)$ around $\omega = \omega_c$ where $\Delta\omega << \omega_c$, we get

$$\theta(\omega + \Delta\omega)|_{\omega=\omega_c} \approx \theta(\omega_c) + \frac{1}{2}\Delta\omega\frac{\partial\theta(\omega)}{\partial\omega}|_{\omega=\omega_c} \quad (2)$$

By putting $\Delta\omega = \omega_m$ and $-\omega_m$ and noting the fact that $\omega_m << \omega_c$, if we substitute these in (1), upon simplification, we get,

$$y(t) = A.|H(\omega)|.cos(\omega_c t+\theta(\omega_c)).cos(\omega_m t+\omega_m\frac{\partial\theta(\omega)}{\partial\omega}|_{\omega=\omega_c}) \quad (3)$$

which can be written equivalently as

$$y(t) = A.|H(\omega)|.cos(\omega_c(t - \tau_p)).cos(\omega_m(t - \tau_g)) \quad (4)$$

where $\tau_p = -\frac{\theta(\omega_c)}{\omega_c}$ is known as phase delay and $\tau_g = -\frac{\partial\theta(\omega)}{\partial\omega}|_{\omega=\omega_c}$ is known as group delay [3].

A modern day amplifier is made of transistors which are inherently non-linear devices. Due to this non-linearity the power gain ($\frac{P_{out}}{P_{in}}$) does not remain constant and drops as we increase the input signal level i.e., the small signal assumption doesn't hold anymore. To make a measurable sense of this non-linearity of an amplifier, of many, a metric termed as 1-dB compression is used. The 1-dB gain compression point ($P_{1dB}$) indicates the input power level that causes the gain to drop by 1 dB from its small signal value [4].

## III. Characterization

The Vector Network Analyzer used in this experiment is **Agilent E5062A** as shown in Fig. 1 which has a frequency range of 300 KHz to 3 GHz. Also, the calibration kit used is **Agilent 85033D** which has a frequency range of operation up to 6 GHz. The various load options are shown in Fig. 2

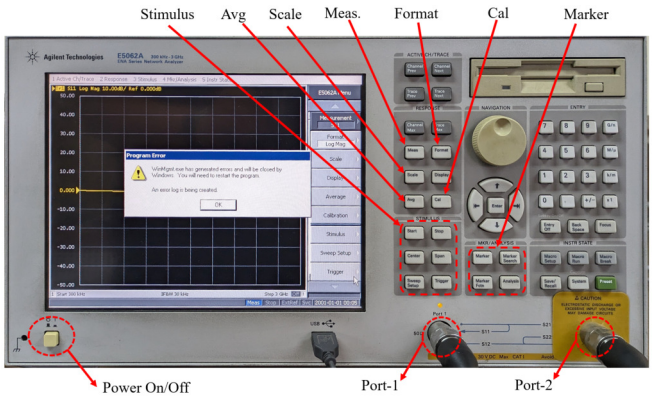


Fig. 1: Agilent E5062A Vector Network Analyzer (VNA)

Fig. 2: Agilent 85033D Calibration Kit loads : Male and Female types (L-R)

### A. Study of Group Delay of a cable using VNA

The experimental setup is shown in Fig. 3. Firstly, the VNA is calibrated using OSLT calibration to fix the reference plane at the end of the VNA probes, as shown in Fig. 3. The VNA was set to a centre frequency of 1.5002 GHz, span of 2.9997 GHz, IF bandwidth of 30 KHz.

An 1m-50Ω SMSM+ cable is connected between the two ports of the VNA. The phase plot is shown in Fig. 4 from which we can calculate the group delay in the cable using the formulation mentioned in Section-II, i.e., $\tau_g = -\frac{\partial\theta(\omega)}{\partial\omega}|_{\omega=\omega_c}$. From the marker locations in Fig. 4, we can observe that $f_1 = 331.91684$ MHz, $\theta_1 = 160^o$ and $f_2 = 524.85754$ MHz, $\theta_1 = -164^o$, hence, $\tau_g = -\frac{\theta_2-\theta_2}{2\pi(f_2-f_1)}$ = 4.664 ns. We have verified this result using the group delay feature of the VNA.

To further investigate the results obtained from the phase plot, we have introduced an electrical delay of $t_d$ = 4.664ns in the VNA and then measured the phase plot which shows no variation of phase with frequency. When an electrical delay is introduced, the reference plane shifts towards the cable as shown in Fig. 3 and by setting $t_d$ = 4.664ns, the entire cable has been taken into consideration. Now, if we set $t_d$ = -4.664 ns, the reference plane shifts towards VNA, and when measured $\tau_g$ from the phase plot, it comes out to be 9.328 ns, which agrees with theoretical prediction.

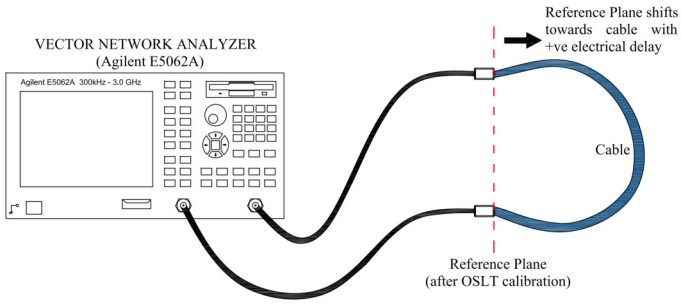


Fig. 3: Experimental setup for measuring group delay of a cable using VNA

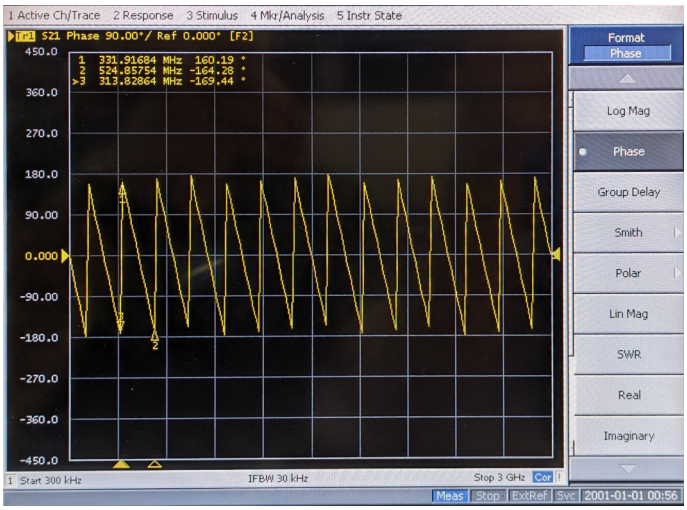


Fig. 4: Phase response of the 50Ω cable

TABLE I: Measurement results of S-Parameters (Magnitudes)

| Frequency | $S_{11}$ (dB) | $S_{12}$ (dB) | $S_{21}$ (dB) | $S_{22}$ (dB) |
|---|---|---|---|---|
| 10 MHz | -16.263 | -48.610 | 13.783 | -12.151 |
| 100 MHz | -31.309 | -39.144 | 23.305 | -19.093 |
| 1 GHz | -17.259 | -39.578 | 22.413 | -14.577 |
| 2 GHz | -12.898 | -40.991 | 22.328 | -32.299 |
| 2.7 GHz | -16.745 | -40.373 | 21.687 | -14.723 |

### *B.* Study of Amplifier Characteristics using VNA

The setup for this experiment is shown in Fig. 5. The VNA is calibrated using OSLT calibration before connecting the amplifier. A sample of the physical connection to the amplifier (Mini Circuits ZKL-2R7) using DC blocks from VNA is shown in Fig. 6. The DC operating point of the amplifier is (11.996V, 0.111A). A complete set of S-parameters are measured between the input (port-1) and the output (port-2) ports of the amplifier using VNA. The measured results are tabulated in Table.I and II. The S-parameter plots are given in Fig.7a to Fig. 9b.

To compute the 1-dB compression point, we have used the power sweep option in the VNA at f = 2.3 GHz. Proper care has been taken considering the RF power handling limit of the VNA and the gain of the amplifier. The input power is swept from -15 dBm to -5dBm. The measurement results of the transfer gain ($S_{21}$) with input power is tabulated at Table.III and the power sweep plot is shown in Fig.9c. The 1-dB compression point is measured as $P_{1dB}$ = -5.3152 dBm from Table.III.

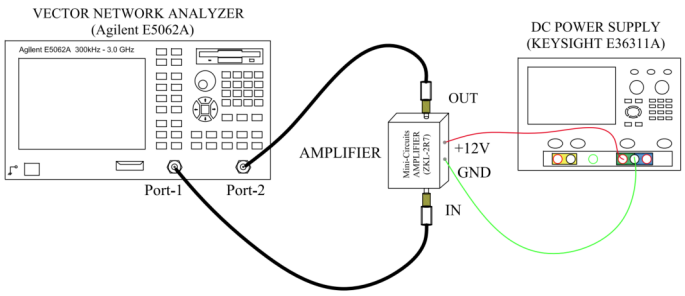


Fig. 5: Experimental setup for characterizing an amplifier


Fig. 6: Amplifier connection using DC-Block

TABLE II: Measurement results of S-Parameters (Phase angle)

| Frequency | $S_{11}$ ($^o$) | $S_{12}$ ($^o$) | $S_{21}$ ($^o$) | $S_{22}$ ($^o$) |
|---|---|---|---|---|
| 10 MHz | -50.101 | -56.698 | -46.537 | -117.64 |
| 100 MHz | -12.298 | -22.779 | -28.315 | 160.40 |
| 1 GHz | 119.86 | 131.73 | 81.577 | -11.578 |
| 2 GHz | -140.42 | -100.20 | 168.31 | 160.92 |
| 2.7 GHz | 62.847 | 98.972 | -33.220 | 121.89 |

TABLE III: Measurement results of $S_{21}$ vs $P_{in}$ at f=2.3GHz

| $P_{in}$ | $S_{21}$ (dB) |
|---|---|
| -14.968 | 23.1 |
| -14.668 | 23.1 |
| -11.667 | 23.0 |
| -10.300 | 23.0 |
| -5.3152 | 22.1 |

## IV. Results and Discussion

The focus of this experiment revolves around the quantification of group delay in a cable and the characterization of an amplifier utilizing a Vector Network Analyzer (SA) [5]. Firstly, in exp.A, we have performed OSLT calibration to fix the reference plane at the end of probes connected to the VNA. Thereafter, from the phase plot obtained in VNA when a cable is connected between the two ports of the VNA, we have calculated the group delay of the cable which has come out to be $\tau_g$ = 4.664 ns. This was verified by introducing electrical delay of 4.664 ns and hence obtaining the phase plot where we observed that the phase is constant with frequency. This verifies the fact that the group delay of the subject cable is indeed 4.664 ns. It is understood that as we introduce an electrical delay in the VNA which is equivalent to that of the cable, the reference plane is re-adjusted such a way that it takes into account the cable length also. To further investigate this, we have introduced an electrical delay of -4.664 ns in the VNA and obtained the phase plot. From the obtained phase plot, we recomputed the group delay to be 9.328 ns, which clearly indicates that due to a negative electrical delay introduced in VNA, the reference plane is shifted from the VNA probe end towards VNA, thus increasing the effective cable length.

In exp.B, the completer S-parameters of an amplifier have been measured at different frequencies using the calibrated

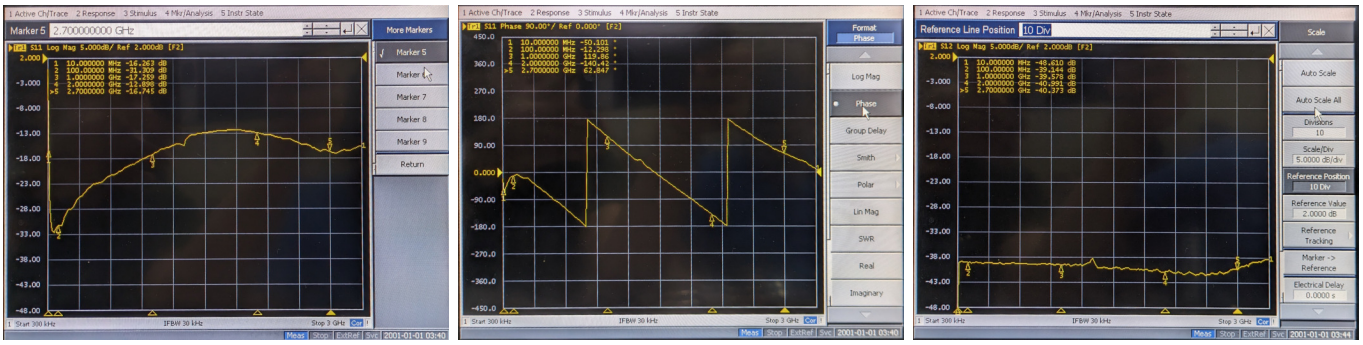

(a) (b) (c)

Fig. 7: (a) Magnitude Plot of $S_{11}$, (b) Phase Plot of $S_{11}$, (c) Magnitude Plot of $S_{12}$

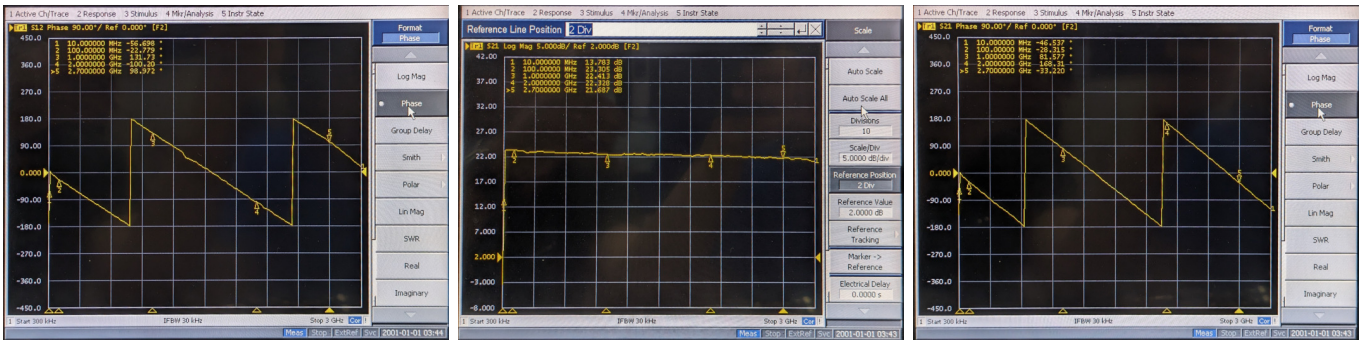

(a) (b) (c)

Fig. 8: (a) Phase Plot of $S_{12}$, (b) Magnitude Plot of $S_{21}$, (c) Phase Plot of $S_{21}$

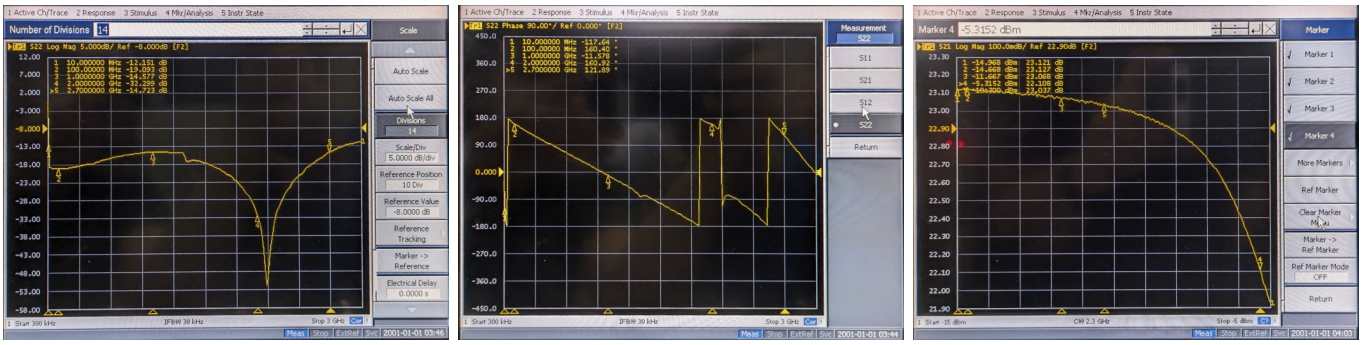

(a) (b) (c)

Fig. 9: (a) Magnitude Plot of $S_{22}$, (b) Phase Plot of $S_{22}$, (c) $S_{21}$ vs. $P_{in}$ at f = 2.3 GHz

VNA. To calibrate the VNA, OSLT calibration has been performed. From the $S_{11}$ magnitude plot, we can infer that the input side (port-1) matching is good as it lies below -10 dB for the entire operating frequency range. $S_{21}$ is reasonably flat at all the frequency range of operation which is around 21 to 23 dB which implies the gain of the amplifier. Also, from the $S_{21}$ vs. input power plot, we have calculated the 1-dB compression point which is around $P_{1dB}$ = -5.3152 dBm. It is worthwhile to note that an accurate power sweep setting is important considering the power handing limit of the VNA.

## V. Conclusion

In this study, a comprehensive series of experimental investigations was conducted to gain a thorough understanding of the group delay measurement of a cable and the S-parameter characterization of an amplifier which gives us numerous insight including input/output matching, gain, bandwidth, 1-dB compression point etc. During the course of this experiment, we encountered a need to re-calibrate the Vector Network Analyzer (VNA) at one point in our study. This necessity arose when we observed a positive value for the $S_{11}$ parameter. Upon further investigation, we identified the root cause of this issue: a faulty female-type $50\Omega$ matched load in the calibration kit used during that particular calibration. To rectify this, we re-calibrated the VNA using male-type loads from the Agilent 85033D Calibration kit. We took meticulous care in selecting the exact reference planes, particularly when dealing with male-to-female converters. This re-calibration process underscored the significance of properly calibrating the VNA before conducting measurements and significantly enhanced our understanding of its operation.

The Vector Network Analyzer (VNA) holds a central and

indispensable role across a broad spectrum of applications within the RF and Microwave engineering field. Its utility extends from testing integrated circuits to a wide range of industrial applications. This research effort has deepened our understanding of the intricate functionalities of the VNA, providing valuable insights that benefit various applications in this field.

## VI. ACKNOWLEDGMENT

Firstly, the author would like to thank his lab-mate Mr. Mayank Anupam for carrying out the experiments together and sharing concepts. The author would also like to acknowledge the efforts of course TAs in conducting the experiments smoothly and finally, Prof. A R Harish for his ever-present guidance and patience to answer all the questions.

## REFERENCES

[1] D. M. Pozar, “Microwave Engineering, 4th ed., Wiley, 2013.”
[2] A. R. Harish, “EE647A:Microwave Measurements and Design Lecture Notes, 2023.”
[3] B. P. Lathi, “Modern Digital And Analog Communication Systems 4th ed., Oxford, 2017.”
[4] B. Razavi, “RF Microelectronics 2nd ed., Prentice Hall, 2011.”
[5] A. R. Harish, “EE647A:Microwave Measurements and Design Lab Handouts, 2023.”

# Experiment No. - 3
# Determination of 1-dB Compression Point and Third Order Intercept (TOI) of a given Amplifier using Spectrum Analyzer

Debashish Nandi, *Graduate Student Member, IEEE*
*Roll No.21204262*

***Abstract*— This study provides a comprehensive analysis of the non-linearity characteristics of a wide-band amplifier, focusing on key performance metrics including the 1-dB compression point, gain flatness, and Third Order Intercept (TOI). The investigation leveraged a Spectrum Analyzer (SA) as an indispensable instrument for scrutinizing and visually representing signal frequency components, underpinning its significance in diverse fields such as integrated circuits testing, telecommunications, audio engineering, and RF testing. Furthermore, the report offers an in-depth examination of various sources of non-linearities. The experimental assessments were conducted at the Microwave Measurement Laboratory, situated within the Electrical Engineering Department of the Indian Institute of Technology Kanpur.**

***Index Terms*— Spectrum Analyzer, 1-dB compression point, TOI, harmonics, non-linearity.**

## I. Introduction

The realm of microwave measurements and design [1], [2] is a critical domain in modern electronics, as it plays an indispensable role in the development and optimization of wireless communication systems, radar technology, satellite communication, and various other applications requiring the transmission and reception of electromagnetic signals within the microwave frequency spectrum. Accurate characterization of microwave components and circuits is paramount to ensure their efficient performance and to mitigate the deleterious effects of non-linearities and other imperfections. In this context, the utilization of a Spectrum Analyzer emerges as an invaluable tool that not only facilitates the visualization and analysis of signal spectra but also provides insights into the intricate behavior of microwave devices.

A Spectrum Analyzer (SA) is an essential instrument in the field of microwave measurements and design. Its primary function is to display the amplitude versus frequency characteristics of an input signal, allowing engineers and researchers to observe and analyze the spectral components of signals in the microwave and radio frequency (RF) bands. This ability to visualize the frequency domain representation of signals makes it a cornerstone in the characterization and troubleshooting of microwave circuits and components. One of the pivotal applications of spectrum analyzers in microwave measurements is the characterization of amplifiers. Amplifiers play a crucial role in amplifying signals across a broad range of frequencies, making them indispensable in modern communication systems. Several key parameters are vital in assessing the performance of these amplifiers, including the 1 dB compression point ($P_{1dB}$), gain flatness, and third-order intercept ($IIP_3$, $OIP_3$) [3].

The $P_{1dB}$ is a critical metric that defines the input power level at which an amplifier's output power deviates by 1 dB from its linear behavior. This parameter serves as an important figure-of-merit (FOM) for assessing the amplifier's dynamic range and linearity. In applications demanding a consistent amplification level across a wide bandwidth, gain flatness becomes paramount. This metric gauges the amplifier's ability to maintain a uniform gain response over the specified frequency range. Third-order-intercepts, i.e., $IIP_3$ and $OIP_3$ parameters unveil the amplifier's non-linear tendencies by pinpointing the juncture at which third-order intermodulation products ($IM_3$) arise. Understanding these non-linearities is vital in applications where interference and distortion can be detrimental.

Microwave measurements, while empowered by Spectrum Analyzers, must also contend with non-linearities originating from various sources within the measurement ecosystem. A comprehensive understanding and mitigation of these non-linearities are pivotal to ensure accuracy and reliability in microwave characterizations. Active microwave components, such as amplifiers, are susceptible to nonlinear behaviors under specific operating conditions. Factors such as gain compression, intermodulation distortion, and harmonic generation can significantly impact measurement accuracy. Spectrum Analyzers, despite their precision, are not immune to non-linearities. Spurious responses, phase noise, and limited dynamic range can introduce inaccuracies into measurements. The signal generator, often employed as a stimulus source in microwave measurements, can introduce non-linearities of its own. These may manifest as phase noise, harmonic distortion, or amplitude variations, which need to be considered during measurements.

In this Experiment-3 which is comprising of three sub-

Debashish Nandi is with the Nanolab, Department of Electrical Engineering, IIT Kanpur, Kanpur 208016, India (e-mail: debashish21@iitk.ac.in)

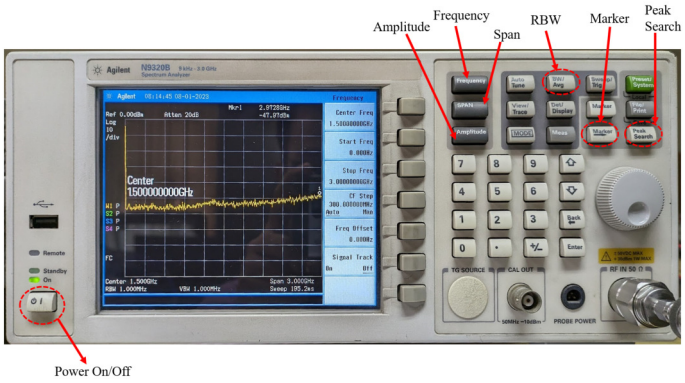


Fig. 1: Agilent N9320B Spectrum Analyzer

experiments, we characterize 1-dB compression point, gain flatness, third-order-intercept of an amplifier, using a spectrum analyzer.

The organization of the report is as follows: The problem formulation is presented in Section II, followed by characterization in Section III. Section IV presents the results and discussions, and we offer the concluding remarks in Section V.

## II. Problem Formulation

The experiments [4] involved in this study are as follows:

*1)* **Study of 1-dB compression point and harmonics of an amplifier:** The principal objective of this experiment is to ascertain the 1-dB compression point ($P_{1dB}$) of the Mini-Circuits ZKL-2R7 amplifier, accomplished through the utilization of a Spectrum Analyzer (SA). Moreover, we endeavor to quantify the power levels of harmonics generated by the inherently non-linear amplifier, specifically for a designated input power level.

*2)* **Study of gain flatness of an amplifier:** This phase of the experiment is dedicated to visualizing the gain flatness characteristics of the Mini-Circuits ZKL-2R7 amplifier. Gain flatness analysis involves creating a plot that depicts the measured gain of the amplifier across a spectrum of frequencies.

*3)* **Study of Third-order-intercept (TOI) of an amplifier:** In this experiment, we aim to thoroughly characterize the Mini-Circuits ZKL-2R7 amplifier through the assessment of its third-order intercept points ($IIP_3$, $OIP_3$) with the aid of a spectrum analyzer. Careful consideration has been given to ensure that the intermodulation products are solely generated by the amplifier itself, rather than the spectrum analyzer, achieved by judiciously adjusting the input power level.

**Theoretical Formulation** : A modern day amplifier is made of transistors which are inherently non-linear devices. Due to this non-linearity the power gain ($\frac{P_{out}}{P_{in}}$) does not remain constant and drops as we increase the input signal level i.e., the small signal assumption doesn't hold anymore. To make a measurable sense of this non-linearity of an amplifier, of many, a metric termed as 1-dB compression is used. The 1-dB gain compression point ($P_{1dB}$) indicates the input power level that causes the gain to drop by 1 dB from its small signal value [3].

Another important measure of non-linearity is third-order intercept (TOI). If two interferers at $f_1$ and $f_2$ are applied to a nonlinear system, the output generally exhibits components which are not harmonics of these frequencies. Called "intermodulation" (IM), this phenomenon arises from "mixing" (multiplication) of the two components as their sum may raise to a power greater than unity. These IM products may very well be adjacent to the signal frequency. Suppose an antenna receives a small desired signal at $f_0 = 2.41GHz$ along with two large interferers at $f_1 = 2.42GHz$ and $f_2 = 2.43GHz$, providing this combination to an amplifier, the third IM product $2f_1 - f_2$ = 2.41 GHz falls exactly at the desired signal frequency, thus corrupting the signal. For modern day narrow-band GHz range operations, the harmonics lie much beyond the range of the band-pass filter used at the output, thus, might give an impression that the system is linear, which may not be the actual case. Hence, IM characterization is of immense importance along with other figure of merits. A common method of IM characterization is the "two-tone" test [3], which is detailed in section-III.

## III. Characterization

The general characterization set-up used in this experiment, is shown in Fig.2a. The spectrum analyzer used in this experiment is Agilent N9320B and the wide-band amplifier under test is Mini-Circuits ZKL-2R7 [5].

### A. Study of 1-dB compression point and harmonics of an amplifier

The setup for this experiment is shown in Fig. 2a. The DC operating point of the amplifier is (12.0V, 0.108A). A 20-dB attenuator has been used between the Spectrum Analyzer (SA) and amplifier output. The signal frequency has been set to $f_1$ = 900 MHz. The input signal power ($P_{in}$) is varied from -18 dBm to +13 dBm and the measured power ($P_{out,mes}$) at fundamental ($f_1$) from the SA, is tabulated in Table.I. However, to cater for the 20-dB attenuation, actual power at the amplifier output is calculated as $P_{out,act}$ dBm = ($P_{out,mes}$ + 20) dBm. The plot of $P_{out,mes}$ vs. $P_{in}$ is shown in Fig.3. From this, the calculated 1-dB gain compression point is $P_{1dB}$ = -5.56 dBm.

We have also measured the powers in harmonics ($2f_1 = 1.8$ GHz, $3f_1 = 2.7$ GHz), produced by the amplifier (generally) and the measured results are tabulated in Table.II. The input power ($P_{in}$) is also varied from -20 dBm to -17 dBm, and power components in harmonics are observed as shown in Fig.4. It is observed that the second harmonic power level is erroneous. Further investigation has been carried out and is detailed in Section-IV.

### B. Study of gain flatness of an amplifier

The setup for this experiment is same as shown in Fig. 2a. The input power ($P_{in}$) is set to -20 dBm and the signal frequency (f) is swept from 700 MHz to 990 MHz and the output power is measured. The actual output power ($P_{out,act}$) is calculated same as mentioned in previous experiment. The

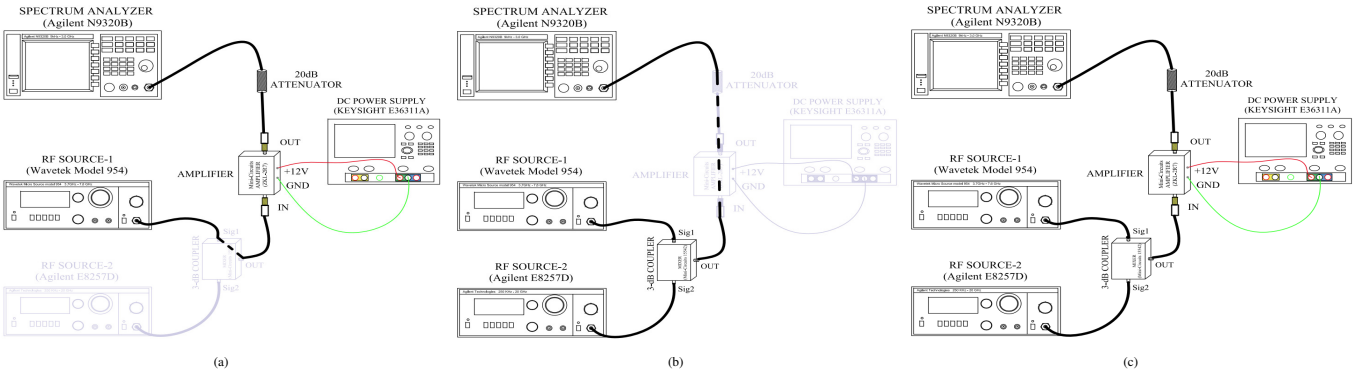


Fig. 2: Measurement set-up for (a) measuring $P_{1dB}$, (b) measuring $P_{in}$ at which no intermodulation product is generated by the SA, (c) measuring TOI of the amplifier

TABLE I: Measurement results of $P_{in}$ sweep for characterizing $P_{1dB}$

| $\mathbf{P_{in}}$ (dBm) | $\mathbf{P_{out,mes}}$ (dBm) | $\mathbf{P_{out,act}}$ (dBm) |
|---|---|---|
| -18 | -17.53 | 2.47 |
| -16 | -15.60 | 4.40 |
| -14 | -13.64 | 6.36 |
| -12 | -11.60 | 8.40 |
| -10 | -9.62 | 10.38 |
| -9 | -8.80 | 11.20 |
| -8 | -7.88 | 12.12 |
| -7 | -7.15 | 12.95 |
| -6 | -6.65 | 13.35 |
| -5.5 | -6.48 | 13.52 |
| -5 | -6.32 | 13.68 |
| -4.5 | -6.14 | 13.86 |
| -4 | -6.08 | 13.92 |
| -2 | -5.73 | 14.27 |
| 0 | -5.55 | 14.45 |
| 2 | -5.57 | 14.43 |
| 4 | -5.70 | 14.30 |
| 8 | -5.61 | 14.39 |
| 13 | -5.28 | 14.72 |

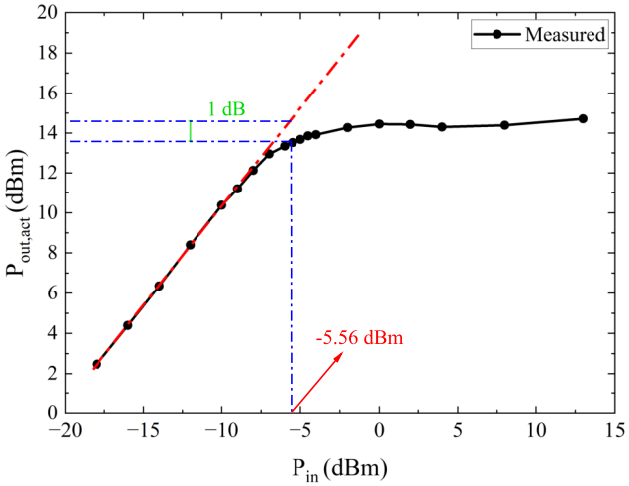


Fig. 3: Output power vs input power to calculate $P_{1dB}$

TABLE II: Measurement results of powers in harmonics (in dBm)

| $\mathbf{P_{in}}$ | $\mathbf{P_{1,mes}}$ | $\mathbf{P_{2,mes}}$ | $\mathbf{P_{3,mes}}$ | $\mathbf{P_{1,act}}$ | $\mathbf{P_{2,act}}$ | $\mathbf{P_{3,act}}$ |
|---|---|---|---|---|---|---|
| -20 | -19.50 | -67.00 | -79.51 | 0.50 | -47.00 | -59.51 |
| -17 | -16.50 | -66.70 | -72.06 | 3.50 | -46.70 | -52.06 |

gain of the amplifier is computed as A = $\frac{P_{out,act}}{P_{in}}$ and tabulated in Table.III. The gain (A) vs freq (f) plot is shown in Fig.5,

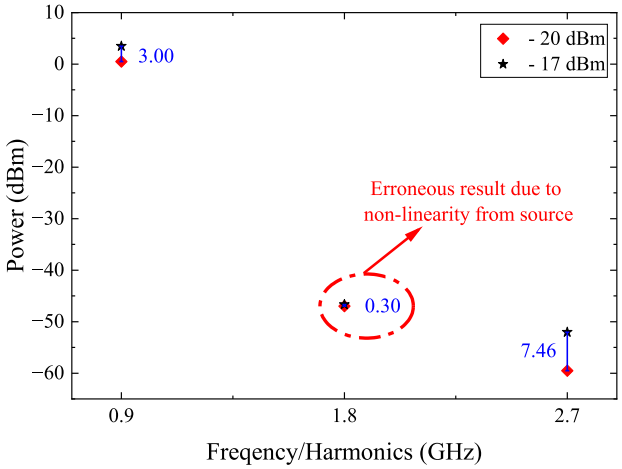


Fig. 4: Powers in fundamental (0.9 GHz) and harmonics (1.8, 2.7 GHz)

TABLE III: Measurement results of Gain Flatness, $P_{in}$ = -20 dBm

| f (MHz) | $\mathbf{P_{out,mes}}$ (dBm) | $\mathbf{P_{out,act}}$ (dBm) | A (dB) |
|---|---|---|---|
| 700 | -18.80 | 1.20 | 21.20 |
| 725 | -18.80 | 1.20 | 21.20 |
| 750 | -19.00 | 1.00 | 21.00 |
| 775 | -19.15 | 0.85 | 20.85 |
| 800 | -19.80 | 0.20 | 20.20 |
| 825 | -19.08 | 0.92 | 20.92 |
| 850 | -19.15 | 0.85 | 20.85 |
| 875 | -19.30 | 0.70 | 20.70 |
| 900 | -19.50 | 0.50 | 20.50 |
| 950 | -19.42 | 0.58 | 20.58 |
| 975 | -19.37 | 0.63 | 20.63 |
| 990 | -19.43 | 0.57 | 20.57 |

which shows that the gain is fairly flat over the mentioned frequency range.

### C. Study of Third-order-intercept (TOI) of an amplifier

The setup for the first part of this experiment is shown in Fig. 2b. Two tones at frequencies $f_1 = 2.1GHz$ and $f_2 = 2.2GHz$ are applied from two RF sources. These signals are then combined using a 3-dB coupler as shown in Fig.2b and then the output of the 'SUM' port is connected to the Spectrum Analyzer (SA). The $f_1$ and $f_2$ are chosen keeping in mind a) the operating range of Microlab/FXR CA-65N 3-dB coupler which is 2.0 - 4.0 GHz and b) the range of the Spectrum Analyzer which is 9 KHz - 3 GHz. Now, by varying

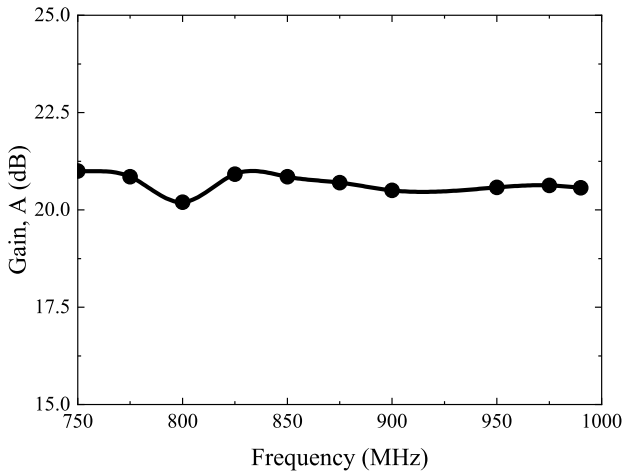


Fig. 5: Amplifier Power Gain vs. Frequency

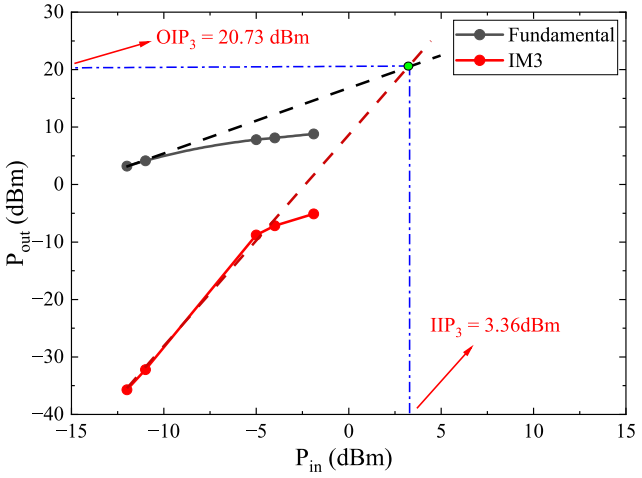


Fig. 6: Output Power components of fundamental and IM3 vs input power, $IIP_3$ and $OIP_3$

TABLE IV: Measurement results of Third-Order-Intercept

| $\mathbf{P_{in}}$ | $\mathbf{P_{1,m}}$ | $\mathbf{P_{IM3L,m}}$ | $\mathbf{P_{IM3R,m}}$ | $\mathbf{P_{IM3L,a}}$ | $\mathbf{P_{IM3R,a}}$ |
|---|---|---|---|---|---|
| -12.00 | -16.78 | -56.75 | -55.71 | -36.75 | -35.71 |
| -11.00 | -15.85 | -52.17 | -52.19 | -32.17 | -32.19 |
| -6.00 | -12.55 | -30.85 | -30.55 | -10.85 | -10.55 |
| -5.00 | -12.20 | -29.05 | -28.78 | -9.05 | -8.78 |
| -4.00 | -11.87 | -27.48 | -27.18 | -7.48 | -7.18 |
| -1.90 | -11.20 | -25.45 | -25.09 | -5.45 | -5.09 |

input power levels of the interferer tones and the attenuation level in the SA, we have observed that below 0 dBm input power, there is no intermodulation products generated by the Spectrum Analyzer. This has been verified by varying the attenuation in SA and finally it has been set to 20 dB.

The setup for the final part of this experiment, where characterize the TOI of the amplifier, is shown in Fig. 2c. The input power ($P_{in}$) is varied from -12 dBm to -1.9 dBm (which is less than 0 dBm, thus ensuring IM3 components are produced by the amplifier only), and the measured output power at fundamental ($P_{1,m}$), IM3 products, i.e, at $2f_1 - f_2$ = 2.0 GHz : $P_{IM3L,m}$ and at $2f_2 - f_1$ = 2.3 GHz : $P_{IM3R,m}$ are tabulated in Table.IV. The actual powers are calculated by adding 20 dB (due to the attenuator) to the measured powers. The output powers ($P_{out}$) at fundamentals and $IM_3$ are plotted with respect to input power ($P_{in}$) in Fig.6. The graphically-calculated third-order-intercepts are $IIP_3$ = 3.36 dBm and $OIP_3$ = 20.73 dBm. The extrapolation range of the output powers at fundamental and IM3 are chosen much below the values corresponding to $P_{1dB}$.

## IV. Results and Discussion

The focus of this experiment revolves around the determination of various figure of merits of an amplifier. The exp.A was focused on determining the 1-dB gain compression point which has come out to be $P_{1dB}$ = -5.56 dBm. The powers in the harmonics are shown in Fig.4. During the measurement it was found that the harmonic powers are not following the desired proportionality, even when input power level is much below $P_{1dB}$. This led us to investigate other sources of non-linearities such as spectrum analyzer and signal generator, which may produce harmonics through their internal non-linear components. By changing the attenuation level of the attenuator present at the input of SA and it was observed that irrespective of the attenuation level, the power levels at fundamental and harmonics remain same. This indicates that the non-linearity is attributed to the signal generator itself. A way to mitigate this issue is to reduce the input signal power level which is being generated by the Signal generator. However, we observed that at $P_{in} = -20dBm$, the second harmonic power level does not settle to expected value while power levels at fundamental and third harmonic show desired proportionality with change in input power. This may be attributed to some issue with the signal generator which remain unknown and needs further investigation.

In exp.B, the gain flatness of the amplifier is characterized as shown in Fig.5. It can be observed that the gain of the amplifier is around 20 - 21 dB.

The focus of the exp.C was to measure and characterize the TOI of the amplifier by means of Two-Tone test. Initially, it was ensured that the IM products are generated by the amplifier only and not by the Spectrum Analyzer, by properly setting the input power of the interferer tones and attenuation level of the SA. The measured TOIs of the amplifier has been found out to be $IIP_3$ = 3.36 dBm and $OIP_3$ = 20.73 dBm. These results agree with the theoretical prediction, i.e., $IIP_3$ - $P_{1dB}$ = 8.92 dB (close to 9.6 dB [3]).

## V. Conclusion

In this study, a comprehensive series of experimental investigations was conducted to gain a thorough understanding of the 1-dB compression point, gain flatness of an amplifier using Spectrum Analyzer. The power levels in the harmonics created by the amplifier which is the manifestation of its inherent non-linearity has also been analyzed. During the measurement it was found that the harmonic powers are not following the desired proportionality, which upon further investigation led to the conclusion that of the presence of other non-linearity in the measurement set-up, i.e., signal generator. We have explored various Detect Schemes in the Spectrum Analyzer display, i.e., Auto, positive peak, negative peak, average etc. Third order intercept of the subject amplifier has also been

studied and validated with theoretical prediction. Proper care has been taken to ensure that the intermodulation products are generated by the amplifier only and not by the Spectrum Analyzer.

The Spectrum Analyzer (SA) holds a central and indispensable role across a broad spectrum of applications within the RF and Microwave engineering field and this fact is further strengthened by our exploration in this experiment. This study has deepened our understanding of the intricate functionalities of the SA, amplifier non-linearities, providing valuable insights that benefit various applications in this field.

## VI. ACKNOWLEDGMENT

Firstly, the author would like to thank his lab-mate Mr. Mayank Anupam for carrying out the experiments together and sharing concepts. The author would also like to acknowledge the efforts of course TAs in conducting the experiments smoothly and finally, Prof. A R Harish for his ever-present guidance and patience to answer all the questions.

## REFERENCES

[1] D. M. Pozar, "Microwave Engineering, 4th ed., Wiley, 2013."
[2] A. R. Harish, "EE647A:Microwave Measurements and Design Lecture Notes, 2023."
[3] B. Razavi, "RF Microelectronics 2nd ed., Prentice Hall, 2011."
[4] A. R. Harish, "EE647A:Microwave Measurements and Design Lab Handouts, 2023."
[5] Mini-Circuits, "Coaxial Amplifier ZKL-2R7+ Technical Manual."

# Experiment No. - 4
# Familiarization with Noise Figure Meter and Noise Figure Analyzer

Debashish Nandi, *Graduate Student Member, IEEE*
*Roll No.21204262*

***Abstract*— This study presents a thorough examination of the Noise Figure Meter and Noise Figure Analyzer, with the primary objective of gaining a comprehensive understanding of these devices and their intricate functionalities. The analysis encompasses various key aspects, including the calibration of the Noise Figure Meter using a standard Noise source within a specified frequency range. Furthermore, it involves the measurement of Noise Figures for a diverse range of Devices Under Test (DUTs), such as IF amplifiers, mixers, attenuators, and various combinations thereof. To validate our findings, we have applied the renowned Friis formula to calculate the Noise Figure of cascaded systems, supported by multiple illustrative examples. The experimental assessments were conducted at the Microwave Measurement Laboratory, situated within the Electrical Engineering Department of the Indian Institute of Technology Kanpur.**

***Index Terms*— Noise Figure, insertion gain, NF meter, NF Analyzer, Friis Formula, Noise source.**

## I. Introduction

IN the ever-evolving field of microwave engineering [1], the demand for efficient and high-performance devices has been growing exponentially. Microwave circuits and components, such as amplifiers, mixers, and attenuators, play a pivotal role in various applications including wireless communication, radar systems, and satellite communication. One of the critical factors influencing the performance of these devices is the presence of noise. Noise, in the context of microwave devices, refers to any unwanted, random electrical signals that can degrade the quality of the desired output signal. To ensure optimal performance, it is essential to understand and quantify the noise characteristics of these devices accurately. This is where Noise Figure (NF) meters and Noise Figure analyzers become indispensable tools. A Noise Figure meter, often referred to as a Noise Figure analyzer or Noise Figure measurement system, is a sophisticated instrument designed for the precise measurement of noise characteristics in microwave devices. It provides a quantitative assessment of the impact of noise on the signal quality, making it an essential tool in the field of microwave measurements and design. A Noise Figure analyzer goes beyond basic noise measurements by providing a comprehensive analysis of noise sources and their contributions in a given device or circuit. It measures the Noise Figure and Noise Temperature, which are essential parameters for understanding the noise behavior of a component. The Noise Figure is a measure of how much additional noise a device adds to the input signal, expressed in decibels (dB), while Noise Temperature is a measure of the equivalent temperature that would produce the observed noise power. Together, these parameters enable engineers and researchers to identify and mitigate noise-related issues effectively.

In amplifiers, which are used to boost weak signals, minimizing noise is paramount. Noise Figure analysis helps in selecting amplifiers with low noise characteristics, ensuring that the amplified signal remains of high quality. Mixers are essential for frequency conversion in various applications, including heterodyne receivers. Noise Figure measurements are crucial to ensure that mixers do not introduce excessive noise during the signal conversion process. Attenuators are used to reduce signal power, and in some cases, they can introduce noise. Noise Figure analysis helps in selecting attenuators that minimize additional noise while providing the desired signal attenuation.

Noise Figure meters and analyzers are indispensable tools in microwave engineering, enabling precise measurement and analysis of noise characteristics in devices and circuits. Their importance extends to various applications, including amplifiers, mixers, and attenuators, where optimal noise performance is critical for achieving superior system performance. These instruments empower engineers and researchers to design and optimize microwave devices that meet the ever-increasing demands of modern communication and technology. In this Experiment-4 which is comprising of two sub-experiments, we get ourselves familiarized with the Noise Figure Meter and Analyzer by means of calibration, measuring Noise Figures of various DUTs, such as IF amplifier, Attenuator, Mixer and cascade combinations of these. We also verify the famous Friis Equation for calculation of Noise Figures of a cascaded systems.

The organization of the report is as follows: The problem formulation is presented in Section II, followed by characterization in Section III. Section IV presents the results and discussions, and we offer the concluding remarks in Section V.

## II. Problem Formulation

The experiments [2] involved in this study are as follows:

Debashish Nandi is with the Nanolab, Department of Electrical Engineering, IIT Kanpur, Kanpur 208016, India (e-mail: debashish21@iitk.ac.in)

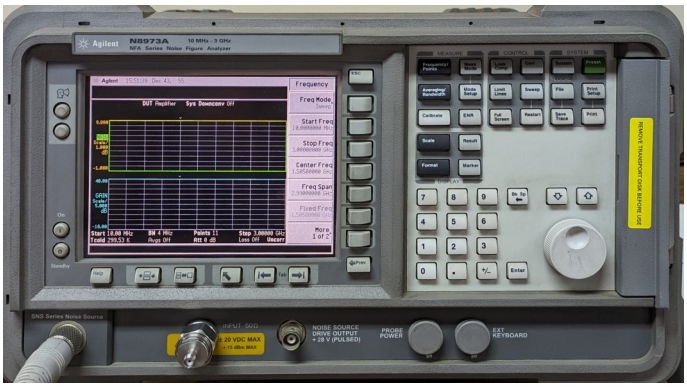


Fig. 1: Agilent N8973A Noise Figure Analyzer

*1)* **Study of Noise Figure (NF) Meter and NF measurement:** The primary aim of this experiment is to acquaint ourselves with the Noise Figure Meter and Analyzer. This entails a comprehensive process, commencing with the calibration of the NF meter across a specific frequency range. Subsequently, we engage in the meticulous measurement of Noise Figures (NF) for distinct components, including an IF amplifier, an attenuator, and their combined configuration. Additionally, we undertake the verification of the Friis equation in the context of Noise Figure calculations for cascaded systems.

*2)* **Study of Noise Figure and insertion gain of a mixer:** This experimental phase is dedicated to the precise measurement of the Noise Figure (NF) and insertion gain for the Anaren Model-74129 Double Balanced Mixer.

**Theoretical Formulation** : The Noise Figure (NF) of a system is given by [3]

$$NF = \frac{SNR_{in}}{SNR_{out}} \tag{1}$$

where $SNR_{in}$ is the signal-to-noise ratio at the input of a system or Device-Under-Test (DUT) and $SNR_{out}$ is the signal-to-noise ratio at the output.

For cascaded stages, the overall Noise Figure of the system is given by

$$NF_{tot} = 1 + (NF_1 - 1) + \frac{NF_2 - 1}{A_{P1}} + ... + \frac{NF_m - 1}{A_{P1}...A_{P(m-1)}} \tag{2}$$

where $NF_i$ is the Noise Figure for the $i^{th}$ stage and $A_{Pi}$ is the power gain of the $i^{th}$ stage.

## III. Characterization

The general characterization set-up used in this experiment, is shown in Fig.2a. The components used in this experiment are a) Noise Figure Analyzer (Agilent N8973A), b) Noise Source (Agilent N4000A), c) IF amplifier (HP 3743A), d) 6-dB attenuator (HP 8491A) and e) Double Balanced Mixer (ANAREN 74129 [4]).

### A. Study of Noise Figure (NF) Meter and NF measurement

The first part of the experiment is to calibrate the Noise Figure meter with a known noise source. The setup for this part is shown in Fig. 2a and the measurement result is given in Fig. 3a. The measured NF and gain is around 0 dB which confirms that the NF meter is calibrated. The frequency range is chosen keeping in mind the operating range of the IF amplifier.

TABLE I: Summarized Results for NF and gain measurement

| S. No. | Connection | NF (dB) | Gain (dB) |
|---|---|---|---|
| 1 | Calibrated | 0 | 0 |
| 2 | IF Amplifier (IFA) | 6.9 | 29.5 |
| 3 | Attenuator | 6.0 | -6.0 |
| 4 | Attenuator + IFA | 13.0 | 23.5 |
| 5 | IFA + Attenuator | 6.9 | 23.5 |
| 6 | Mixer | 3-4 | -3.0 |

In this part, the NF is measured for an IF amplifier and an attenuator individually. The measurement set-ups are shown in Fig.2b and 2c respectively. The measurement result is furnished in Fig.3b and 3c. The NF of the IF amplifier is measured as approx. 6.9 dB and the gain as approx. 29.5 dB. The NF of the attenuator is measured as approx. 6.0 dB and the gain as approx. -6.0 dB.

Now a series connection of the attenuator followed by the IF amplifier is made as shown in Fig.4a and the $NF_{tot}$ is measured as approx. 13.0 dB as given in Fig.5a. When the series connection is reversed, i.e., the IF amplifier followed by the attenuator as shown in Fig.4b, the $NF_{tot}$ is measured as approx. 6.9 dB as given in Fig.5b. The measured gain in both the cases is approx. 23.5 dB. These results have been verified with theoretical predictions and is detailed in Section-IV.

### B. Study of Noise Figure and Insertion gain of a mixer

The experimental set-up for this part is shown in Fig.6. The purpose of this experiment is to find out the NF and insertion gain of the mixer. The Local Oscillator input power is set at 12 dBm and frequency of 10 GHz as per the mixer specification [4]. The measurement result is furnished in Fig.7. The NF of the mixer is measured as approx. 3 - 4 dB and the insertion gain as approx. -3.0 dB.

## IV. Results and Discussion

The focus of this experiment revolves around the determination of Noise Figures (NF) of various components such as attenuator, IF amplifier, mixer and their series combinations as detailed in Section - III. The results obtained are tabulated in TableI.

The Friis equation (2) is verified for the cases mentioned in S.No. 4, 5 in Table.I. For the case of attenuator followed by IF Amplifier, the NF if calculated from (2), is approx. 12.9 dB (agreeing with the measured 13.0dB). For the case of IF Amplifier followed by attenuator, the NF if calculated from (2), is approx. 6.9 dB (agreeing with the measured 6.9 dB). It brings out the fact that the first stage of the RF receiver chain (an amplifier) has to be a low noise stage.

## V. Conclusion

In this comprehensive study, we have delved into the intricacies of the Noise Figure Meter and Analyzer, gaining a

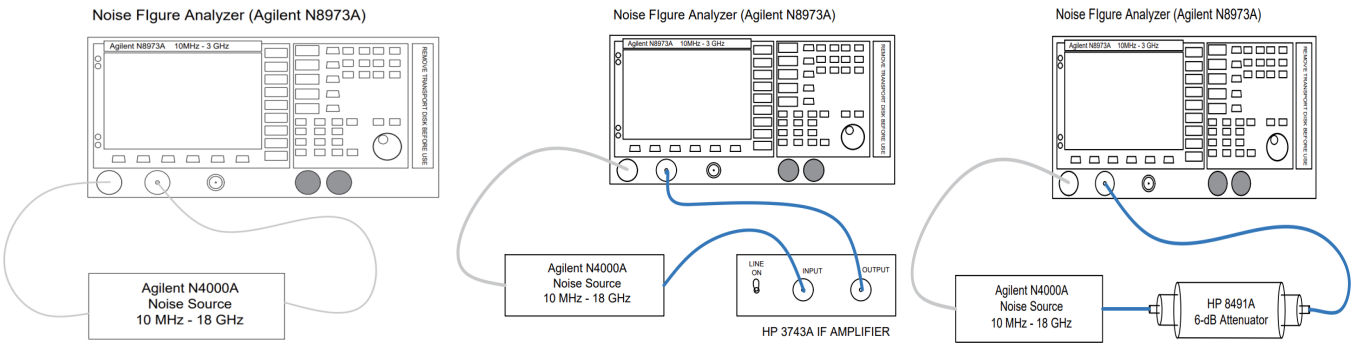


(a) (b) (c)

Fig. 2: Measurement set-up for (a) Calibration of NF meter, (b) measuring NF of an IF amplifier, (c) measuring NF of an attenuator

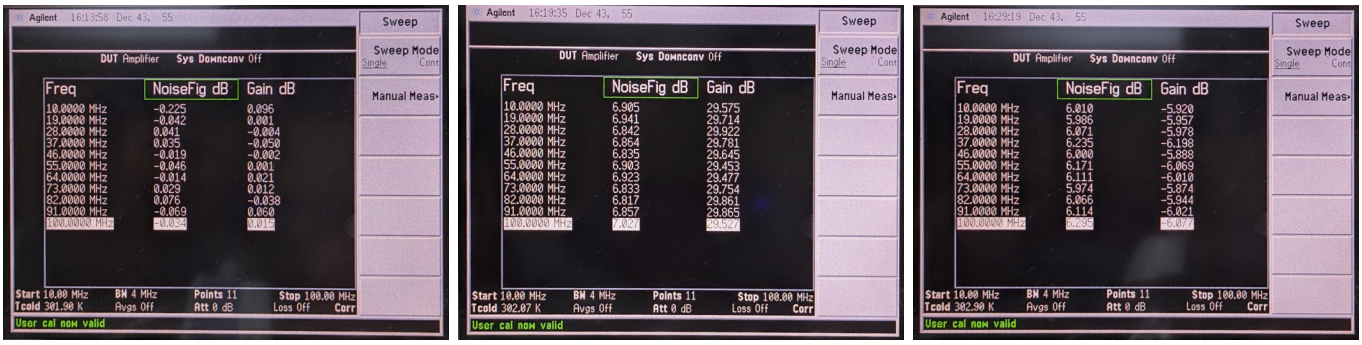


(a) (b) (c)

Fig. 3: Measurement results of Noise Figures for (a) a calibrated NF meter (b) an IF amplifier, and (c) an attenuator

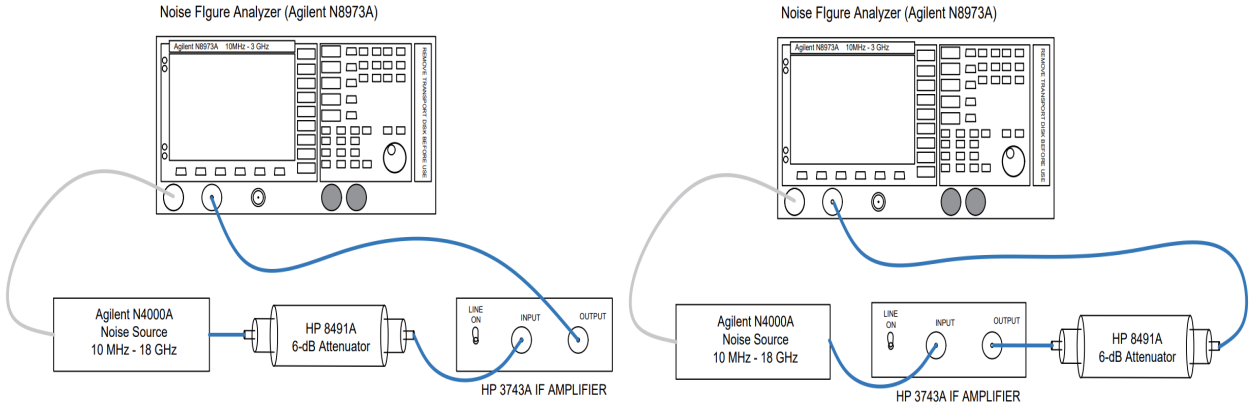


(a) (b)

Fig. 4: Noise Figure measurement set-up for (a) an attenuator followed by an amplifier, (b) an amplifier followed by an attenuator

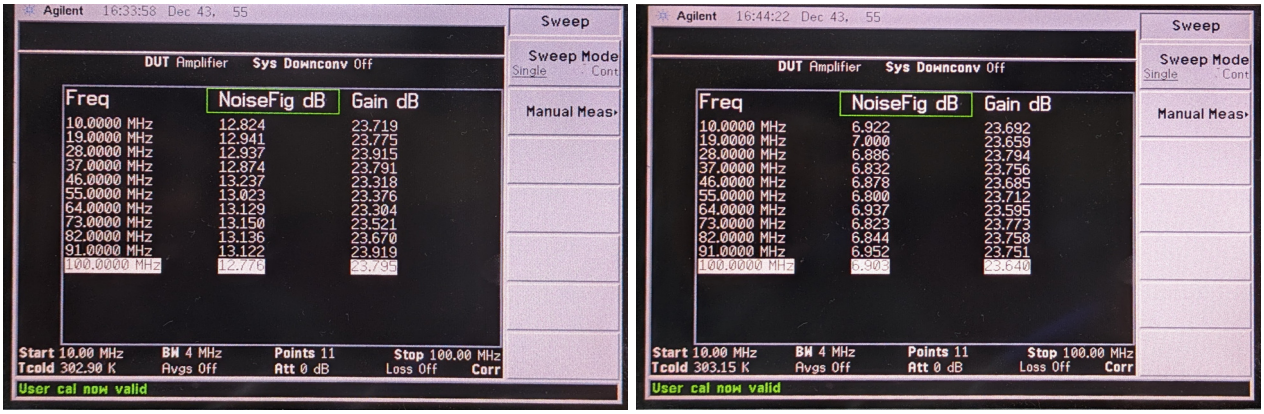


(a) (b)

Fig. 5: Measurement results of Noise Figures for (a) an attenuator followed by an amplifier (b) an amplifier followed by an attenuator

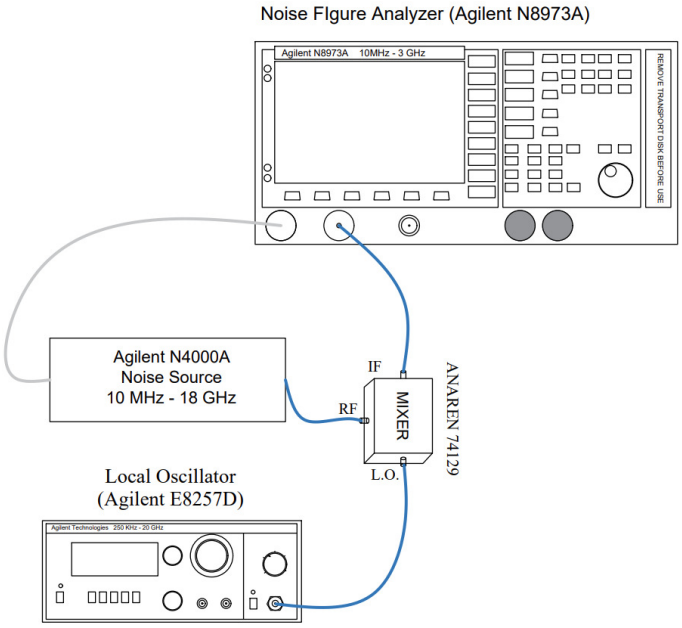


Fig. 6: Measurement set-up for measuring the NF of a mixer


Fig. 7: Measurement results for NF and insertion gain of the mixer

profound understanding of their multifaceted functionalities. A crucial aspect of our experimentation involved calibrating the Noise Figure meter with a known noise source, establishing a reliable standard for our subsequent measurements. Our investigation encompassed the determination of Noise Figure values for both an IF amplifier and an attenuator, shedding light on their individual noise characteristics. Furthermore, we explored the combined Noise Figure when these two components were integrated, revealing insightful patterns. Notably, our observations unveiled that when the amplifier assumed the role of the first stage, the dominant contributor to the overall noise was the amplifier itself, with the contribution from the second stage diminishing in significance due to the first stage's gain factor. Conversely, when the attenuator assumed the lead role, both stages played a significant role in the overall noise figure, as the Noise Figure contribution of the second stage was amplified. This phenomenon underscores the rationale behind employing a Low Noise Amplifier (LNA) as the first stage in an RF receiver. As a comprehensive capstone to our study, we meticulously measured the noise figure of a mixer, further enriching our understanding of noise characteristics in microwave systems.

## VI. ACKNOWLEDGMENT

Firstly, the author would like to thank his lab-mate Mr. Mayank Anupam for carrying out the experiments together and sharing concepts. The author would also like to acknowledge the efforts of course TAs in conducting the experiments smoothly and finally, Prof. A R Harish for his ever-present guidance and patience to answer all the questions.

## REFERENCES

[1] A. R. Harish, "EE647A:Microwave Measurements and Design Lecture Notes, 2023."
[2] ——, "EE647A:Microwave Measurements and Design Lab Handouts, 2023."
[3] B. Razavi, "RF Microelectronics 2nd ed., Prentice Hall, 2011."
[4] Anaren, "Double Balanced Mixers - Model 74129, Technical Datasheet."

# Experiment No. - 5
# Directional Coupler Characteristics and Realization of Scalar Network Analyzer

Debashish Nandi, *Graduate Student Member, IEEE*
*Roll No.21204262*

***Abstract*— This study offers a comprehensive analysis of a Directional Coupler through the utilization of a Power Sensor. This encompassing investigation involves the measurement of cable loss through the power sensor, with meticulous attention paid to its incorporation in the Directional Coupler's characterization process. Furthermore, we employed a dual Directional Coupler to establish a Scalar Network Analyzer, which served as a crucial tool for the characterization of a Device under test (DUT) - specifically, a Band Pass Filter. These experimental evaluations were executed within the confines of the Microwave Measurement Laboratory, housed within the distinguished Electrical Engineering Department at the Indian Institute of Technology Kanpur.**

***Index Terms*— Noise Figure, insertion gain, NF meter, NF Analyzer, Friis Formula, Noise source.**

## I. Introduction

Microwave measurement and design [1] are critical aspects of modern technology, spanning various domains such as telecommunications, radar systems, satellite communication, and microwave circuits. Accurate measurement and analysis of microwave components are fundamental to ensuring the performance and reliability of these systems. In this context, power sensors and directional couplers play pivotal roles, providing crucial insights into the behavior of microwave devices and enabling the construction of Network Analyzers. This experiment aims to elucidate the significance of power sensors and directional couplers in microwave measurement and design, emphasizing their characteristics and usage in the development of Network Analyzers.

Power sensors are indispensable tools for accurately measuring microwave power levels. They enable engineers and researchers to quantify the power output or input of microwave devices, ensuring that they operate within specified limits. This is crucial for assessing the performance and safety of microwave systems. Directional couplers are passive microwave devices that facilitate the splitting and combining of microwave signals. Understanding their characteristics is essential for designing and optimizing microwave circuits and systems. Power sensors play a pivotal role in characterizing the insertion loss, coupling factor, and isolation of directional couplers. Power sensors, in conjunction with directional couplers, form the foundation of Network Analyzers. These analyzers are essential for measuring and analyzing the complex scattering parameters (S-parameters) of microwave components and systems. Accurate S-parameter measurements are crucial for the design and optimization of microwave circuits, antennas, and filters.

Debashish Nandi is with the Nanolab, Department of Electrical Engineering, IIT Kanpur, Kanpur 208016, India (e-mail: debashish21@iitk.ac.in)

Power sensors come in various types, including thermocouple-based, diode-based, and thermal-based sensors. They offer wide dynamic range, high accuracy, and low insertion loss. Modern power sensors often feature digital interfaces for precise data acquisition and analysis. Directional couplers are known for their high coupling efficiency, low insertion loss, and excellent isolation. They are available in different coupling ratios and frequency ranges, making them versatile tools for a wide range of applications. Scalar Network Analyzers utilize power sensors to measure only the magnitude of S-parameters (amplitude information). SNAs are well-suited for characterizing passive microwave components like filters and attenuators. They are simpler in design and operation compared to vector network analyzers. Vector Network Analyzers utilize both power sensors and phase-sensitive detectors to measure both the magnitude and phase of S-parameters. VNAs are capable of characterizing active and passive components with superior accuracy. They provide a complete picture of the microwave behavior, including phase information, making them invaluable for complex microwave systems and non-linear device characterization.

In this Experiment-5 which is comprising of three sub-experiments, we utilize the Power sensors for calculating cable loss over a frequency range, followed by characterization of a dual directional coupler which forms basis of Network Analyzers. Additionally, we implement a Scalar Network Analyzer with help of the dua directional coupler and power sensors which is used to characterize a Band Pass Filter.

The organization of the report is as follows: The problem formulation is presented in Section II, followed by characterization in Section III. Section IV presents the results and discussions, and we offer the concluding remarks in Section V.

## II. Problem Formulation

The experiments [2] involved in this study are as follows:

*1)* **Measurement of Cable Loss:** The primary aim of this experiment is to measure loss of a co-axial cable with the help of a power sensor. This information is later used to characterize a directional coupler.

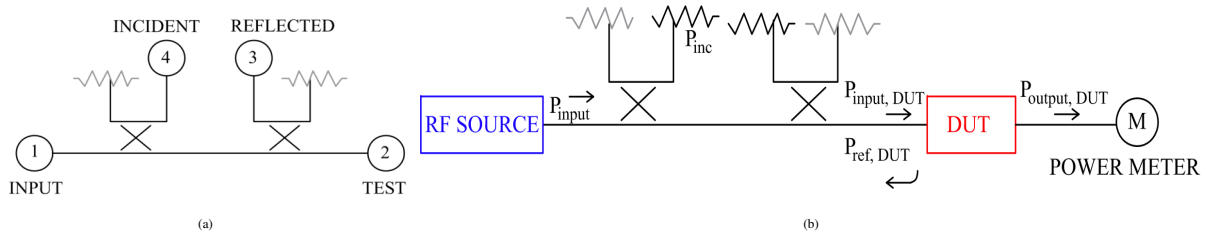


Fig. 1: (a) Block Diagram of a dual Directional Coupler (b) Block diagram for measuring $P_{output,DUT}$ of a DUT

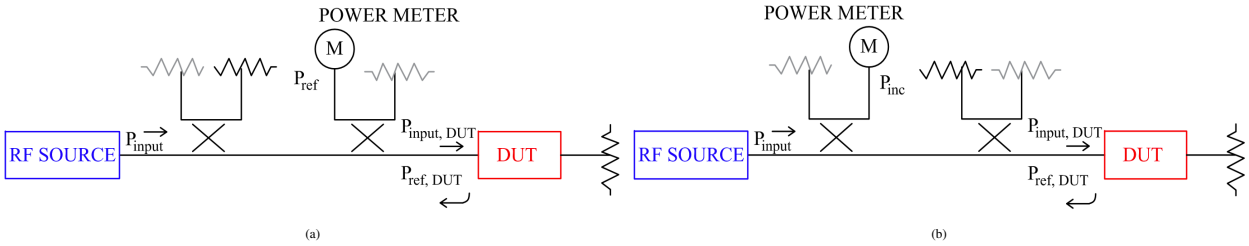


Fig. 2: (a) Block diagram for measuring $P_{ref}$ of a DUT, (b) Block diagram for measuring $P_{inc}$ of a DUT

*2)* **Measurement of Directional Coupler Characteristics:** This experimental phase is dedicated to characterize the Directional coupler in terms of its coupling factor, isolation, directivity. A RF source and a power sensor are used in this regard.

*3)* **Implementation of a Scalar Network Analyzer:** In this part, we use the dual Directional Coupler to implement a Scalar Network Analyzer and characterize a Band Pass Filter (BPF) by means of the amplitude of its scattering parameters.

**Theoretical Formulation** : The block diagram of a dual directional coupler is shown in Fig.1a [2]. The measurement procedure of $S_{11}$ and $S_{21}$ is shown below:

*a) Calculation of* $|S_{11}|$*:* A typical block-diagram for calculation of $S_{11}$ is shown in Fig.2a, where the powers measured at Input, Incident, Reflected and Test ports are denoted by $P_{input}$, $P_{inc}$, $P_{ref}$ and $P_{test}$ respectively, all in dB scale (e.g., dBm). As the coupler is labelled as 20 dB, we can write

$$P_{input} = P_{inc} + 20 \tag{1}$$

Assuming the coupler to have a low insertion loss, $P_{test}$ = $P_{input}$. Since, the power at TEST port is fed into the DUT (as shown in Fig.2b), we can write

$$P_{input,DUT} = P_{test} \approx P_{inc} + 20 \tag{2}$$

The reflected power from the DUT is coupled to the REFLECTED port via the directional coupler (as shown in Fig.2a), hence,

$$P_{ref,DUT} = P_{ref} + 20 \tag{3}$$

Therefore, using (2) and (3), we have,

$$\begin{aligned} |S_{11-DUT}| &= P_{ref,DUT} - P_{input,DUT} \\ &= (P_{ref} + 20) - (P_{inc} + 20) \\ &\quad or, \\ |S_{11-DUT}| &= P_{ref} - P_{inc} \end{aligned} \tag{4}$$

*b) Calculation of* $|S_{21}|$*:* A typical block-diagram for calculation of $S_{21}$ is shown in Fig.1b, where $P_{output-DUT}$ is in dB scale, the $|S_{21}|$ can be written as

$$\begin{aligned} |S_{21-DUT}| &= P_{output,DUT} - P_{input,DUT} \\ &\quad or, \\ |S_{21-DUT}| &= P_{output,DUT} - (P_{inc} + 20) \end{aligned} \tag{5}$$

## III. Characterization

The general characterization set-up used in this experiment, is shown in Fig.3. The components used in this experiment are a) Average Power sensor including PC (Agilent U2004A), b) RF Signal Source (Anritsu MG3692C), c) 20-dB dual Directional Coupler (HP 777D), d) Band Pass Filter (Mini-Circuits ZFBP-2400-S+) and e) Co-axial Cable.

### A. Measurement of Cable Loss

The first part of the experiment is to measure the loss ($L_c$ in a co-axial cable over a range of frequency. The input power from the RF source is set at 0-dBm and the frequency range is chosen based on the dual Directional Coupler operating frequency. The setup for this part is shown in Fig. 3 and the measurement result is given in Table. I. The cable loss vs frequency is plotted in Fig. 5a.

### B. Measurement of Directional Coupler Characteristics

The set-up for this part of the experiment is shown in Fig. 4a, 4b and 4c. The input power from the RF source is maintained at 0-dBm throughout the experiment. The measured powers at TEST port ($P_{test}$), INCIDENT port ($P_{inc}$) and REFLECTED port ($P_{ref}$) is given in Table. II. The calculated coupling factor (C), isolation (I) and Directivity (D) are given in Table. III, which considers the cable losses. The respective plots of Coupling Factor (C) vs. Frequency and Directivity (D) vs. Frequency are shown in Fig. 5b and Fig. 5c.

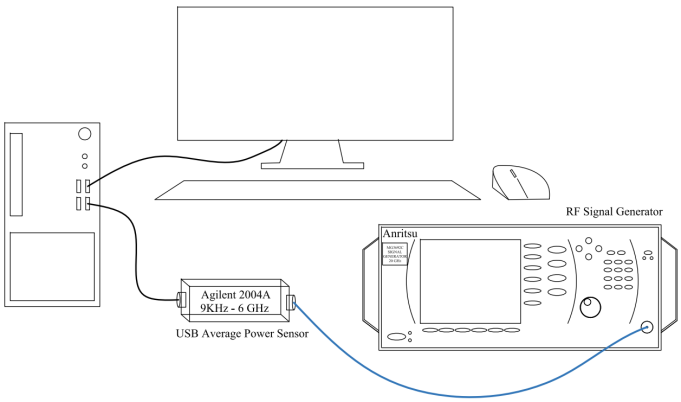


Fig. 3: Measurement set-up for measuring the cable loss of a co-axial cable

TABLE I: Measurement results of Cable Loss at various freq. for $P_{in} = 0dBm$

| freq. (GHz) | $P_{out}$ (dBm) | $L_c$ (dB) |
|---|---|---|
| 1.8 | -0.63 | 0.63 |
| 2.0 | -0.68 | 0.68 |
| 2.2 | -0.72 | 0.72 |
| 2.3 | -0.50 | 0.50 |
| 2.4 | -0.50 | 0.50 |
| 2.6 | -0.59 | 0.59 |
| 2.8 | -0.62 | 0.62 |
| 3.0 | -0.65 | 0.65 |
| 3.2 | -0.69 | 0.69 |
| 3.4 | -0.71 | 0.71 |
| 3.6 | -0.75 | 0.75 |
| 3.8 | -0.77 | 0.77 |
| 4.0 | -0.80 | 0.80 |

TABLE II: Measurement results of output powers at different ports for $P_{in} = 0dBm$

| freq. (GHz) | $P_{test}$ (dBm) | $P_{inc}$ (dBm) | $P_{ref}$ (dBm) |
|---|---|---|---|
| 1.8 | -0.95 | -20.89 | -60 |
| 2.0 | -1.03 | -20.80 | -60 |
| 2.2 | -1.03 | -20.73 | -60 |
| 2.4 | -0.86 | -20.47 | -55.87 |
| 2.6 | -0.90 | -20.50 | -51.68 |
| 2.8 | -0.93 | -20.51 | -48.64 |
| 3.0 | -0.96 | -20.50 | -46.90 |
| 3.2 | -1.01 | -20.53 | -46.18 |
| 3.4 | -1.06 | -20.53 | -46.15 |
| 3.6 | -1.10 | -20.53 | -46.70 |
| 3.8 | -1.13 | -20.51 | -48.28 |
| 4.0 | -1.22 | -20.55 | -50.36 |

TABLE III: Insertion Loss, Coupling, Isolation and Directivity of the Directional Coupler

| freq. (GHz) | IL (dB) | C (dB) | I (dB) | D (dB) |
|---|---|---|---|---|
| 1.8 | 0.32 | 20.26 | 59.37 | 39.11 |
| 2.0 | 0.35 | 20.12 | 59.32 | 39.20 |
| 2.2 | 0.31 | 20.01 | 59.28 | 39.27 |
| 2.4 | 0.36 | 19.97 | 55.37 | 35.40 |
| 2.6 | 0.31 | 19.91 | 51.09 | 31.18 |
| 2.8 | 0.31 | 19.89 | 48.02 | 28.13 |
| 3.0 | 0.31 | 19.85 | 46.25 | 26.40 |
| 3.2 | 0.32 | 19.84 | 45.49 | 25.65 |
| 3.4 | 0.35 | 19.82 | 45.44 | 25.62 |
| 3.6 | 0.35 | 19.78 | 45.95 | 26.17 |
| 3.8 | 0.36 | 19.74 | 47.51 | 27.77 |
| 4.0 | 0.42 | 19.75 | 49.56 | 29.81 |

### C. Implementation of a Scalar Network Analyzer

The experimental set-up for this part is shown in Fig.6a. In this study, a scalar network analyzer has been realized using the dual Directional Coupler and power sensor. A band pass filter has been characterized using the scalar network analyzer where the $|S_{11}|$ and $|S_{21}|$ has been calculated over the range of its operating frequency. The measurement set-ups for measuring output powers at different ports of the dual Directional Coupler, i.e., $P_{test}$, $P_{inc}$ and $P_{ref}$ have been shown in Fig.6a, 6b and 6c respectively. The measured results are tabulated in Table.IV. $S_{11}$ and $S_{21}$ are calculated using (4) and (5) respectively and tabulated in Table.V. The plots of $S_{11}$ and $S_{21}$ are shown in Fig.7a and 7b.

TABLE IV: Measurement results of output powers at different ports for $P_{in} = 0dBm$

| freq. (GHz) | $P_{ref}$ (dBm) | $P_{inc}$ (dBm) | $P_{OUT,DUT}$ (dBm) |
|---|---|---|---|
| 2.11 | -23.12 | -20.57 | -11.49 |
| 2.14 | -24.71 | -20.96 | -9.38 |
| 2.17 | -26.96 | -20.85 | -6.42 |
| 2.20 | -31.11 | -20.54 | -5.0 |
| 2.23 | -39.57 | -20.40 | -3.91 |
| 2.26 | -46.76 | -20.43 | -3.70 |
| 2.29 | -41.17 | -20.42 | -3.68 |
| 2.32 | -41.16 | -20.43 | -3.74 |
| 2.35 | -43.62 | -20.43 | -3.77 |
| 2.38 | -46.86 | -20.44 | -3.88 |
| 2.41 | -46.46 | -20.43 | -3.96 |
| 2.44 | -45.16 | -20.44 | -4.08 |
| 2.47 | -46.56 | -20.45 | -4.24 |
| 2.50 | -53.62 | -20.46 | -4.42 |
| 2.53 | -49.22 | -20.46 | -4.81 |
| 2.56 | -49.55 | -20.49 | -5.72 |
| 2.59 | -34.17 | -20.41 | -8.40 |

TABLE V: Calculated magnitudes of $S_{11}$ and $S_{21}$ for a Band Pass Filter

| freq. (GHz) | $S_{11}$ (dB) | $S_{21}$ (dB) |
|---|---|---|
| 2.11 | -2.55 | -10.92 |
| 2.14 | -3.75 | -8.42 |
| 2.17 | -6.11 | -5.57 |
| 2.20 | -10.57 | -4.46 |
| 2.23 | -19.17 | -3.51 |
| 2.26 | -26.33 | -3.27 |
| 2.29 | -20.75 | -3.26 |
| 2.32 | -20.73 | -3.31 |
| 2.35 | -23.19 | -3.34 |
| 2.38 | -26.42 | -3.44 |
| 2.41 | -26.03 | -3.53 |
| 2.44 | -24.72 | -3.64 |
| 2.47 | -26.11 | -3.79 |
| 2.50 | -33.16 | -3.96 |
| 2.53 | -28.76 | -4.35 |
| 2.56 | -29.06 | -5.23 |
| 2.59 | -13.76 | -7.99 |

## IV. Results and Discussion

The focus of this experiment revolves around the utilization of a power sensor and dual Directional Coupler to establish a scalar network analyzer. Firstly, the loss of a cable is characterized over a range of frequency and the characteristics is shown in Fig.5a. The non-monotonous behaviours of the cable loss may be attributed to a) multiple reflections at the ends of the cables which may add in or out of phase, b) due to random noise in the measurement set-up.

A 20-dB dual directional coupler has been characterized in terms of its coupling, directivity, isolation and insertion loss and the results are detailed in Section-III. From Fig.5b, it can be observed that the coupling is fairly constant over the range of frequency which is around 20 dB. However, the directivity of the directional coupler varies significantly over frequency,

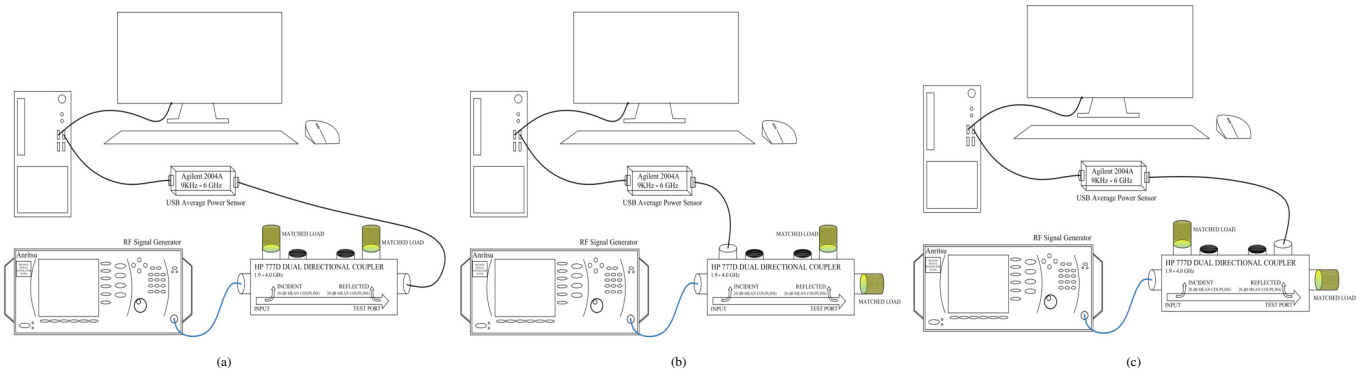


Fig. 4: Measurement set-up for (a) $P_{test}$, (b) $P_{inc}$, (c) $P_{ref}$

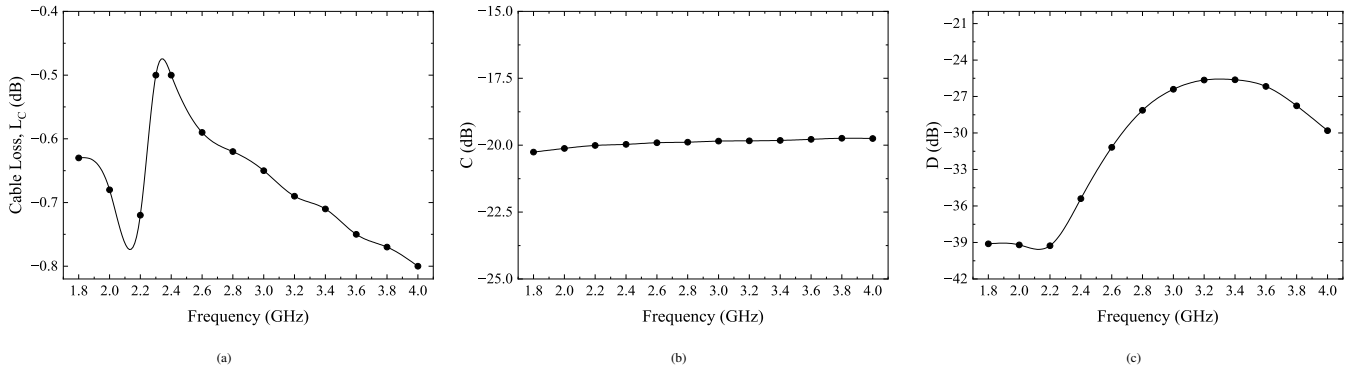


Fig. 5: (a) Cable Loss vs. Frequency (b) Coupling vs Frequency of the Directional Coupler, and (c) Directivity vs Frequency of the Directional Coupler

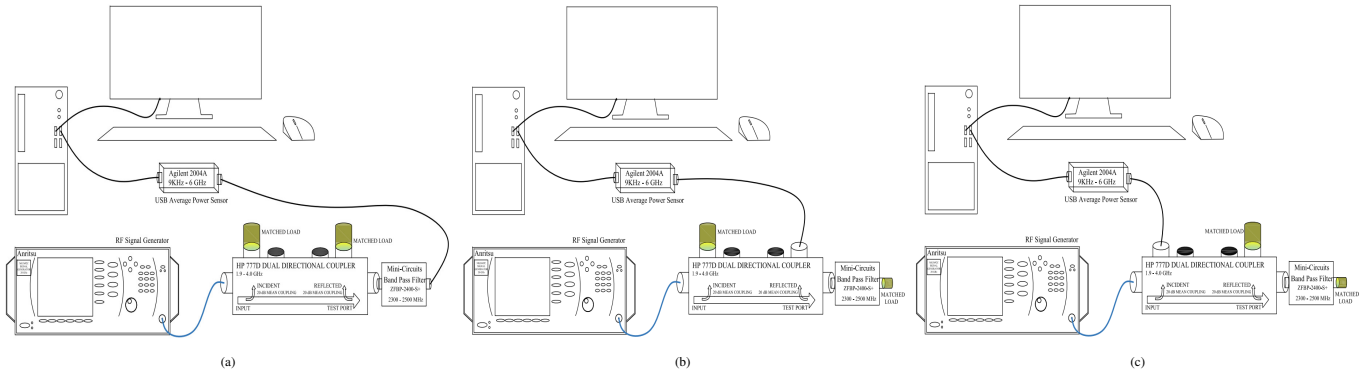


Fig. 6: Measurement set-up for measuring (a) $P_{test}$ (b) $P_{ref}$, and (c) $P_{inc}$

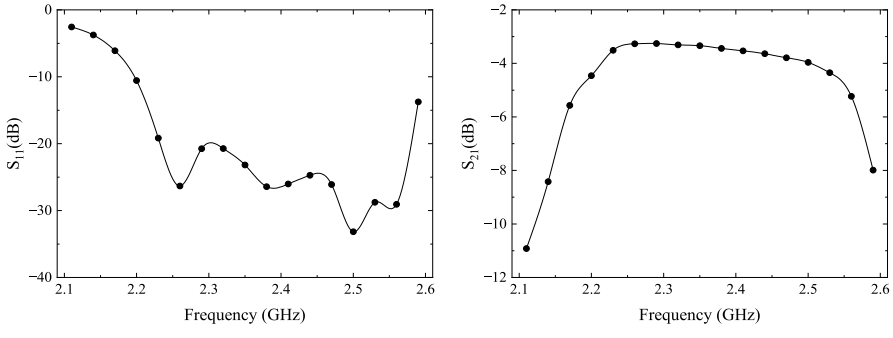


Fig. 7: (a) $S_{11}$ vs. Frequency (b) $S_{21}$ vs. Frequency of a Band Pass Filter

as can be seen from Fig.5c, which can be attributed to the discontinuities within the circuit. These mismatches can occur on either at the input port or the isolated port.

A scalar network analyzer which was realized using the dual directional coupler and power sensor, has been used to measure magnitudes of $S_{11}$ and $S_{21}$ of a Band Pass Filter and the results are shown in Fig.7a and 7b.

## V. Conclusion

In this expansive exploration, we have probed deeply into the nuances of characterizing a Directional Coupler through the employment of a power sensor, meticulously considering the measurement of cable losses. Additionally, we have successfully implemented a Scalar Network Analyzer by harnessing the capabilities of the directional coupler and the power sensor, which were subsequently employed to meticulously scrutinize the behavior of a band pass filter. This investigation underscores the indispensable role of power sensors and directional couplers as foundational instruments in the realm of microwave measurement and design, empowering the construction of Network Analyzers for the precise and comprehensive characterization of microwave components and systems.

## VI. Acknowledgment

The author would like to acknowledge the efforts of course TAs in conducting the experiments smoothly and Prof. A R Harish for his ever-present guidance and patience to answer all the questions.

## References

[1] A. R. Harish, “EE647A:Microwave Measurements and Design Lecture Notes, 2023.”
[2] ——, “EE647A:Microwave Measurements and Design Lab Handouts, 2023.”

# Experiment No. - 6
# One Port Error Model of VNA

Debashish Nandi, *Graduate Student Member, IEEE*
*Roll No.21204262*

***Abstract*— This manuscript conducts a comprehensive analysis of the One Port Error Model for a Vector Network Analyzer (VNA), highlighting its ability to mitigate systematic errors inherent to VNAs. The efficacy of this error model is illustrated by its utilization in determining the reflection coefficient of a Band-Pass Filter, which is subsequently verified through 1 port Open-Short-Load Calibrated measurements. Furthermore, the paper offers an extensive exploration of the error model coefficients and their variability over a wide frequency range. The experimental evaluations were executed within the confines of the Microwave Measurement Laboratory, housed within the distinguished Electrical Engineering Department at the Indian Institute of Technology Kanpur.**

***Index Terms*— VNA, OSL Calibration, Error model, Systematic Errors, Band-Pass-Filter.**

## I. Introduction

Microwave measurements are integral in various fields of science and technology, ranging from telecommunications and radar systems to materials characterization and research in microwave engineering. These measurements often rely on the precision and accuracy of Vector Network Analyzers (VNAs) to assess the performance of microwave components, such as filters, amplifiers, and antennas. VNAs have evolved to become indispensable tools, enabling engineers and researchers to extract vital information about the electrical behavior of devices operating at microwave frequencies. However, like any measurement system, VNAs are not without their challenges, and a fundamental aspect of their operation lies in their susceptibility to various sources of error. These errors can significantly impact the accuracy and reliability of the measurements obtained. Understanding and mitigating these errors is essential for ensuring the trustworthiness of VNA-based measurements. This paper explores the One Port Error Model for VNAs and its role in addressing systematic errors to enhance measurement precision and reliability.

VNAs are susceptible to several types of errors, which can be categorized into three main groups: systematic errors, random errors and drift errors. Systematic errors are predictable and reproducible, while random errors are unpredictable and can vary between measurements. Among the most common systematic errors in VNAs are mismatches, drifts, and imperfections in the VNA's own electronics. Mismatches occur when the characteristics of the measurement setup (e.g., connectors, cables) differ from the reference conditions, leading to reflection and transmission errors. Drifts are gradual variations in VNA performance over time, which can introduce measurement errors. Imperfections in the VNA's electronics, such as cross-talk and residual responses, can also contribute to systematic errors. To enhance the accuracy and reliability of VNA measurements, systematic errors need to be systematically addressed and minimized. Several strategies have been developed to remove or mitigate these errors. These include the use of calibration techniques, which correct for known errors in the measurement system. One of the most common calibration methods is the Open-Short-Load-Thru (OSLT). For 1-port reflection measurements, OSL calibration is dominant.

The One Port Error Model is a calibration technique designed specifically to tackle systematic errors in one-port measurements, often used to characterize passive microwave components like antennas and filters. This method provides a systematic approach to eliminate or reduce the effects of systematic errors in VNA measurements. By characterizing the systematic errors and their dependence on frequency, the One Port Error Model allows for precise error correction, ensuring that measurements accurately reflect the intrinsic behavior of the DUT (Device Under Test). In this manuscript, we provide a detailed examination of the One Port Error Model for VNAs, highlighting its utility in minimizing systematic errors and enhancing the accuracy of microwave measurements. We also demonstrate the effectiveness of this error model through its application to measure the reflection coefficient of a Band-Pass Filter, validated using 1-port Open-Short-Load Calibrated results. Additionally, we offer comprehensive insights into the error model coefficients and their variations across a broad frequency spectrum, providing valuable information for researchers and engineers working in the field of microwave measurements.

The organization of the report is as follows: The problem formulation is presented in Section II, followed by characterization in Section III. Section IV presents the results and discussions, and we offer the concluding remarks in Section V.

## II. Problem Formulation

The experiments [1] involved in this study are as follows:

*1)* **Determination of 1 Port Error Model Coefficients:** The primary aim of this experiment is to characterize the 1-Port error model coefficients $E_D$, $E_R$ and $E_S$. This is achieved by measuring the reflection coefficients ($S_{11}$) of the Open-Short-Load (OSL) standards.

Debashish Nandi is with the Nanolab, Department of Electrical Engineering, IIT Kanpur, Kanpur 208016, India (e-mail: debashish21@iitk.ac.in)

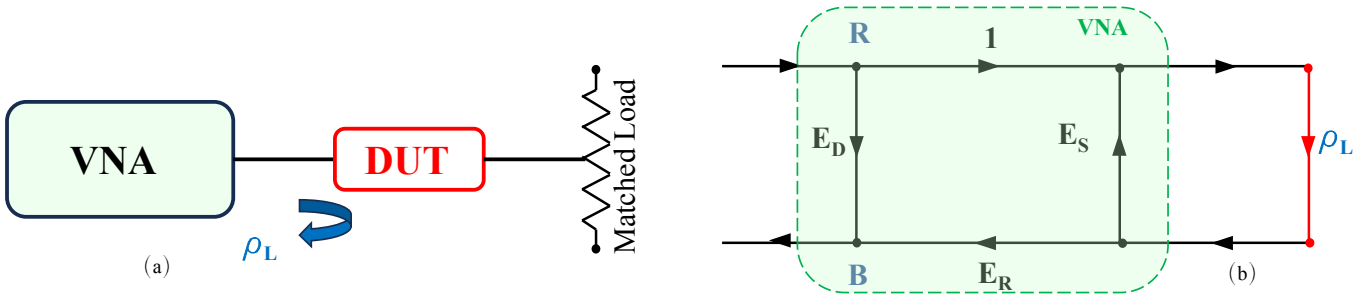


Fig. 1: (a) Typical Measurement Set-up, (b) Signal Flow Graph of 1-Port error model for the VNA

*2)* **Validation of the 1 Port Error Model with OSL Calibrated Measurement:** This experimental phase is dedicated to the characterization of a DUT. A Band-Pass-Filter (BPF) is used as a DUT in our experiment. The $S_{11}$ of the BPF is measured without calibration which is later corrected by incorporating the error coefficients (calculated in previous stage) of the VNA and validated against the $S_{11}$ measured with calibrated VNA.

**Theoretical Formulation** : A typical block diagram of the 1-port reflection measurement set-up dual directional coupler is shown in Fig.1a. The 1-port error model of the VNA can be represented as shown in Fig.1b. Here, $E_D$ is known as Directivity error, $E_R$ as Transmission error or Reflection Tracking and $E_S$ as Effective Source error or Source Match [2].

*a) Calculation of $E_D$, $E_R$ and $E_S$:* If $\rho_L$ is the actual reflection coefficient of any standard (open, short or match), and $S_{11,M}$ is the measured reflection coefficient, then using the Signal Flow Graph (SFG) shown in Fig.1b, we can write

$$S_{11,M} = \frac{B}{R} = E_D + \frac{\rho_L.E_R}{1 - E_S.\rho_L} \tag{1}$$

For an open load, $\rho_{L,open}$ = 1, for a short load, $\rho_{L,short}$ = -1 and for a match load $\rho_{L,match}$ = 0. Hence, while connecting match as load and substituting $\rho_L$ = 0 in (1), we get $E_D$ = $S_{11,match}$. Similarly by substituting $\rho_L$ = 1 and -1 respectively for open and short loads in (1), we get the following equations

$$(S_{11,open} - E_D) - E_S.(S_{11,open-E_D} = E_R \tag{2}$$

$$(S_{11,short} - E_D) + E_S.(S_{11,short-E_D} = -E_R \tag{3}$$

Solving (2) and (3), we get

$$E_S = \frac{S_{11,open} + S_{11,short} - 2.E_D}{S_{11,open} - S_{11,short}} \tag{4}$$

$$E_R = \frac{-2.(S_{11,open} - E_D).(S_{11,short} - E_D)}{S_{11,open} - S_{11,short}} \tag{5}$$

*b) Calculation of $\rho_L$:* Now, from (1), if we assume the measured reflection coefficient of a DUT is $S_{11,M}$ and $\rho_L$ is the actual reflection coefficient, we can compute $\rho_L$ as

$$\rho_L = \frac{S_{11,M} - E_D}{E_R + E_S.(S1,1,M - E_D)} \tag{6}$$

TABLE I: Coefficients of Short and Open standard loads of CalKit - Agilent 85032F

| Short Coeff. | Value | Open Coeff. | Value |
|---|---|---|---|
| $C_0$ | 8.9939e-14 F | $L_0$ | 0 H |
| $C_1$ | 2.5368e-24 F | $L_1$ | 0 H |
| $C_2$ | -2.6499e-34 F | $L_2$ | 0 H |
| $C_3$ | 1.34e-44 F | $L_3$ | 0 H |
| Delay | 4.119e-11 s | Delay | 4.5955e-11 s |
| Loss | 9.3e08 $\Omega/s$ | Loss | 1.087e9 $\Omega/s$ |
| $Z_0$ | 50 $\Omega$ | $Z_0$ | 49.99 $\Omega$ |

*c) Calculation actual $\rho_{L,open}$, $\rho_{L,short}$:* The actual value of the $\rho_{L,o}$ is calculated as $\rho_{L,o} = \frac{Z_C - Z_0}{Z_C - Z_0}$, where $Z_C = \frac{1}{j\omega C}$. The actual value of the $\rho_{L,s}$ is calculated as $\rho_{L,s} = \frac{Z_L - Z_0}{Z_L - Z_0}$, where $Z_L = j\omega L$.

The C and L are empirically modelled as

$$C = C_0 + C_1.f + C_2.f^2 + C_3.f^3 \tag{7}$$

$$L = L_0 + L_1.f + L_2.f^2 + L_3.f^3 \tag{8}$$

where $C_0$, $C_1$, $C_2$, $C_3$, $L_0$, $L_1$, $L_2$, and $L_3$ are arbitrary constants are provided by the manufacturer of the Calkit, f is the frequency of operation. If delay of the standards are provided as $l$, the final values of the reflection coefficients will be

$$\rho_{L,open} = \rho_{L,o} \exp(-j2\beta l) \tag{9}$$

$$\rho_{L,short} = \rho_{L,s} \exp(-j2\beta l) \tag{10}$$

## III. Characterization

The general characterization set-up used in this experiment, is shown in Fig.1a. The components used in this experiment are a) Vector Network Analyzer (Agilent 8714ET), b) Band-Pass-Filter (Mini-Circuits VBFZ-2000-S+), c) Calibration Kit (Agilent 85032F), d) connectors and e) Co-axial Cable.

### A. Determination of 1 Port Error Model Coefficients

The first part of the experiment is to measure the reflection coefficients of the Open, Short and Match standards from Calkit. The VNA is set to the following:

- Centre Frequency: 2 GHz
- Span:1000 MHz
- IF Bandwidth: 250Hz
- Number of points: 201

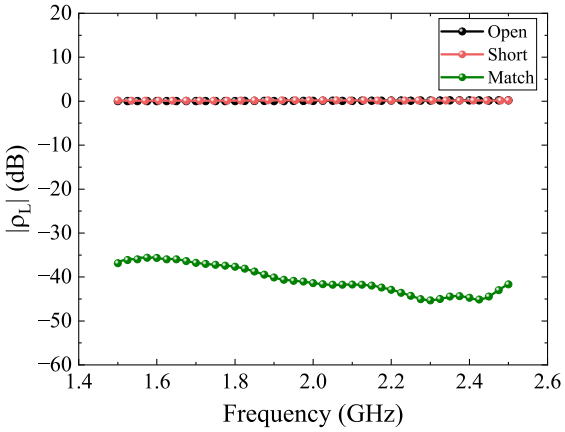


Fig. 2: Magnitude of $\rho_{L,open}$, $\rho_{L,short}$ and $\rho_{L,match}$ vs. Frequency

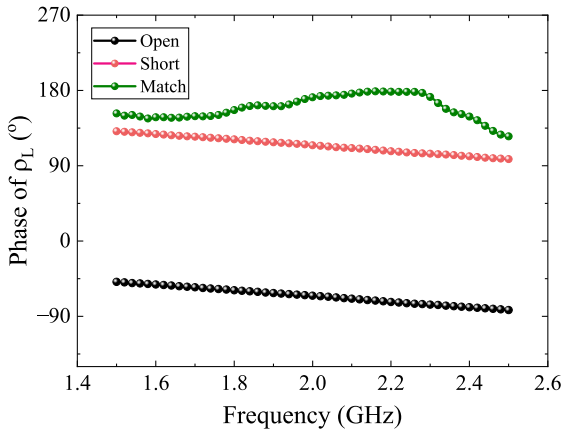


Fig. 3: Phase Response of $\rho_{L,open}$, $\rho_{L,short}$ and $\rho_{L,match}$ vs. Frequency

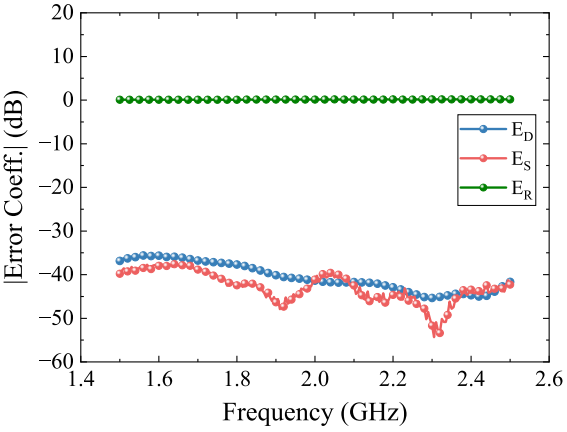


Fig. 4: Magnitude of $E_D$, $E_S$ and $E_R$ vs. Frequency

- Calibration: User Kit A
- Measurement: Reflection

The measured $\rho_{L,open}$, $\rho_{L,short}$ and $\rho_{L,match}$ are shown in Fig.2 and 3. The error coefficients of the 1-port error model, i.e., $E_D$, $E_S$ and $E_R$ are computed using (4) and (5). The obtained values are then plotted over a frequency range as shown in Fig.4 and 5.

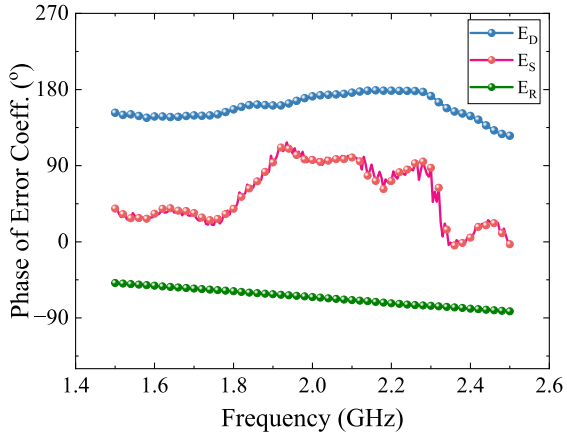


Fig. 5: Phase Response of $E_D$, $E_S$ and $E_R$ vs. Frequency

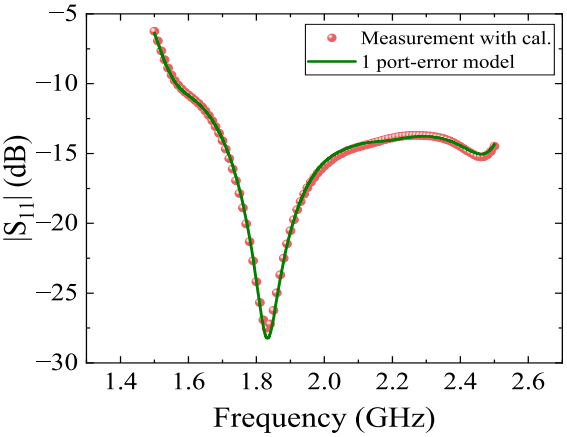


Fig. 6: Magnitude Plot of $S_{11}$ vs. Frequency of a Band-Pass-Filter

### *B.* Validation of the 1 Port Error Model with OSL Calibrated Measurement

In this part of the experiment the $S_{11,M}$ of the Band-Pass-Filter is measured using the same VNA setting as mentioned in previous measurement. The final value of reflection coefficient ($\rho_L$) is calculated using (6).

Furthermore, an OSL calibration has been performed on the VNA. The coefficients of short and open standards has been verified in the VNA, prior employing the OSL calibration. The reflection coefficient of the Band-Pass-Filter is again measured, now with the calibrated VNA. The comparison with the result of $\rho_L$ is presented in Fig.6 and 7.

## IV. Results and Discussion

This experiment centers on the formulation and validation of the 1-Port error model for a Vector Network Analyzer (VNA). We have systematically characterized and depicted the 1-port error model coefficients $E_D$, $E_R$, and $E_S$ in Fig. 4 and 5. Notably, the characterization reveals that $E_R$ approaches approximately 0 dB, while both $E_D$ and $E_S$ register below -30 dB. These findings collectively affirm the VNA's overall competence.

Furthermore, we applied this 1-Port error model to characterize the reflection coefficients of a Band-Pass Filter. To assess its effectiveness, we compared the calculated $S_{11}$ using

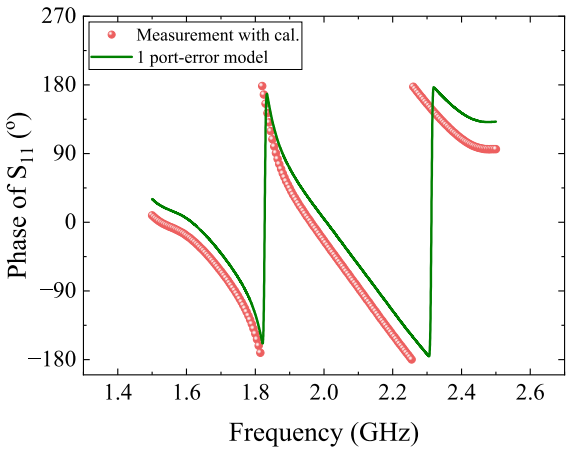


Fig. 7: Phase Response of $S_{11}$ vs. Frequency of a Band-Pass-Filter

the VNA's 1-Port error model with the measured $S_{11}$ obtained via OSL calibration. The validation results are presented in Fig. 6 and 7, illustrating a strong correlation between the 1-Port error model of the VNA and the OSL calibrated results. This alignment underscores the model's efficacy in accurately characterizing the device's performance.

## V. Conclusion

In this comprehensive investigation, we delved deep into the systematic errors associated with Vector Network Analyzers (VNAs) and successfully employed the 1-Port error model to address them. Error models serve as indispensable tools for rectifying these errors and are primarily accomplished through calibration techniques. Among the various calibration methods available, our focus centered on the Open-Short-Load (OSL) calibration technique and its corresponding error model, which we rigorously validated for a Band-Pass Filter. While the primary emphasis of our work revolves around 1-Port reflection measurements, it is worth noting that the same concept, with higher-order error models, can be extended to encompass two-port transmission measurements as well. Our experimental efforts have not only contributed to a more profound understanding of VNA error modeling but have also effectively bridged the gap between theoretical coursework and practical, real-world applications. This has significantly enriched our knowledge and appreciation of the capabilities of Vector Network Analyzers as versatile instruments for precise microwave measurements.

## VI. Acknowledgment

Firstly, the author would like to thank his lab-mate Mr. Mayank Anupam for carrying out the experiments together and sharing concepts. The author would also like to acknowledge the efforts of course TAs in conducting the experiments smoothly and finally, Prof. A R Harish for his ever-present guidance and patience to answer all the questions.

## References

[1] A. R. Harish, "EE647A:Microwave Measurements and Design Lab Handouts, 2023."
[2] ——, "EE647A:Microwave Measurements and Design Lecture Notes, 2023."

# Experiment No. - 7
# Measurement of Radiation Characteristics of Antenna and Time-Gating

Debashish Nandi, *Graduate Student Member, IEEE*
*Roll No.21204262*

***Abstract*— This report delves into a thorough investigation of radiation characteristics in antenna measurement, complemented by time domain reflectometry for the analysis of frequency selective surfaces. The assessment of the antenna under test (AUT) encompasses the determination of its reflection coefficient, antenna gain, and the radiation patterns in both co-polarization and cross-polarization configurations. Additionally, the characterization of a frequency selective surface involves the utilization of the time-gating feature of a network analyzer to examine its reflection coefficient. These experimental evaluations were meticulously conducted within the Microwave Measurement Laboratory, situated in the Electrical Engineering Department at the Indian Institute of Technology Kanpur.**

***Index Terms*— Antenna Under Test (AUT), Radiation Pattern, Absorber, Anechoic chamber, Time-gating.**

## I. Introduction

IN the realm of microwave measurements and design, the precise characterization of antenna radiation characteristics is imperative for advancing communication systems, radar technology, and satellite applications. Antenna radiation characteristics are pivotal in determining the efficacy of electromagnetic wave propagation and reception. The reflection coefficient, antenna gain, and radiation patterns represent key parameters that dictate the antenna's performance in varied operational scenarios. The radiation pattern of an antenna, delineating the spatial distribution of its radiated energy, is a critical aspect influencing the overall performance of communication systems. The comprehension and precise measurement of these radiation patterns, encompassing co-polarization and cross-polarization characteristics, are imperative for the optimal design and functionality of antenna systems in microwave applications. Anechoic chambers serve as controlled environments designed to minimize reflections of electromagnetic waves, providing an isolated and echo-free space for accurate antenna measurements. The significance of employing an anechoic chamber in antenna characterization lies in its ability to mitigate unwanted interference and external influences, thereby ensuring that the measured radiation patterns are representative of the antenna's intrinsic behavior. This controlled setting becomes particularly crucial when assessing the co-polarization and cross-polarization characteristics, where even slight external reflections could introduce inaccuracies in the measurements.

Moreover, this report sheds light on the indispensable role of frequency selective surfaces (FSS) and absorbers in the contemporary landscape of microwave technology. FSS, known for its ability to selectively filter or allow certain frequencies to pass through while reflecting others, finds their application in Antenna design, modern meta-materials, defence etc. Furthermore, the utilization of time domain reflectometry, specifically through time gating features of advanced network analyzers, adds a layer of sophistication to the characterization process. Time domain reflectometry facilitates a detailed analysis of electromagnetic wave interactions, allowing for a precise determination of reflection coefficients. This technique proves instrumental in unraveling the complex nature of frequency selective surfaces and absorbers, contributing to a more nuanced understanding of their behavior in the microwave domain. All the measurements done in this report are as per [1] and [2].

The organization of the report is as follows: The problem formulation is presented in Section II, followed by characterization in Section III. Section IV presents the results and discussions, and we offer the concluding remarks in Section V.

## II. Problem Formulation

The experiments [3] involved in this study are as follows:

*1)* **Reflection Coefficient Measurement of an AUT:** The primary aim of this experiment is to characterize the Antenna under test (AUT) by means of its reflection coefficient ($S_{11}$). In this step, we also find out the resonance frequency of the AUT.

*2)* **Antenna Pattern Measurement:** This experimental phase is dedicated to the characterization of an AUT by means of its radiation pattern. The radiation pattern of the AUT is measured for all the principle planes in both co-polarized and cross-polarized fashion with the source antenna.

*3)* **Antenna Gain Measurement:** In this step, we measure the transmission coefficient of the AUT with help of a standard gain horn antenna. The gain of the AUT is thereafter characterized by means of Friis formula [3].

*4)* **Reflection Coefficient Measurement of an absorber:** In this part of the experiment, an absorber is characterized by

Debashish Nandi is with the Nanolab, Department of Electrical Engineering, IIT Kanpur, Kanpur 208016, India (e-mail: debashish21@iitk.ac.in)

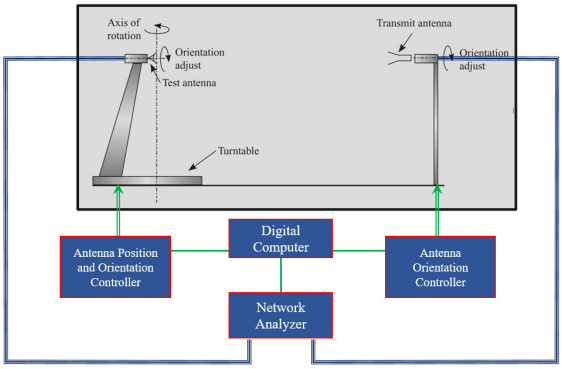


Fig. 1: Typical experimental set-up for Antenna radiation measurement [4]

means of its absorptivity with respect to a copper plate. In this experiment the Time-Gating feature of the Network Analyzer has been explored.

**Theoretical Formulation** : The Friis formula for antenna gain can be written as

$$\frac{P_r}{P_t} = (\frac{c}{4.\pi.f.R})^2.G_t.G_r \quad (1)$$

where,
$f$ = Resonance frequency of AUT
$R$ = Distance between the reference and test antenna
$c$ = Speed of light
$P_r$ = Power delivered by reference antenna
$P_t$ = Power received by test antenna
$G_t$ = Gain of test antenna
$G_r$ = Gain of reference antenna

Equation (1) can be written in dB scale as

$$P_{r,dBm} - P_{t,dBm} = 20.log_{10}(\frac{c}{4.\pi.f.R}) + G_{t,dB} + G_{r,dB} \quad (2)$$

The far-field condition of the antenna is given by

$$R > \frac{2.D^2}{\lambda} \quad (3)$$

where, R is the distance between the source antenna and AUT, D is the maximum dimension of the antenna and $\lambda$ is the wavelength at the resonant frequency.

## III. Characterization

The general characterization set-up used in this experiment, is shown in Fig.1. The components used in this experiment are a) Antenna Under Test (AUT), b) A standard gain Horn Antenna, c) Vector Network Analyzer (Agilent Technologies E5071C), d) Anechoic Chamber along with antenna mounting arrangements, turntable, e) computer controller, f) Antenna measurement studio, g) CCTV cameras, h) Connecting cables, i) Measuring and levelling equipment, j) Cu-plate and absorber plate.

### A. Reflection Coefficient Measurement of an AUT

The first part of the experiment is to measure the reflection coefficient of the Antenna under test (AUT). The VNA is calibrated to the following:

- Centre Frequency: 3.5 GHz
- Span:3 GHz (2-5 GHz)
- IF Bandwidth: 100Hz
- Number of points: 301
- Avg. Factor: 16

The measured $S_{11}$ is plotted in Fig.3. The resonant frequency of the antenna has been characterized as $f = 3.11$ GHz.

### B. Antenna Pattern Measurement

In experimental set-up for this part of the experiment is shown in Fig.1. The entire experiment has been carried out in an anechoic chamber as shown in Fig.2. The far-field condition (3) between the AUT and source antenna has been ensured. The max. dimension of the AUT is d = 27.365 cm (L = 19.3 cm, W = 19.4 cm) and $\lambda = \frac{c}{f} = \frac{3x10^10}{3.11x10^9} cm = 9.655cm$. Hence, the distance between the AUT and the source antenna (R) has to be greater than $\frac{2d^2}{\lambda} = 1.55m$. In our experimental set-up the R = 2.93 m which ensures the far-field condition.

The radiation pattern is measured at all the principle plane cuts by fixed-line-of-sight method [1]. Computer controlled turntables are used in this regard as shown in Fig.2. The measurement is carried out by connecting a standard gain horn antenna at one port of the VNA and the AUT to the other port, thus measuring the transmission coefficient ($S_{21}$). The E-plane co-polarized and cross-polarized radiation patterns are measured and plotted in Fig.4. The H-plane co-polarized and cross-polarized radiation patterns are measured and plotted in Fig.5. The radiation patterns are plotted for the resonant frequency f = 3.11 GHz.

The possible sources of errors in this part of the experiments can be from the leakages/reflections from door openings of the anechoic chamber, misalignment/levelling of the standard gain horn antenna and AUT, cables and connectors. Therefore, calibration of VNA, proper alignment and levelling of the antennas, appropriate connections of cables and connectors, closing the anechoic chamber door and other norms of using an anechoic chamber have been followed strictly to minimize the measurement errors.

### C. Antenna Gain Measurement

In this part of the experiment the AUT and the standard gain horn antennas are kept in such a way that their main beams are pointing towards each other. The transmission coefficient $S_{21}$ has been measured which corresponds to the $P_{r,dBm} - P_{t,dBm}$ in the Friis equation mentioned in (2). The gain of the AUT is thereafter characterized using (2) over a frequency range 2-4 GHz, where, c = 3 x $10^8$ m/s, R = 2.93m, $G_{r,dB}$ has been provided. The characterized gain of the AUT is shown in Fig.6. Cable loss over the frequency range has been incorporated while calculating the gain of the AUT using Friis formula.

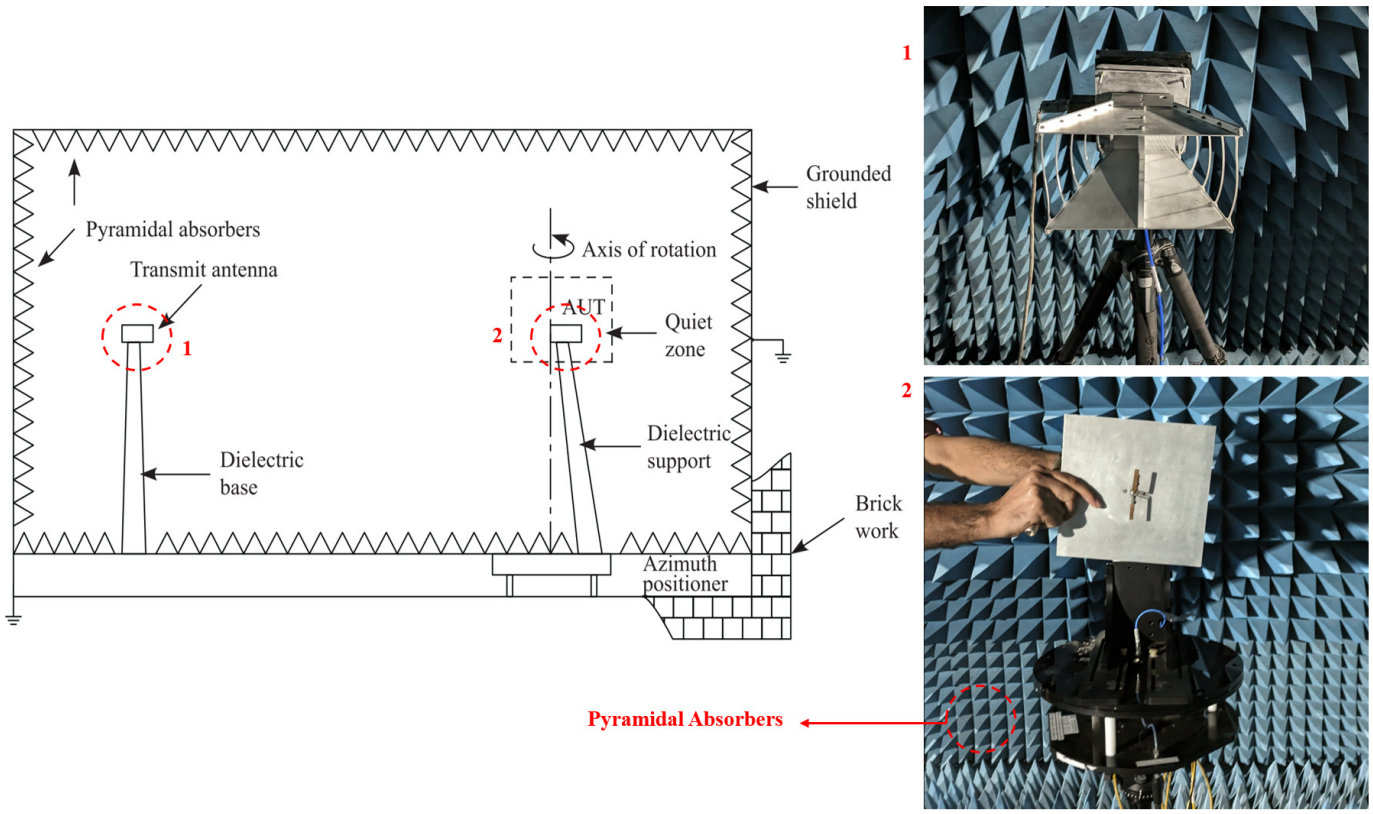


Fig. 2: Schematic of the Anechoic Chamber in the experimental set-up [4]

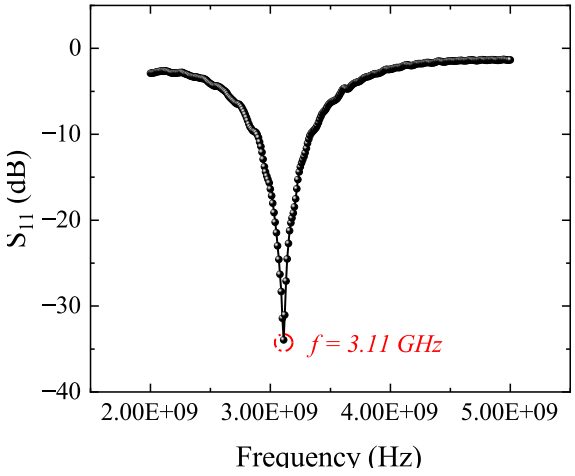


Fig. 3: $S_{11}$ vs. frequency for the Antenna under test (AUT)

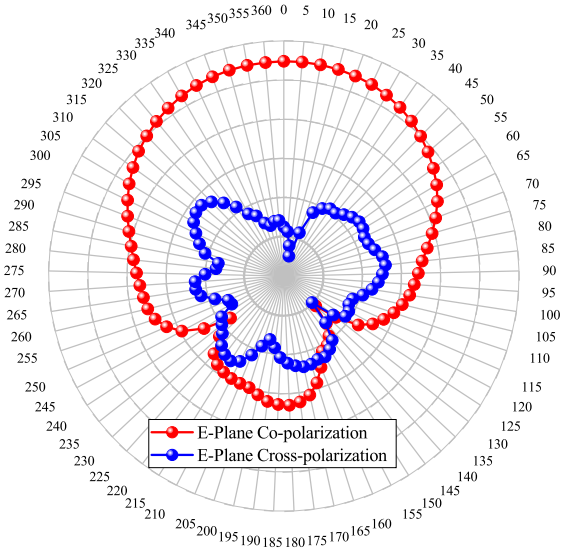


Fig. 4: Principle E-Plane radiation patterns (normalized) for co-polarized and cross-polarized configurations with the source antenna

### *D.* Reflection Coefficient Measurement of an absorber

The experimental configuration for this phase, depicted in Fig.1, replaces the Antenna Under Test (AUT) with a Cu-plate and an absorber sequentially. Fig.7 illustrates a time-domain comparison of the measured $S_{11}$ with and without the presence of the Cu-plate. Overlaying these results in Fig.7 identifies a specific time window around 115 ns, corresponding to the reflection from the Cu-plate to the antenna. Subsequently, the frequency domain response within this identified time window (time gate) is measured. A parallel methodology is employed for the absorber under test, with results presented in Fig.8. The absorber's absorptivity is characterized as ($S_{11,absorber}$ - $S_{11,Cu-plate}$) and graphically depicted in Fig.9..

## IV. Results and Discussion

This experiment focuses on assessing the reflection coefficient, antenna radiation pattern at principal plane cuts, and antenna gain of an AUT. The measured reflection coefficient ($S_{11}$) is depicted in Fig.3, revealing the resonant frequency as f = 3.11 GHz. Ensuring the far-field condition (minimum

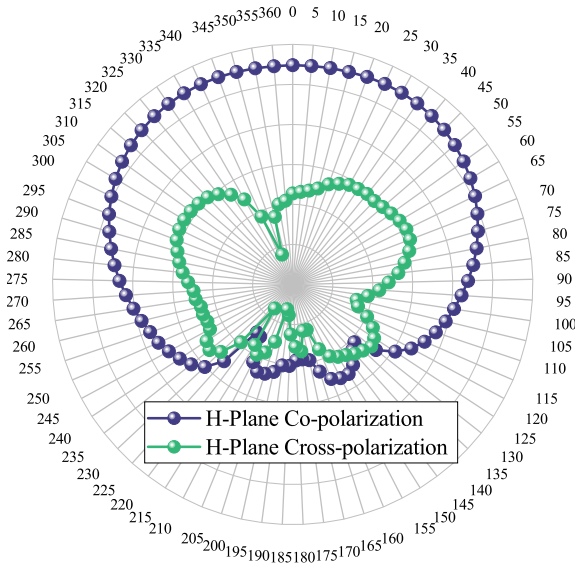


Fig. 5: Principle H-Plane radiation patterns (normalized) for co-polarized and cross-polarized configurations with the source antenna

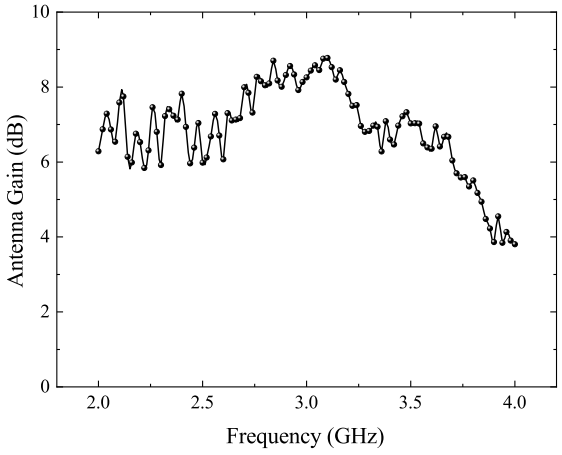


Fig. 6: AUT gain (calculated via Friis equation (2) vs. frequency

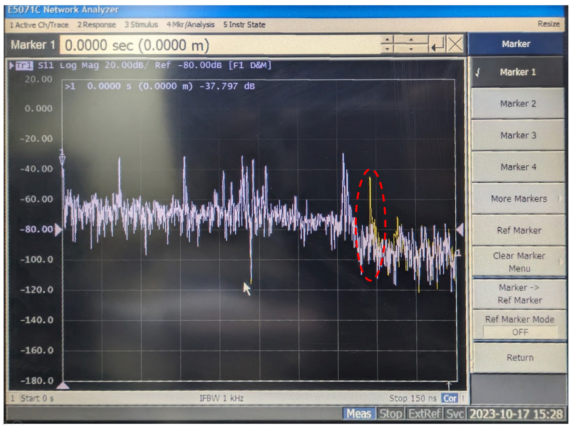


Fig. 7: Comparison of measured $S_{11}$ with (yellow) and without (grey) Cu-plate in the time-domain mode of VNA

distance between AUT and standard horn antenna) for accurate measurements is maintained at 1.55 m. The normalized radiation patterns for principal E-plane and H-planes are presented in Fig.4 and 5, respectively. Antenna gain, determined to be approximately $6dB$ using the Friis formula (2), is graphically

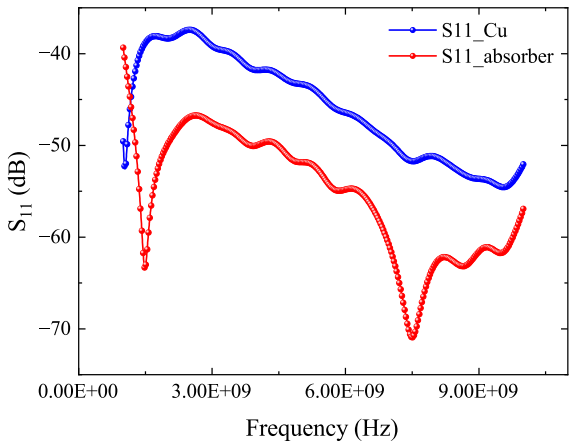


Fig. 8: Measured $S_{11}$ of a Cu-plate and an absorber

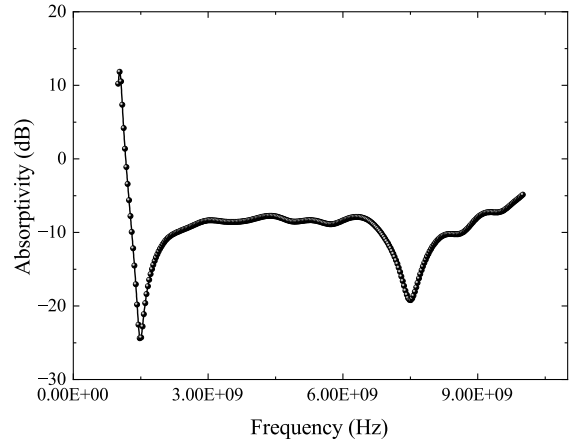


Fig. 9: Absorptivity of an absorber under test with respect to a Cu-plate

illustrated across a frequency range in Fig.6.

Additionally, the time-gating feature of the VNA is employed to measure the reflection coefficients of a Copper plate and an absorber under test, as depicted in Fig.8. The absorber's characterized absorptivity is further detailed in Fig.9. This multifaceted experimental approach provides a comprehensive understanding of the antenna's electromagnetic behavior and extends its applications to the assessment of materials like absorbers through advanced measurement techniques.

## V. Conclusion

In this comprehensive investigation, we delved deep into the measurement intricacies of Antenna measurement. This experiment has yielded crucial insights into parameters such as reflection coefficient, antenna gain, and radiation patterns. Furthermore, the application of time domain reflectometry and time gating to characterize the reflection coefficient of an absorber not only demonstrated their practical utility but also provided a nuanced understanding of their dynamic behavior. These findings contribute to the advancement of communication systems and radar technology. The incorporation of temporal aspects through time domain reflectometry enhances the characterization process, offering a holistic view of antenna and absorber responses to varying temporal stimuli.

## VI. ACKNOWLEDGMENT

Firstly, the author would like to thank his lab-mate Mr. Mayank Anupam for carrying out the experiments together and sharing concepts. The author would also like to acknowledge the efforts of course TAs in conducting the experiments smoothly and finally, Prof. A R Harish for his ever-present guidance and patience to answer all the questions.

## REFERENCES

[1] "IEEE Recommended Practice for Antenna Measurements," *IEEE Std 149-2021 (Revision of IEEE Std 149-1977)*, pp. 1–207, 2022.
[2] "IEEE Standard Definitions of Terms for Antennas," *IEEE No 145-1969*, pp. 1–10, 1969.
[3] A. R. Harish, "EE647A:Microwave Measurements and Design Lab Handouts, 2023."
[4] ——, "EE647A:Microwave Measurements and Design Lecture Notes, 2023."

# Experiment No. - 8
# Single Stub and Double Stub Matching for a given Load using Vector Network Analyzer

Debashish Nandi, *Graduate Student Member, IEEE*
*Roll No.21204262*

***Abstract*— This report presents a comprehensive exploration of single stub matching and double stub matching techniques for an unidentified load utilizing a Vector Network Analyzer (VNA). The traditional methods of single stub and double stub matching are examined in-depth, considering their respective advantages and drawbacks. Additionally, the report delves into the intricacies of the portable VNA and the electronic calibration (e-calibration) process. These experimental evaluations were meticulously conducted within the Microwave Measurement Laboratory, situated in the Electrical Engineering Department at the Indian Institute of Technology Kanpur.**

***Index Terms*— Single stub, Double Stub, Matching, VNA, E-cal, Forbidden Zone.**

## I. Introduction

Impedance matching is a crucial aspect in the realm of radio frequency (RF) and microwave engineering, playing a pivotal role in optimizing power transfer between different components within a communication system. The efficient matching of impedances ensures maximum power transfer and minimizes signal reflections, contributing to enhanced system performance. This introduction delves into the significance of impedance matching, focusing on two widely employed techniques: single stub matching and double stub matching.

Single stub matching is a conventional and versatile method employed to match an unknown load with a transmission line. This technique involves the insertion of a single adjustable stub, typically a short-circuited or open-circuited transmission line, at a specific location along the main transmission line. The goal is to achieve the desired impedance transformation that matches the load impedance with the characteristic impedance of the transmission line. While single stub matching is relatively simple and can provide effective impedance matching in certain cases, it has limitations, particularly in dealing with complex loads or those with varying frequency responses. Double stub matching is an extension of the single stub matching technique, offering greater flexibility and precision. In this method, two adjustable stubs are strategically placed along the transmission line to achieve a more accurate impedance match. The iterative nature of double stub matching allows for fine-tuning and optimization, making it suitable for a broader range of load impedances. However, this increased precision comes at the cost of added complexity and the requirement for more intricate tuning procedures.

The Vector Network Analyzer (VNA) serves as an indispensable tool in impedance matching experiments. VNAs enable the precise measurement of complex impedance, providing valuable insights into the performance of the matching networks. The ability to characterize the impedance behavior over a range of frequencies is instrumental in designing effective matching circuits. Moreover, VNAs facilitate the visualization of reflection and transmission coefficients, aiding engineers in optimizing the matching network for specific applications. Accurate measurements with a VNA necessitate calibration procedures to account for systematic errors and uncertainties. Electronic calibration, or e-calibration, is a critical step in ensuring the reliability of VNA measurements. This process involves the calibration of the VNA using electronic standards to enhance measurement accuracy and reduce errors introduced by the test setup. Proper e-calibration is imperative for obtaining precise impedance measurements and ensuring the validity of impedance matching strategies.

The organization of the report is as follows: The problem formulation is presented in Section II, followed by characterization in Section III. Section IV presents the results and discussions, and we offer the concluding remarks in Section V.

## II. Problem Formulation

The experiments [1] involved in this study are as follows:

*1)* **Single Stub Matching:** The primary aim of this experiment is study the VNA by means of Single stub matching. This part of the experiment comprises of familiarization of the VNA, e-calibration, normalization of $S_{11}$ trace with a matched load, measuring guide wavelength from Smith Chart in VNA, measuring stub susceptance as a function of its depth, matching three unknown loads to the VNA port and characterizing the bandwidth of single stub matching (with Standing wave ratio (SWR) $< 2$).

*2)* **Double Stub Matching:** This experimental phase is dedicated to exploration of double stub matching by means of three unknown loads to the VNA port. Here, we also characterize the bandwidth of double stub matching (with SWR $< 2$).

**Theoretical Formulation** : For a lossless transmission line, the reflection coefficient $\Gamma_L$ can be defined as

Debashish Nandi is with the Nanolab, Department of Electrical Engineering, IIT Kanpur, Kanpur 208016, India (e-mail: debashish21@iitk.ac.in)

$$\Gamma_L = \frac{Z_L - Z_0}{Z_L + Z_0} \tag{1}$$

where, $Z_L$ is the load resistance and $Z_0$ is the characteristic impedance of the mentioned transmission line. The Voltage Standing wave ratio is defined as

$$SWR = \frac{1 + |\Gamma_L|}{1 - |\Gamma_L|} \tag{2}$$

For a rectangular wave guide the cut-off frequency is given by

$$f_c = \frac{1}{2\pi\sqrt{\mu\epsilon}} \cdot \sqrt{(\frac{m\pi}{a})^2 + (\frac{n\pi}{b})^2} \tag{3}$$

where, $\mu$ is the permeability of the medium, $\epsilon$ is the permittivity of the medium, a is the length and b is the width of the wave-guide cross section. m and n are integers and define the modes of propagation the wave guide [2]. The dominant mode for a rectangular wave guide is $TE_{10}$ mode (m = 1, n = 0) and hence the cut-off frequency using (3) can be written as

$$f_c = \frac{1}{2\pi\sqrt{\mu\epsilon}} \cdot \frac{\pi}{a} \tag{4}$$

The guide wavelength of a rectangular wave guide $\lambda_g$ is given as

$$\lambda_g = \frac{\lambda}{\sqrt{1 - (\frac{f_c}{f})}} \tag{5}$$

where $\lambda$ is the wavelength of the electromagnetic wave at frequency f and $f_c$ is the cut-off frequency of the mode of propagation.

## III. Characterization

The general characterization set-up used in this experiment, is shown in Fig.1. The components used in this experiment are a) Vector Network Analyzer (Agilent Technologies, FieldFox N9912A, 6 GHz), b) A single-tub matching test bench, c) Double-stub tuners e) mounting screws and drivers, f) Unknown loads (three types) and g) connecting cables, connectors.

### A. Single Stub Matching

The first part of the experiment is to explore the Single Stub matching technique for three unknown loads. For $TE_{10}$ mode to propagate in the wave guide, the operating frequency has to be greater than the cut-off frequency ($f_c$) which is calculated using (4) as $f_c$ = 4.285 GHz (a = 3.5 cm). The VNA is calibrated using e-calibration for the frequency range of 4.28 - 6 GHz, IF bandwidth = 1 KHz, no. of points = 201. The frequency range is chosen considering the operating range of the VNA. The calibration is done to fix the reference plane at the end of the connecting cable of the VNA.

For this part of the experiment, the VNA is set to Smith Chart mode with desired frequency of matching $f_0$ = 5.9 GHz. This frequency is chosen by considering the operating range of matched load, i.e., 5.8 - 8.2 GHz. Firstly, the $S_{11}$ trace is normalized by connecting a short (short circuit load) at the end of the adaptor. This was achieved by using the $Trace/Math$ & $Memory/Data/Memory/\frac{Data}{Math}/Done$ features in the VNA.

Thereafter, to measure the guide wavelength ($\lambda_g$) from the Smith Chart, the single stub tuner with a matched load termination has been introduced. The $S_{11}$ has been set to the real axis of the $\Gamma$ plane. By changing the distance of the stub from the load end (d) we tried to reach the same conductance value, i.e., one revolution in the Smith Chart ($\frac{\lambda_g}{2}$). Hence, the measured result is found out to be d = $\frac{\lambda_g}{2}$ = 3.6 cm. The measured $\lambda_g$ = 7.2 cm which approximately agrees with the theoretically calculated guide wavelength using (5), i.e., 7.39 cm.

The stub susceptance has been measured for various stub-depths and the measured results are given in Table.I. Fig.2 shows the plot of stub susceptance vs. stub depth.

The single stub matching has been carried out for three types of loads and the measured results are shown in Table.II. The bandwidth has been calculated for $SWR < 2$ and the measurement results tabulated assuming that the dip in SWR is symmetric around $f_0$ = 5.9 GHz.

TABLE I: Measurement results of Stub depth and admittance

| Stub depth $l_s$(mm) | Admittance Reading ($\Omega^{-1}$) |
|---|---|
| 10.5 | 48.8 + j 157.0 |
| 11.0 | 49.4 + j 126.6 |
| 11.5 | 50.0 + j 104.1 |
| 12.0 | 50.7 + j 86.8 |
| 12.5 | 51.1 + j 72.0 |
| 13.0 | 51.6 + j 60.4 |
| 13.5 | 51.9 + j 50.4 |
| 14.0 | 52.0 + j 42.4 |

TABLE II: Measurement results of Single Stub Matching for $f_0$ = 5.9 GHz

| Load Aperture type | Bandwidth (GHz) | d (cm) | Stub depth $l_s$(mm) |
|---|---|---|---|
| □ Wide | 0.342 | 3.55 | 15.525 |
| □ Narrow | 0.212 | 3.10 | 13.037 |
| ○ Circular | 0.010 | 2.0 | 9.022 |

TABLE III: Measurement results of Double Stub Matching for $f_0$ = 5.9 GHz

| Load Aperture type | Bandwidth (GHz) |
|---|---|
| □ Wide | 0.257 |
| □ Narrow | 0.148 |
| ○ circular | Matching not possible |

### B. Double Stub Matching

The double stub matching has been carried out for three types of loads and the measured results are shown in Table.III. The bandwidth has been calculated for $SWR < 2$ and the measurement results tabulated assuming that the dip in SWR is symmetric around $f_0$ = 5.9 GHz. The double stub tuner is added for this part of the experiment and the stub used for single stub matching has been kept loose, so that it doesn't get activated as a third stub. The circular aperture load could not be matched using double stub matching and upon further investigation as mentioned in [3], it was found to be in the forbidden zone [2].

## IV. Results and Discussion

This experiment focuses on exploration of the single and double stub matching techniques for three unknown loads.

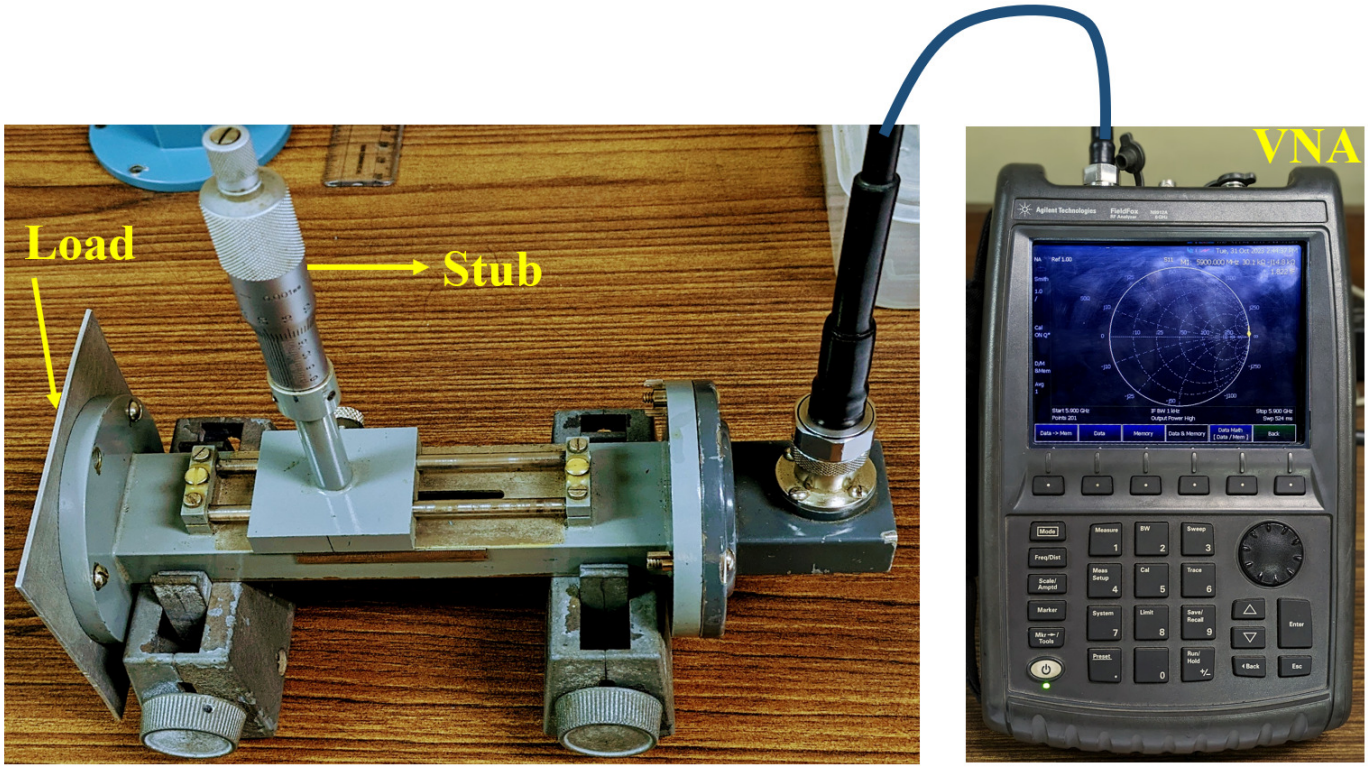


Fig. 1: Experimental set-up used for single and double stub matching

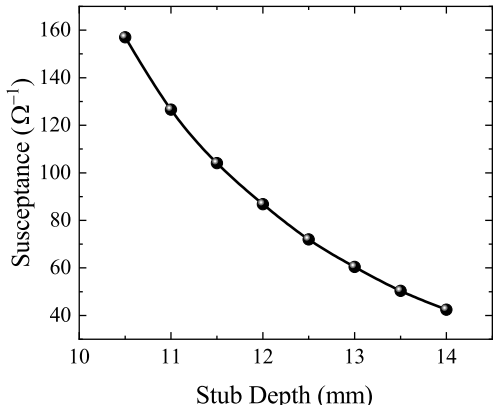


Fig. 2: Stub susceptance vs. Stub depth

The cut-off frequency of the wave guide for $TE_{10}$ mode is found to be $f_c$ = 4.285 GHz. The operating frequency has been chosen to be $f_0$ = 5.9 GHz. In the single stub matching, the stub-susceptance has been measured for various stub-depths and the results are shown in Table.I and plotted in Fig.2. The distance between the load and the stub (d), the stub depth ($l_s$), bandwidth of matching (for SWR $<$ 2) have been measured for single stub matching and are given in Table.II. The results of double stub matching are tabulated in Table.III.

## V. Conclusion

In this comprehensive investigation, we delved deep into the measurement intricacies of single and double stub matching techniques. The experiment has provided invaluable insights into e-calibration, Math-Memory and the Smith Chart features of the Vector Network Analyzer (VNA). Both single stub and double stub matching techniques were employed to match three unknown loads to the VNA port. A noteworthy finding emerged when attempting to match a load with a circular aperture using double stub matching, revealing its confinement within a speculated forbidden zone [2]. However, this load could be easily matched using three stubs, showcasing the efficacy of alternative techniques. While single stub matching appears simpler than its double stub counterpart, its reliance on movable parts renders it generally costlier. In contrast, double stub matching, despite its precision, faces limitations, particularly with loads that may fall into the aforementioned forbidden zone. An interesting observation is that the matching achieved with both techniques is inherently narrow-band. Consequently, for wide-band applications, multi-section matching techniques [2] emerge as the preferred choice. This comprehensive investigation not only advances our understanding of impedance matching intricacies but also underscores the nuanced considerations and trade-offs inherent in selecting the most suitable matching technique for diverse applications.

## VI. Acknowledgment

Firstly, the author would like to thank his lab-mate Mr. Mayank Anupam for carrying out the experiments together and sharing concepts. The author would also like to acknowledge the efforts of course TAs in conducting the experiments smoothly and finally, Prof. A R Harish for his ever-present guidance and patience to answer all the questions.

## References

[1] A. R. Harish, “EE647A:Microwave Measurements and Design Lab Handouts, 2023.”
[2] D. M. Pozar, “Microwave Engineering, 4th ed., Wiley, 2013.”
[3] A. R. Harish, “EE647A:Microwave Measurements and Design Lecture Notes, 2023.”

# Experiment No - 10 Familiarization with Spectrum Analyzer (SA), Study of Modulated Waveforms and Range Extension of SA

Debashish Nandi, *Graduate Student Member, IEEE*
*Roll No.21204262*

***Abstract*— In this work, we present a detailed report on the study of Spectrum Analyzer (Agilent N9320B). Spectrum Analyzers (SA) help us visualize signal powers, noise powers etc. in frequency domain which holds a great significance in testing of RF, Microwave and Integrated Circuits. A detailed analysis of Amplitude Modulated (AM) waveform, Frequency Modulated (FM) waveform and RF Pulsed signals have been carried out by looking into their power Spectral densities (PSD) in the SA. Also, an attempt has been made for range extension of the Spectrum Analyzer using an external mixer. All the measurements have been carried out in the Microwave Measurement Laboratory in the Electrical Engineering Department of IIT Kanpur.**

***Index Terms*— Microwave Measurement, Spectrum Analyzer, AM, FM, Puled RF, IF, Local Oscillator.**

## I. Introduction

IN the realm of contemporary wireless communication and electromagnetic research, precise and comprehensive Microwave Measurements [1], [2] stand as a bedrock for understanding signal behaviors and optimizing their applications. Within this landscape, the Spectrum Analyzer (SA) emerges as an indispensable tool, offering an unparalleled window into the spectral intricacies of electromagnetic waveforms. This experiment embarks on an in-depth voyage into the domain of Microwave Measurements facilitated by the Spectrum Analyzer. With a deliberate focus on well-known examples, including Amplitude Modulation (AM) and Frequency Modulation (FM) [3], the study delves into the subtle interplay between modulation techniques and their spectral manifestations. Beyond modulation, the analysis extends to the exploration of pulsed RF signals, deftly highlighting the Spectrum Analyzer's prowess in capturing transient phenomena with remarkable precision. Moreover, this study delves into the subtleties of Noise Floor via its Power Spectral Densities, unraveling their significance in discerning signal quality amidst noise-laden environments. By the assistance of these examples, our study not only underscores the instrumental role of Spectrum Analyzers in unraveling microwave intricacies but also advances a holistic comprehension of the intricate relationships binding modulation, spectral composition, and signal fidelity.

Debashish Nandi is with the Nanolab, Department of Electrical Engineering, IIT Kanpur, Kanpur 208016, India (e-mail: debashish21@iitk.ac.in)

In this Experiment-10 which is comprising of five sub-experiments we familiarize ourselves with the Spectrum Analyzer by means of analyzing AM, FM, pulsed RF waveforms, Noise Floor etc.

The organization of the report is as follows: The problem formulation is presented in Section II, followed by characterization in Section III. Section IV presents the results and discussions, and we offer the concluding remarks in Section V.

## II. Problem Formulation

The experiments involving the study of Spectrum Analyzer (SA) are as follows:

*1)* **Study of various features of Spectrum Analyzer:** In this experiment we familiarize ourselves with the Agilent N9320B Spectrum Analyzer (Fig. 1) by exploring its various operations and features. This includes measurement of 3dB bandwidth of the IF filter using a continuous wave (CW) source for various resolution bandwidth (RBW) settings. Also, we inspect the effect of RBW on the Noise Floor.

*2)* **Study of Amplitude Modulated (AM) wave spectrum:** The objective of this experiment is to visualize the Amplitude Modulated (AM) wave spectrum for various AM depth settings. Additionally, we measure the carrier and sideband power levels and characterize the modulation index.

*3)* **Study of Frequency Modulated (FM) wave spectrum:** In this experiment we visualize and perform measurement on the Frequency Modulated (FM) wave spectrum in the SA for various frequency deviations and calculate the FM modulation indices. An appropriate display setting in the SA is essential for visualizing the FM spectra.

*4)* **Study of Pulsed RF spectrum:** In this case, we study the Pulsed RF spectrum in SA. A precise display setting is mandatory for visualizing the spectrum in SA. Measurement of the first zero-crossing of the spectrum envelope, distance between spectral lines are also carried out and pulse width and pulse period are calculated.

*5)* **Range extension of Spectrum Analyzer:** In this experiment, we made an attempt to extend the range of Spectrum Analyzer by connecting an external mixer. Here, we tried to measure the conversion loss of the mixer.

**Available information** : The following information regarding the Experiment-10 is provided [3], [4]:

For an Amplitude Modulated (AM) wave,

$$m = \frac{A_m}{A_c} \tag{1}$$

where m is the AM modulation index, $A_m$ is the peak of modulating signal and $A_c$ is the peak of carrier signal. The total power $P_t$ in terms of carrier power $P_c$ is given by

$$P_t = P_c \times (1 + \frac{m^2}{2}) \tag{2}$$

whereas the total sideband power is given by $P_{SB} = P_c\frac{m^2}{2}$. Hence

$$m = 2 \times \sqrt{\frac{P_{SB1}}{P_c}} \tag{3}$$

where $P_c$ is the carrier power in watts and $P_{SB1}$ is the power in one sideband in watts.

For a frequency modulated (FM) wave, the useful bandwidth (BW) is given by

$$BW = 2 \times (\Delta f + f_m) \tag{4}$$

where $f_m$ is the modulating signal frequency and $\Delta f$ is the frequency deviation. For a Narrow-band FM (NBFM), the bandwidth is $BW \approx 2\Delta f$. The FM modulation index is given by

$$m = \frac{\Delta f}{f_m} \tag{5}$$

The conversion loss (CL) of a mixer is defined as the difference in power between the input RF signal power and the output IF signal power levels. It is given by

$$CL = P_{RF} - P_{IF} \tag{6}$$

where $P_{RF}$ and $P_{IF}$ are in dBm and CL is in dB.

## III. Characterization

The setup shown in Fig. 2 has been used in general to demonstrate all the experiments mentioned in Section-II. The **Agilent N9320B** has been used as the spectrum analyzer and **Agilent N9310A** as the signal generator, both of which has an operating range of 9 KHz to 3.0 GHz. For the last part of the experiment, another signal generator **Wavetek 954** (operating range: 3.7-7.6 GHz) and an external mixer have been used.

### A. Study of various features of Spectrum Analyzer

Fig. 1 shows the subject Spectrum Analyzer which is under study. In this experiment some of the very important features such as the display settings (amplitude, span, centre frequency), Resolution Bandwidth (RBW), reading of data using multiple markers, peak search etc. have been exploited.

Additionally, we have measured the 3dB bandwidth of the IF filter present in the SA using a continuous wave (CW) signal from the signal generator as shown in Fig. 2. A sinusoidal input signal of frequency 0.9 GHz and power 0 dBm has been used. The results are mentioned in Table I where $P_0$ is the power at centre frequency $f_0$ = 0.9 GHz and NF is the noise floor measured in dBm.

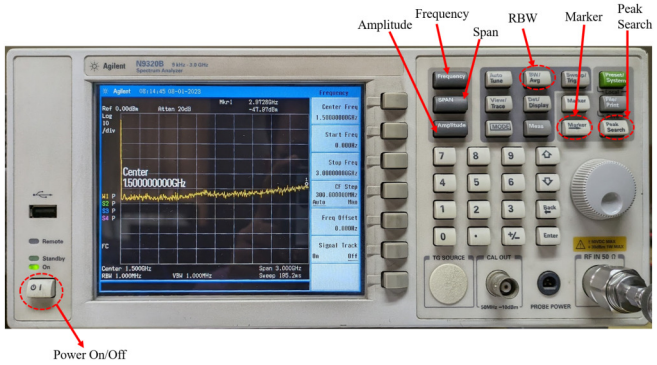


Fig. 1: Agilent N9320B Spectrum Analyzer

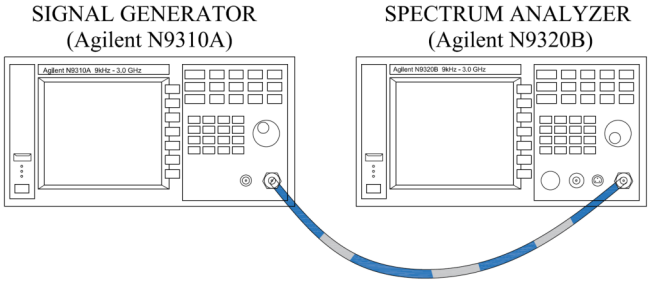


Fig. 2: A typical experimental set-up with a Signal Generator and a Spectrum Analyzer

TABLE I: Measurement results for 3dB bandwidth of IF filter

| RBW (KHz) | $P_0$ (dBm) | $\Delta f_{3dB}$ (KHz) | NF (dBm) |
|---|---|---|---|
| 1 | -6.76 | 1.087 | -90 |
| 3 | -6.50 | 3.066 | -85 |
| 10 | -6.46 | 10.066 | -80 |
| 30 | -6.40 | 30.500 | -75 |
| 100 | -6.38 | 98.326 | -68.8 |

Firstly, we can observe that the 0 dBm input power has dropped to approx. -6.5 dBm. This 6.5 dB loss encountered between the generator to SA is mainly from the cable used for connection. It is observed that the Resolution Bandwidth (RBW) actually signifies the 3dB bandwidth of the IF filter. Additionally we can observer that the Noise Floor increases with the increase in RBW which actually makes sense as the higher 3dB bandwidth will take into account larger contribution from noise.

### B. Study of Amplitude Modulated (AM) wave spectrum

In this experiment, the same set-up has been used as shown in Fig. 2. The carrier signal has frequency $f_c$ = 1.3 GHz and power level of 0 dBm whereas the sinusoidal modulating signal has a frequency $f_m$ = 50 KHz and modulation depth $m_d$ = 50%. The obtained spectrum in SA is shown in Fig. 3. The formation of side bands is evident from Fig. 3. The modulation index m is calculated using (3) and is found out to be m = 0.484 (48.4%) which is almost equal to the input modulation depth. The similar steps have been performed for $m_d$ = 10%, 20%, 40%, 70%, 80% and the results are provided in Table. II. For maintaining brevity of the report, only the spectrum related to $m_d$ = 50% has been shown and results for other values of $m_d$ are tabulated. Here $P_L$ denotes the power level of left side band and $P_R$ denotes the power level of right side band.

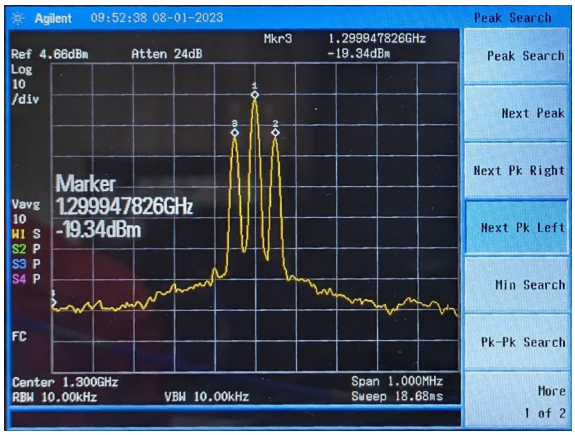


Fig. 3: Amplitude Modulated Wave Spectrum for $f_c$ = 1.3 GHz and $m_d$ = 50%

TABLE II: Measurement results from Amplitude Modulated Wave spectrum

| $\mathbf{m_d}$ (%) | $\mathbf{P_0}$ (dBm) | $\mathbf{P_L}$ (dBm) | $\mathbf{P_R}$ (dBm) | m |
|---|---|---|---|---|
| 50 | -6.97 | -19.3 | -19.2 | 0.484 |
| 10 | -7.22 | -33.5 | -33.5 | 0.097 |
| 20 | -7.23 | -27.5 | -27.4 | 0.195 |
| 40 | -7.21 | -21.5 | -21.4 | 0.388 |
| 70 | -7.22 | -16.7 | -16.6 | 0.675 |
| 80 | -7.22 | -15.6 | -15.5 | 0.767 |

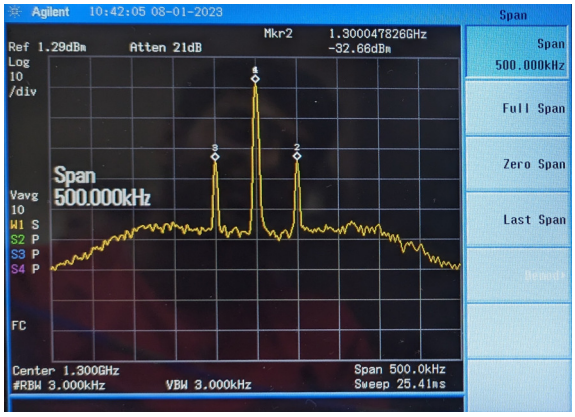


Fig. 4: Frequency Modulated Wave Spectrum for $f_c$ = 1.3 GHz and $f_d$ = 5 KHz

## C. Study of Frequency Modulated (FM) wave spectrum

In this experiment, the same set-up has been used as shown in Fig. 2. The carrier signal has frequency $f_c$ = 1.3 GHz and power level of 0 dBm whereas the sinusoidal modulating signal has a frequency $f_m$ = 50 KHz and frequency deviation $f_d$ = 5 KHz. The obtained spectrum in SA is shown in Fig. 4 for which the span of the SA has been set to 0.5 MHz and RBW as 3 kHz. Ideally there should be infinite side bands for a FM spectrum [3]. The similar steps have been performed for $f_d$ = 25, 50, 75, 100 KHz and the results are provided in Table. III where $P_0$ is the power level measured at centre frequency. For maintaining brevity of the report, only the spectrum related to $f_d$ = 50 KHz has been shown in Fig. 5 and results for other values of $f_d$ are tabulated. Fig. 5 clearly brings out the fact of forming multiple side bands in a FM spectrum. We have also calculated the useful FM bandwidth (BW) considering 50 dB bandwidth, $\Delta f$ and modulation index m = $\frac{\Delta f}{f_m}$, using (4), (5) and are given in Table. III.

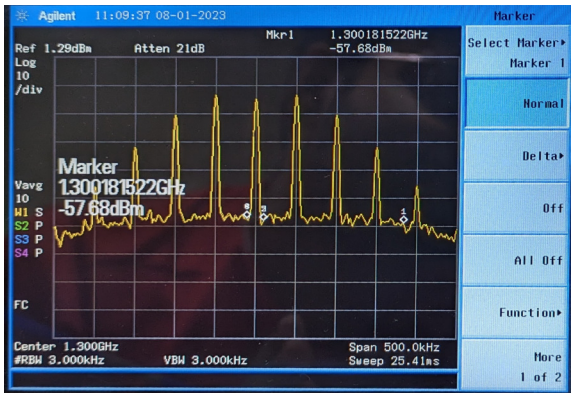


Fig. 5: Frequency Modulated Wave Spectrum for $f_c$ = 1.3 GHz and $f_d$ = 50 KHz

TABLE III: Measurement results from Frequency Modulated Wave spectrum

| $\mathbf{f_d}$ (KHz) | $P_0$ (dBm) | BW (KHz) | $\Delta f$ (KHz) | m |
|---|---|---|---|---|
| 5 | -7.10 | 100 | 0 | 0.00 |
| 25 | -7.10 | 200 | 50 | 1.00 |
| 50 | -9.70 | 300 | 100 | 2.00 |
| 75 | -14.12 | 624 | 262 | 5.24 |
| 100 | -22.5 | 823 | 361.5 | 7.23 |

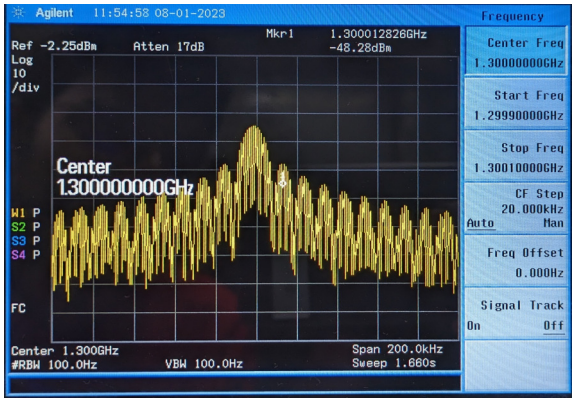


Fig. 6: Pulsed RF Wave Spectrum for $f_c$ = 1.3 GHz, $\tau$ = 1ms and T = 100$\mu s$

TABLE IV: Power levels of the frequency components captured in SA

| Parameters | Freq. (GHz) | Amplitude (dBm) |
|---|---|---|
| $f_z$ (right) | 1.300009087 | -82.0 |
| $f_z$ (left) | 1.299988326 | -85.0 |
| peak 1 | 1.299998500 | -26.7 |
| peak 2 | 1.299997522 | -27.0 |

## D. Study of Pulsed RF spectrum

In this experiment, the set-up used is shown in Fig. 2. The RF signal has frequency $f_c$ = 1.3 GHz and power level of 0 dBm whereas the pulse used has a pulse period $\tau$ = 1ms ($f_\tau$ = 1 KHz) and pulse width of T = 100$\mu s$ ($f_T$ = 10 KHz). For obtaining the spectrum as shown in Fig. 6, a careful display setting has been set by considering span = 200 KHz (one order greater than $f_T$) and RBW = 100 Hz (One order lesser than $f_\tau$). The first zero crossing ($f_z$) of the spectrum envelope, distance between spectral lines ($f_T$) have been measured and results are tabulated in IV.

The first zero crossing ($f_z$) of the spectrum envelope is measured as $f_T = \frac{f_z(right) - f_z(left)}{2}$ = 10.038 KHz. The distance between the spectral lines are calculated as the difference

TABLE V: Power levels of the frequency components captured in SA

| Frequency (GHz) | Power level (dBm) |
|---|---|
| 1.63 | -42.00 |
| 1.80 | -21.88 |
| 1.96 | -18.40 |

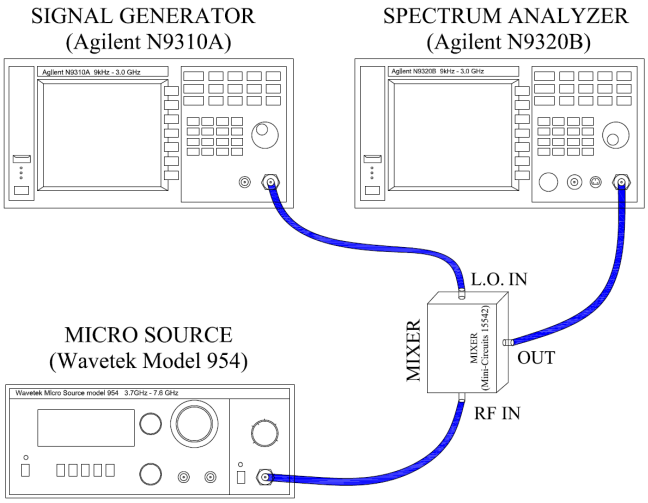


Fig. 7: A Transmission line terminated at a capacitive load.

between frequencies where peak1 and peak2 are measured, i.e., $f_\tau$ = 0.978 KHz. The calculated pulse period $\tau = \frac{1}{f_\tau}$ = 1.022 ms and pulse width of T = $\frac{1}{f_T}$ = $99.6\mu s$. The measured results matches the settings on the pulse modulator.

### E. Range extension of Spectrum Analyzer

In this experiment as shown in Fig. 7, an additional RF signal generator and an external mixer have been used. The idea is to use Agilent N9310A as a Local Oscillator (LO) and Wavetek 954 as RF signal generator and produce an IF signal through an external mixer. The RF source is set to $f_1$ = 3.8 GHz and the LO is set to $f_2$ = 1.8 GHz. Due to the non-linearities in the system, there will be presence of higher order harmonics and inter-modulated signals which have been tried to visualize in the Spectrum Analyzer. The span of the SA has been set to full-screen (9 KHz - 3.0 GHz) and all the frequency components within the SA range were measured. The input power from the RF source has been set to its maximum and LO power is at 0 dBm, during measurement. The results are furnished at Table. V.

The following frequency components were observed in Spectrum Analyzer under full span: $f_2$ = 1.8 GHz , $f_1 - f_2$ = 2 GHz (1.96 GHz) and $3f_2 - f_1$ = 1.6 GHz (1.63 GHz). The conversion loss could not be measured due to non-availability of the input RF power level.

## IV. Results and Discussion

This experiment is centred around the study of Spectrum Analyzer (SA). Firstly, in exp.A, we have explored various features of the SA including display settings, resolution bandwidth (RBW), attenuation, reading outputs, measuring 3dB bandwidth of the IF filter, Noise Floor etc. From the measured results given in Table.I, we concluded that the RBW is indeed the 3dB bandwidth of the IF filter. A few interesting observations were made while visualizing spectrum of a continuous wave (monotone) in the SA, i.e., a spectral line at the very low frequency ( DC) and higher order harmonics along with the fundamental frequency component. From the presence of harmonics, it can be concluded that there is non-linearity in the system and the spectral line at DC is due to LO leakage/free thru. We have further inspected the source of non-linearity by changing the attenuation level of the attenuator present at the input of SA and it was observed that irrespective of the attenuation level, the power levels at fundamental, $1^{st}$ harmonic and $2^{nd}$ harmonic remain same. This signifies that the non-linearity is attributed to the signal generator itself. From the relationship of noise floor and RBW, we can infer that as RBW is increased, the noise floor is also increased and has been discussed in detail in Section-III.

From the AM spectrum, we have calculated the modulation indices for various AM depths as mentioned in Table.II, and the characterized results seem to match the input setting. It was observed that as we increase the modulation depth the deviation from input setting is more. Similarly, FM and pulsed RF spectrum have been studied and measurement results are furnished in Table.III and IV respectively.

An attempt has been made for the range extension of the Spectrum Analyzer and results are furnished in Section-III. However, due to unavailability of the RF power readings, the conversion loss (CL) could not be calculated.

## V. Conclusion

A comprehensive series of experimental investigations was conducted to cultivate a profound familiarity with the diverse capabilities inherent to the Agilent N9320B Spectrum Analyzer. Within this exploratory framework, the analysis focused on the meticulous examination of two well-established modulation techniques: Amplitude Modulation (AM) and Frequency Modulation (FM). These techniques were scrutinized through a comprehensive exploration of their respective Power Spectral Densities, facilitated by the Spectrum Analyzer's precision in measurement. Additionally, the visualization of RF Pulsed spectra was achieved through meticulous adjustments of parameters such as span and resolution bandwidth (RBW) within the Spectrum Analyzer. An insightful exploration into the impact of RBW on the Noise Floor was undertaken and effectively demonstrated within the context of the Spectrum Analyzer. An attempt was made into enhancing the operational range of the Spectrum Analyzer through the integration of an external mixer, showcasing the adaptability and extensibility of the instrument.

It is noteworthy that the Spectrum Analyzer (SA) stands as a pivotal tool across diverse domains within the realm of RF and Microwave engineering, boasting a wide array of applications ranging from the testing of integrated circuits to broader industrial applications. This experimental endeavor not only established a comprehensive foundation for proficiently operating the Spectrum Analyzer but also facilitated a deeper comprehension of its intricate functionalities.

## VI. ACKNOWLEDGMENT

Firstly, the author would like to thank his lab-mate Mr. Mayank Anupam for carrying out the experiments together and sharing concepts. The author would also like to acknowledge the efforts of course TAs in conducting the experiments smoothly and finally, Prof. A R Harish for his ever-present guidance and patience to answer all the questions.

## REFERENCES

[1] D. M. Pozar, "Microwave Engineering, 4th ed., Wiley, 2013."
[2] A. R. Harish, "EE647A:Microwave Measurements and Design Lecture Notes, 2023."
[3] H. Taub and D. L. Schilling, "Principles of Communication Systems, 4th ed., McGraw-Hill, 2013."
[4] A. R. Harish, "EE647A:Microwave Measurements and Design Lab Handouts, 2023."

# Experiment No - 9
# Study of Terminated Transmission lines - Time Domain and Frequency Domain Measurements

Debashish Nandi, *Graduate Student Member, IEEE*
*Roll No.21204262*

***Abstract*— In this work, we present a detailed report on the study of Terminated Transmission lines where multiple experiments have been carried out in both the time domain and the frequency domain. A $50\Omega$ coaxial cable is used as the transmission line. In time domain measurements, the main focus has been imparted on demonstration of the concept of Time Domain Reflectometry (TDR) where in case of frequency domain response, the experiments revolve around the concept of quarter wave transformers. All the measurements have been carried out in the Microwave Measurement Laboratory in the Electrical Engineering Department of IIT Kanpur.**

***Index Terms*— Microwave Measurement, Transmission Line, TDR, Quarter wave transformer.**

## I. Introduction

Microwave measurement and design [1], [2] form a critical nexus within the realm of electromagnetic engineering, catering to a wide array of applications spanning telecommunications, radar systems, satellite communications, and more. Microwave measurements involve quantifying the behavior of electromagnetic waves within the microwave frequency spectrum, typically ranging from 300 MHz to 300 GHz. Engineers and researchers employ an assortment of techniques, such as vector network analysis, spectrum analysis, and time domain reflectometry, to characterize microwave devices, components, and systems. Accurate measurement of parameters such as S-parameters, insertion loss, and return loss enables the optimization of microwave circuits and the validation of theoretical models. Meanwhile, microwave design involves the creation of intricate components like antennas, filters, amplifiers, and oscillators, often with the intention of achieving specific performance criteria such as high gain, low noise, or precise frequency selection. Advanced simulation tools such as electromagnetic simulators (e.g. Keysight ADS, HFSS etc.) aid engineers in designing and refining these complex structures before fabrication, saving time and resources. In essence, microwave measurement and design are symbiotic processes that underpin the evolution of modern wireless technologies, enabling us to harness the full potential of the electromagnetic spectrum.

In this Experiment-9 which is comprising of eight sub-experiments we study the concepts of Time Domain Reflectometry and Frequency Domain response of terminated Transmission lines. The important concepts of Reflection Coefficient, phase velocity, quarter wave transformers have been discussed and experimental validations have been furnished.

The organization of the report is as follows: The problem formulation is presented in Section II, followed by characterization in Section III. Section IV presents the results and discussions, and we offer the concluding remarks in Section V.

Debashish Nandi is with the Nanolab, Department of Electrical Engineering, IIT Kanpur, Kanpur 208016, India (e-mail: debashish21@iitk.ac.in)

## II. Problem Formulation

The experiments involving the time domain reflectometry (TDR) are as follows:

*1)* **Measurement of output impedance:** In this experiment we measure the output impedance of the signal source (function generator) for step and sinusoidal signals.

*2)* **Measurement of phase velocity in the cable:** In this experiment we measure the timed domain response of a transmission line terminated at an open-circuit and a short-circuit to compute the phase velocity and dielectric constant of the material filling the cable.

*3)* **Measurement on Transmission line terminated on a matched load:** Here we characterze the reflectection coefficient by terminating the transmission line in three types of load, i.e., a matched load, a load greater than the characteristic impedance of the line and a load lesser than the characteristic impedance of the line.

*4)* **Measurement on Transmission line with source mismatch:** In this case, we study the time domain response of the transmission line with a source mismatch for various loads.

*5)* **Measurement on Transmission line with capacitive termination:** In this experiment, we study the time domain response of the transmission line with a capacitive load.

*6)* **Capacitive discontinuity in a Transmission line:** In this experiment, a capacitive discontinuity is connected between two transmission line which models many real life scenarios and we study the impact of this in the time domain.

For all of the above cases, $50\Omega$ coaxial lines are used as Transmission lines. In Frequency domain experiments we mainly study and demonstrate the concept of Quarter Wave Transformer with the following experiments:

*7)* **Frequency Domain response of a terminated Transmission line:** In this experiment we compute the frequency at which the aforementioned co-axial line behaves as a quarter wave transformer. Here we also demonstrate how the frequency

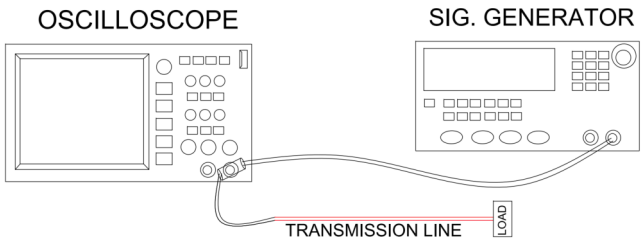


Fig. 1: A typical experimental set-up

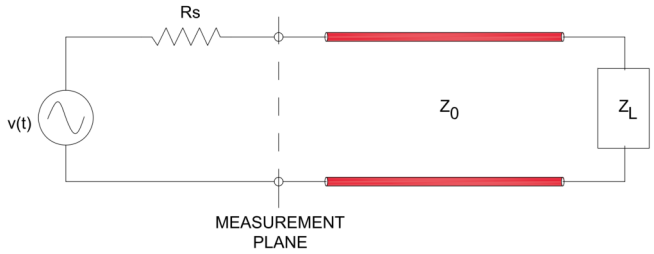


Fig. 2: An equivalent circuit representation of the experimental set-up

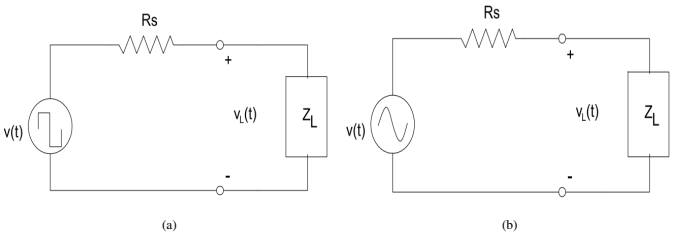


Fig. 3: Measurement of output impedance for (a) step/rectangular signal (b) sinusoidal signal

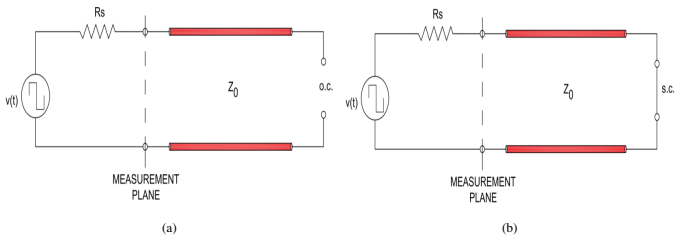


Fig. 4: Terminated Transmission line at (a) an open-circuit load (b) a short-circuit load

domain response will look like around the centre frequency (the frequency at which the Transmission line behaves as a quarter wave transformer).

*8)* **Impedance Matching with a quarter wave Transmission line:** Quarter wave transformers are very often used as a matching section between two impedance. In this experiment we demonstrate this very phenomena of impedance matching with quarter wave transformer.

**Available information** : The following information regarding the co-axial cables is provided [3]: Characteristic impedance of the lossless coaxial cables used: $Z_0$ = 50Ω, velocity of light: c = 3 x $10^8$ m/s.

Capacitance per unit length in the transmission line is given by

$$C = \frac{2\pi\epsilon}{\ln(b/a)} F/m \tag{1}$$

where a and b are the radii of the inner and outer conductors of the co-axial cable filled with a dielectric material with dielectric constant $\epsilon_r$. The length of the cable is 12.55 m.

Inductance per unit length in the transmission line is given by

$$L = \frac{\mu}{2\pi} \ln(b/a) H/m \tag{2}$$

Characteristic impedance of the transmission line is given by

$$Z_0 = \sqrt{L/C} = \frac{60}{\sqrt{\epsilon_r}} \ln(b/a)\Omega \tag{3}$$

Finally, the phase velocity of a lossless transmission line is given by

$$v_p = \frac{1}{\sqrt{LC}} m/s \tag{4}$$

## III. Characterization

The setup shown in Fig. 1 has been used in general to demonstrate all the experiments mentioned in Section-II. An equivalent circuit diagram of the setup has been shown in Fig. 2 where $R_s$ is the source resistance, $Z_0$ is the characteristic impedance of the lossless transmission line and $Z_L$ is the load. The measurement plane is fixed as shown at the output of the signal generator, for all of the experiments.

### A. Measurement of output impedance

Fig. 3a and 3b show the equivalent circuit diagram of the set-up used to determine the output impedance of the source which in our case is the signal generator. In our experiment, $Z_L$ has been chosen to be 100Ω (actual value measured was 101.1Ω) and a peak to peak voltage of 1V (actual value measured was 1.08 V). By measuring the voltage at the measurement plane, i.e., $v_L(t)$ we can determine the value of $R_s$ by simple voltage division formula. The peak-to-peak voltage measured for $v_L(t)$ is 0.73 V. Hence, the value of $R_s$ is computed as 48.47Ω.

### B. Measurement of phase velocity in the cable

In this experiment, we terminate the co-axial cable under open-circuit or short-circuit loads, as shown in Fig. 4a and 4b. The response at the measurement plane is shown in Fig. 5. When a voltage wave is launched from the signal generator, the wave gets completely reflected back from the open-circuit or short-circuit load and arrives at the measurement plane. If the length of the T.L. is L and the time taken by the wave to come back at the measurement plane if $\tau$, then the phase velocity can be simply calculated by $v_p = 2L/\tau$. The discontinuity at the measured voltage as seen in Fig. 5 gives us information regarding $\tau = 126ns$ (o.c.) and $\tau = 128ns$ and L was given to be 12.55m. Hence, the computed phase velocities are $v_p = 2.00 \times 10^8 m/s$ for the open circuit load and $v_p = 1.96 \times 10^8 m/s$. From (3) and (4), we can compute the L and C for the T.L. Therefore, from (1) and (3), the dielectric constant ($\epsilon_r$) of the dielectric filling in the coaxial cable is calculated. For the open circuit termination, $\epsilon_r = 2.22$ and for short circuit termination, $\epsilon_r = 2.30$.

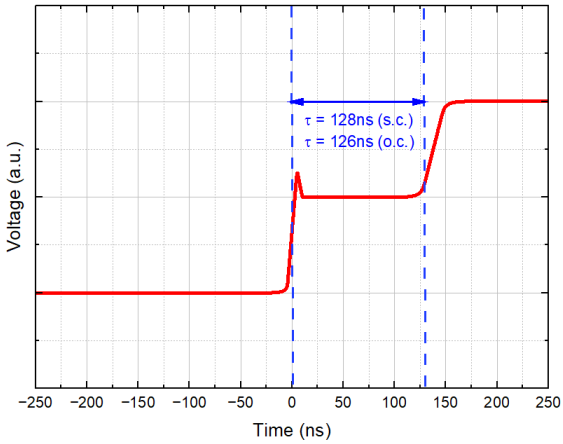


Fig. 5: Measured time domain response (for simplicity same figure is shown for both o.c. and s.c.)

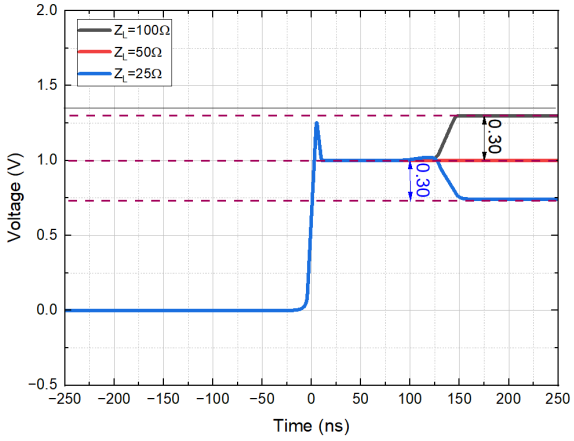


Fig. 6: Measured time domain response for $Z_L = 50\Omega$, $Z_L = 25\Omega$ and $Z_L = 100\Omega$.

## C. Measurement on Transmission line terminated at a matched load

The experimental set-up is the same as shown in Fig. 2. The input signal is taken as a 1KHz square wave (step input) with 2V peak-to-peak voltage and a 1V DC offset. The measured voltages at the measurement plane are shown in Fig. 6. for the cases of (a) $Z_L = 50\Omega$, (b) $Z_L = 25\Omega$ and (c) $Z_L = 100\Omega$. We know that for an impedance mismatch at the load (Case b, c), a part of the voltage wave will be reflected back, and we can see a step like nature at the measured voltage. By noting the difference in magnitude levels of these steps, we can compute the reflection coefficients at load ($\Gamma_L$) for all the cases. The reflection coefficients of the aforementioned cases are calculated as (a) $\Gamma_L = 1$, (b) $\Gamma_L = -0.3$ and (c) $\Gamma_L = 0.3$.

## D. Measurement on Transmission line with source mismatch

In this experiment, a mismatch at the source end is introduced by connecting impedance in series ($Z_s > Z_0$) and in shunt ($Z_s < Z_0$) respectively as shown in Fig. 7a and 7b The T.L. is kept open circuited at the load end (to take advantage of the full reflection at the load end). The measured responses are shown Fig.8.

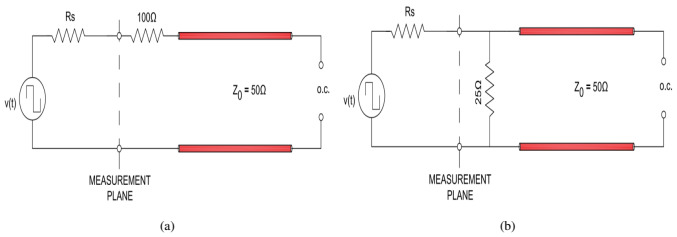


Fig. 7: Introducing Source mismatch (a) in series to make $Z_s > Z_0$ and (b) in shunt to make $Z_s < Z_0$

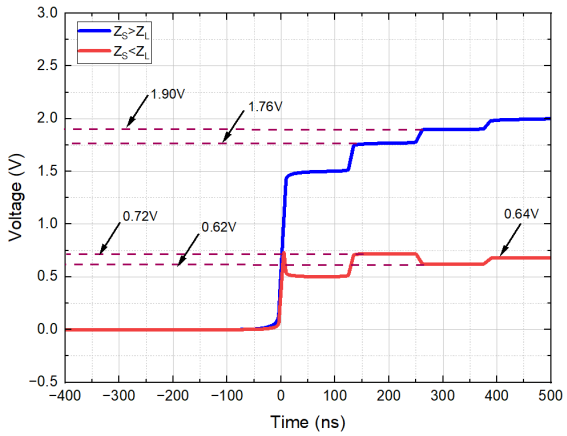


Fig. 8: Measured time domain response for the cases of source mismatch where $Z_s > Z_0$ and $Z_s < Z_0$

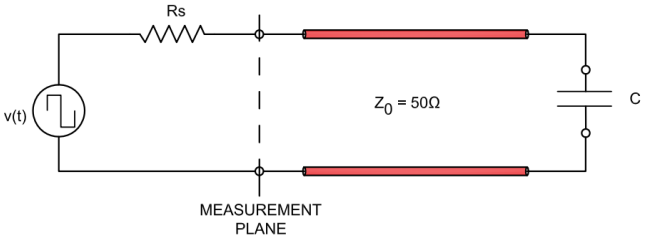


Fig. 9: A Transmission line terminated at a capacitive load.

## E. Measurement on Transmission line with capacitive termination

In this experiment, the transmission line is terminated at a capacitive load. From the equivalent circuit shown in Fig. 9, we can see that the Thevenin's resistance is $98.47\Omega$ where $R_s = 48.47\Omega$. Hence, to achieve a time constant of $0.1\mu s$, we need a capacitor of C = 2.02 nF. The time-domain response is shown in Fig. 10. The approximate time constant calculated from the measure results is $0.12\mu s$ which matches the theoretical value.

## F. Capacitive discontinuity in a Transmission line

In this experiment, another open-circuit transmission line is connected to the first transmission line as shown in Fig. 11. The measured time-domain response is shown in Fig. 12. We can see that due to the increased total length of the transmission lines, the delay is increased compared to the case in experiment B.

Now, we introduce a capacitive discontinuity at the junction of the two transmission lines by adding a 1.5 nF capacitor in

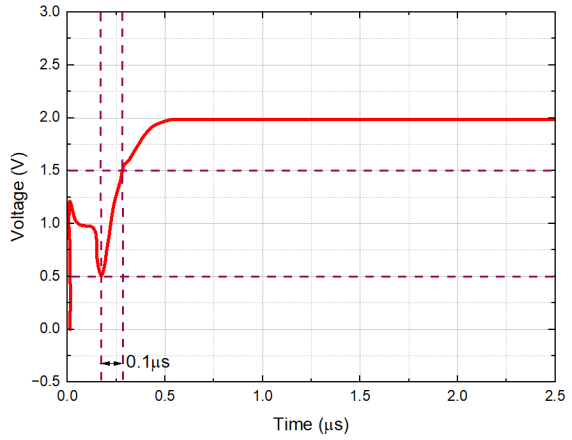


Fig. 10: Measured time domain response of a Transmission line terminated to a capacitive load.

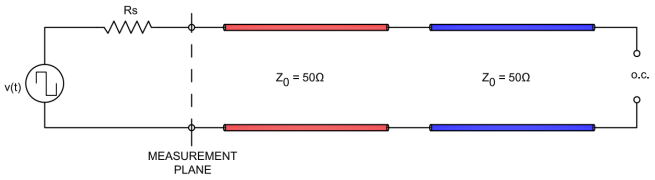


Fig. 11: A Transmission line terminated at another open circuited transmission line.

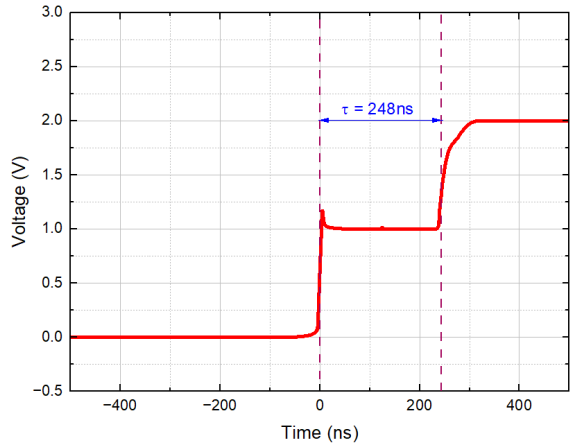


Fig. 12: Time domain response of a Transmission line terminated at another open circuited transmission line.

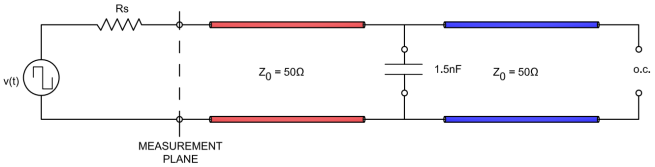


Fig. 13: A Transmission line terminated at another open circuited transmission line with a shunt capacitance at the junction

shunt, as shown in Fig. 13. The time domain response is shown in Fig. 14.

## G. Frequency Domain response of a terminated Transmission line

The experimental set-up for this frequency domain experiment is same as shown in Fig. 2. For the T.L. to behave as a quarter-wave transformer, we sweep the frequency of the

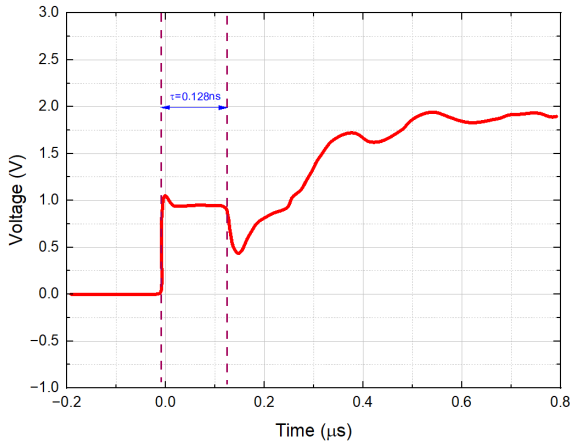


Fig. 14: Time domain response of a Transmission line terminated at another open circuited transmission line with a shunt capacitance at the junction.

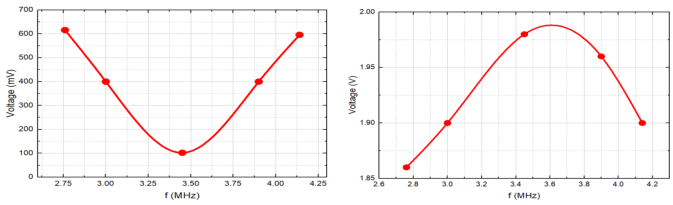


(a) (b)

Fig. 15: Frequency response of the voltage at measurement plane for a T.L. terminated with (a) an open circuit load and (b) a short circuit load.

generator signal (2V peak to peak) and measure the voltage at the input of the T.L. $Z_L = 100\Omega$ has been used and hence the impedance appearing the the input of the T.L. (looking in to the load) is $25\Omega$ (as $Z_{in} = Z0^2/Z_L$). The frequency at which the input voltage (peak to peak) was close to $f_0 = 3.45MHz$. Hence, we consider at $f_0 = 3.45MHz$, the T.L. acts as a quarter wave transformer.

For an open circuit (o.c.) termination, at $f = f_0$, the input impedance $Z_{in}$ (looking into the load) is $0\Omega$ and the measured voltage is 102mV and the same for a short circuit (s.c.) termination is measured to be 1.98V. The frequency variation of the voltage measured at the measurement plane for both o.c. and s.c. are shown in Fig. 15a and 15b respectively.

## H. Impedance Matching with a quarter wave Transmission line

The first step is to connect a $150\Omega$ resistance in series with the source which makes the effective source resistance seen by the Transmission line as $200\Omega$. To ensure this, we connect the source (including $150\Omega$ series resistance) with the load $Z_L = 200\Omega$ and measure $V_m(t)$, as shown in 16. We have used a sinusoidal input of 2V peak to peak and the measured voltage at the measurement plane is measured as 1.8V peak to peak ( $1.75V_{pp}$). This ensures that the source resistance is indeed $200\Omega$. Considering effective source impedance to be $200\Omega$, this is the matched load condition.

Our goal is to match a load of $Z_L = 12.5\Omega$ to this source resistance of $200\Omega$. First we connect a load resistance of $Z_L = 12.5\Omega$ directly to the source as shown in Fig. 16. The measured voltage $V_m(t)$ is 1.58V peak to peak, for the same input of

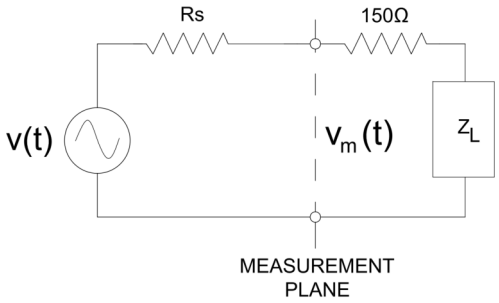


Fig. 16: Equivalent circuit diagram of the experiment H.

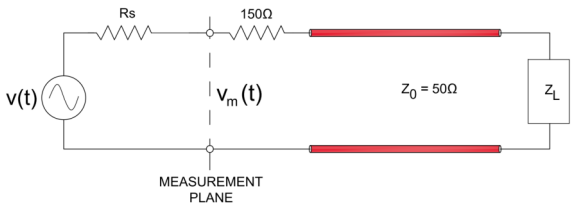


Fig. 17: Terminated Transmission line at load of $Z_L = 12.5\Omega$ with the source mismatch.

2V peak to peak. This shows that the load is not matched to the source.

We know from the previous experiment that the subject T.L. behaves as a quarter wave transformer at $f_0 = 3.45MHz$. Hence, we transform the load impedance of $12.5\Omega$ by this quarter-wave transformer prior connecting to the source, as shown in Fig. 17. The measured voltage $V_m(t)$ is indeed 1.8V peak to peak, which ensures the matched condition.

## IV. Results and Discussion

From the time domain response studies done from exp. A to F, mentioned in Section III, we found out the source impedance to be $R_s = 48.47\Omega$, phase velocity $v_p = 2.00 \times 10^8 m/s$ for open circuited load and $v_p = 1.96 \times 10^8 m/s$ for the short circuited load. We also calculated the di-electric constant of the Transmission line medium to be $\epsilon_r = 2.22$ 2.30. Various cases of load and source mismatch conditions have been examined which hold a great significance in the real world scenario. The capacitive discontinuity at the junction of two transmission lines is a direct manifesto from a real world scenario, i.e., a case when the co-axial cable gets damaged and the two conductors of the cables come very close to each other creating a capacitive discontinuity. This experiment helps us in fault diagnosis. Finally, in the frequency response experiments (G, H), we have found out the frequency $f_0 = 3.45MHz$ at which the subject transmission line/coaxial cable behaves as a quarter wave transformer and the same has been used in impedance matching in experiment H mentioned in Section II.

## V. Conclusion

A comprehensive set of experiments have been carried out to study terminated co-axial lines and their time domain and frequency domain responses. The importance of Time Domain Reflectometry has been emphasised upon and examined through various type of terminations and mismatches in the co-axial cables. The concept of transmission line behaving as a quarter wave transformer has been observed and demonstrated. While these experiments bridged the theoretical understanding and practical phenomena, laid basis for understanding advanced concepts.

## VI. Acknowledgment

Firstly, the author would like to thank his lab-mate Mr. Mayank Anupam for carrying out the experiments together and sharing concepts. The author would also like to acknowledge the efforts of course TAs in conducting the experiments smoothly and finally, Prof. A R Harish for his ever-present guidance and patience to answer all the questions.

## References

[1] D. M. Pozar, “Microwave Engineering, 4th ed., Wiley, 2013.”
[2] A. R. Harish, “EE647A:Microwave Measurements and Design Lecture Notes, 2023.”
[3] ——, “EE647A:Microwave Measurements and Design Lab Handouts, 2023.”